Control relevant modeling and nonlinear state estimation applied to SOFC-GT power systems

Rambabu Kandepu

Control relevant modeling and nonlinear state estimation applied to SOFC-GT power systems

Thesis for degree of philosophiae doctor

Trondheim, August 2007

Norwegian University of Science and Technology
Faculty of Information Technology, Mathematics and Electrical Engineering
Department of Engineering Cybernetics

NTNU
Norwegian University of Science and Technology

Thesis for degree of philosophiae doctor

Faculty of Information Technology, Mathematics and Electrical Engineering
Department of Engineering Cybernetics

ISBN 978-82-471-3778-9 (printed ver.)
ISBN 978-82-471-3781-9 (electronic ver.)
ISSN
ITK Report 2007-4-w

Thesis at NTNU, 2007:172

Summary

With today's increasing concern about global warming and climate change and further increase in energy demand, there is an incentive to investigate power processes that operate efficiently, and thus reducing the amount of emitted pollutants per produced energy unit. It is widely accepted that fuel cells are power sources that will become increasingly important, due to high efficiency, low levels of pollution and noise, and high reliability. A fuel cell converts chemical energy in a fuel directly to electrical energy without direct combustion. One of the most promising fuel cell technologies is the Solid Oxide Fuel Cell (SOFC), due to its solid state design and internal reforming of gaseous fuels, in addition to its high efficiency. Since SOFCs operate at high temperatures (about 1000°C), natural gas can be used directly as fuel. The electrical efficiency of a SOFC can reach 55%. Another significant advantage of the SOFC is that since it operates at high temperature and its efficiency increases when pressurized, it naturally lends itself as a heat source for a gas turbine (GT) cycle. The combined (hybrid) cycle can theoretically have an overall electrical efficiency of up to 70% with a power range from a few hundred kWs to a few MWs. The main applications of the hybrid system include remote area power supply and distributed power generation.

To understand the process dynamics and further to design a control structure, it is useful to have a control relevant model of the hybrid system. The first part of the thesis focuses on developing control relevant models of all the components of the SOFC-GT hybrid system using first principles. The SOFC model developed is tested against a very detailed model and the results show that the control relevant model captures the dynamics of the process and thus can be used to design a control structure. Next, a regulatory controller is designed in order for the hybrid system to be able to follow the dynamic load changes while SOFC temperature is controlled.

In a SOFC-GT system, as well as many other process systems, state

estimation may be important for monitoring and control. Thus, the final part of the thesis concentrates on nonlinear state estimation. The Unscented Kalman Filter (UKF) is investigated for the state estimation in comparison with Extended Kalman Filter (EKF). One of the results is a simple and promising constraint handling method for UKF.

Preface

This dissertation is submitted in partial fulfillment of the requirements for the degree Ph.D. at the Norwegian University of Science and Technology (NTNU). The work was carried out at the Department of Engineering Cybernetics at the Faculty of Information Technology, Mathematics and Electrical Engineering during the period from August 2003 to August 2007, and at the department of Chemical and Materials Engineering, University of Alberta during the period June to December 2006. The work was carried with Professor Bjarne Foss as the main supervisor, and Dr. Lars Imsland and Professor Olav Bolland as co-supervisors.

The project was funded by the Gas Technology Center and the Norwegian Research Council, Norway.

Acknowledgements

First of all I want to thank my supervisor, Professor Bjarne Foss, without his guidance, support and patience the work would never have been conducted. It has been a great pleasure to work with you. I would like to thank Dr. Lars Imsland for his guidance, patience for a lot queries. I would also like to thank Professor Biao Huang from University of Alberta for his guidance, and help during my stay at Alberta, Canada.

I want to acknowledge Christoph Stiller and Bjørn Thorud for introducing me to the SOFC-GT world and for the productive collaboration during the project. I want to thank my the colleagues, Arjun Singh, Hardy Siahaan, Nadi Bar, Jose Marcal, Morten Alver, Gisle Otto Eikrem, Kristin Hestetun, Steinar Kolås, Professor Ole Morten Aamo, Jostein Bakkeheim, Bjønar Bøhagen, Dagfinn Snarheim, Jørgen Spjøtvold and Petter Tøndel for helping me in one way or another and to make the working place a friendly environment. I would like to acknowledge the administration staff Tove Johansen, Eva Amdahl and Unni Johansen for their kind support. The colleagues from University of Alberta, Govind, Salim, Yutong and Seyi are acknowledged for their help and support during the stay at Alberta. I would like to acknowledge the financial support from the Gas technology Center and the Norwegian Research Council.

My deepest gratitude to Venakatapathi Tharigopula and Sridevi Tharigopula for treating me as one of their family members and bearing with me during the stay. Their support and encouragement were worthless. My gratitude to Rama Krishna Uyyuru, Dasharatha Achani, Satyanarayana Kokkula, Linga Reddy, Vasanth Gokul, Rahul Anantharaman, Vinay Kariwala, Kameshwar Singh, Kanak Parmar Singh, all other members of ISF and their family members for their support.

My family (Nageswara Rao Kandepu, Siva Kumari, Madhavi, Sambasiva Rao and Srinivasa Rao) was always standing behind me and giving me the

moral support whenever I needed it.

And last, but not least, I want to thank my wife Vishnu Priya for her love and strong support during the final year of my work.

Contents

Summary **v**

Preface **vii**

Acknowledgements **ix**

Contents **xi**

1 Introduction **1**
1.1 Challenges in energy sector 1
1.2 Fuel cells 4
1.3 Solid Oxide Fuel Cell and hybrid system 5
1.4 Nonlinear state estimation 8
1.5 Publications 10
1.5.1 Journal articles 10
1.5.2 Conferences 10
1.5.3 External Seminars 11
1.5.4 Technical reports 11
1.6 Overview of thesis 12
1.6.1 Paper I: Modeling and control of a SOFC-GT-based autonomous power system 12
1.6.2 Paper II: Modeling and control of a SOFC-GT hybrid system with single shaft configuration 12
1.6.3 Paper III: State estimation of SOFC/GT hybrid system using UKF 13
1.6.4 Paper IV: Applying the Unscented Kalman Filter for Nonlinear State Estimation 13
1.7 Contributions 14

1.8 Conclusions 14
1.9 Directions for Further Work 15
References 15

2 Modeling and control of SOFC-GT **17**
2.1 Introduction 18
2.2 Process description 19
2.3 SOFC modeling 20
2.3.1 SOFC process description 20
2.3.2 Model assumptions 22
2.3.3 Mass balance 23
2.3.4 Energy balance 25
2.3.5 Voltage 26
2.3.6 Model aggregation 26
2.4 Power system modeling 28
2.4.1 Pre-reformer 28
2.4.2 Heat exchanger 28
2.4.3 Combustion chamber 28
2.4.4 Gas turbine 29
2.4.5 Inverter 30
2.4.6 Synchronous generator 30
2.4.7 Autonomous power grid 31
2.5 SOFC model evaluation 33
2.5.1 Discussion 36
2.6 Hybrid system control and simulation 40
2.6.1 Discussion 42
2.7 Conclusions and further work 44
2.8 Acknowledgements 45
2.9 Nomenclature 45
References 46

3 SOFC-GT with single shaft **49**
3.1 Introduction 49
3.2 Process description 51
3.3 Modeling 52
3.3.1 SOFC stack 52
3.3.2 Pre-reformer 52

3.3.3 Combustor . . . 53
3.3.4 Heat exchanger . . . 53
3.3.5 Gas turbine cycle . . . 53
3.3.6 Electrical components . . . 53
3.4 Control design . . . 54
3.5 Simulation . . . 56
3.6 Conclusions . . . 60
3.7 Acknowledgements . . . 61
References . . . 61

4 State estimation of SOFC-GT 63
4.1 Introduction . . . 63
4.2 Process description . . . 66
4.3 Modeling . . . 66
4.3.1 SOFC stack . . . 67
4.3.2 Pre-reformer . . . 67
4.3.3 Combustor . . . 67
4.3.4 Heat exchanger . . . 68
4.3.5 Gas turbine cycle . . . 68
4.3.6 Electrical components . . . 68
4.4 Regulatory controller . . . 69
4.5 State estimation using UKF . . . 70
4.5.1 The SOFC/GT hybrid system description . . . 75
4.5.2 Simulations and results . . . 75
4.6 Conclusion and further work . . . 78
4.7 Acknowledgements . . . 79
References . . . 79

5 UKF for state estimation 81
5.1 Introduction . . . 81
5.2 The EKF and UKF algorithms for nonlinear state estimation 83
5.2.1 EKF principle and algorithm . . . 83
5.2.2 UKF principle and algorithm . . . 85
5.2.3 Discussion . . . 88
5.3 State estimation with constraints . . . 91
5.4 Simulation studies . . . 94
5.4.1 Van der Pol oscillator . . . 95

5.4.2 State estimation in an induction machine 101
5.4.3 State estimation with constraints: A reversible reaction example 106
5.4.4 SOFC/GT hybrid system 109
5.5 Discussion 112
5.6 Conclusions 114
5.7 Acknowledgements 114
References 114

A Additional articles **117**
A.1 ACC 2006 118
A.2 ICCA 2007 124

B Modeling report **131**
B.1 Solid Oxide Fuel Cell (SOFC) 132
B.1.1 Introduction 132
B.1.2 Model assumptions 133
B.1.3 Parameters and variables 134
B.1.4 Interfaces 134
B.1.5 Equations 137
B.1.6 Discretization 142
B.1.7 SOFC stack 145
B.2 Reformer 145
B.2.1 Introduction 145
B.2.2 Model assumptions 146
B.2.3 Parameters and variables 146
B.2.4 Interfaces (Ports) 149
B.2.5 Equations 149
B.3 Combustion chamber 152
B.3.1 Introduction 152
B.3.2 Model assumptions 152
B.3.3 Parameters and variables 153
B.3.4 Interfaces 153
B.3.5 Equations 155
B.4 Heat exchanger 157
B.4.1 Introduction 157
B.4.2 Model assumptions 157

B.4.3 Parameters and variables . . . 157
B.4.4 Interfaces . . . 158
B.4.5 Equations . . . 158
B.5 Compressor . . . 160
B.5.1 Introduction . . . 160
B.5.2 Model assumptions . . . 160
B.5.3 Parameters and variables . . . 160
B.5.4 Interfaces . . . 160
B.5.5 Equations . . . 162
B.5.6 Compressor map . . . 163
B.6 Turbine . . . 163
B.6.1 Introduction . . . 163
B.6.2 Model assumptions . . . 164
B.6.3 Parameters and variables . . . 164
B.6.4 Interfaces . . . 166
B.6.5 Equations . . . 166
B.7 Shaft . . . 167
B.7.1 Introduction . . . 167
B.7.2 Parameters and variables . . . 167
B.7.3 Interfaces . . . 168
B.7.4 Equations . . . 168
References . . . 168

Chapter 1

Introduction

1.1 Challenges in energy sector

The demand for energy is growing rapidly worldwide. The International Energy Agency (IEA) [2] predicts an average growth rate of 1.6% per annum for primary energy worldwide. The main contributions to the energy demand increase are population growth worldwide and industrialization of the fast-growing economies of the developing world. Every three years, the world's population is increasing by 300 million.

Figure 1.1 shows the prediction of energy demand and its production with respect to different fuels. Fossil fuels such as coal, oil and natural gas will remain the largest energy source, supplying about 85% of the world's primary energy needs. The dependency on natural gas as a primary energy source is going to increase in the coming decades. The stocks of fossil resources are finite. It is predicted that the mineral oil stocks will be exhausted around 2050 if we continue our present way of technology. Natural gas will last longer (some 75 years) and coal will last the longest (more than 200 years). Furthermore, the global warming problem is linked to the carbon emissions to atmosphere from using fossil fuels. Figure 1.2 shows the amounts of the carbon emissions from different fossil fuels during the period 1800-2000.

The following are the possible solutions to the challenges mentioned:

1. Increasing the efficiency of energy conversion

2. Using technology with low emissions

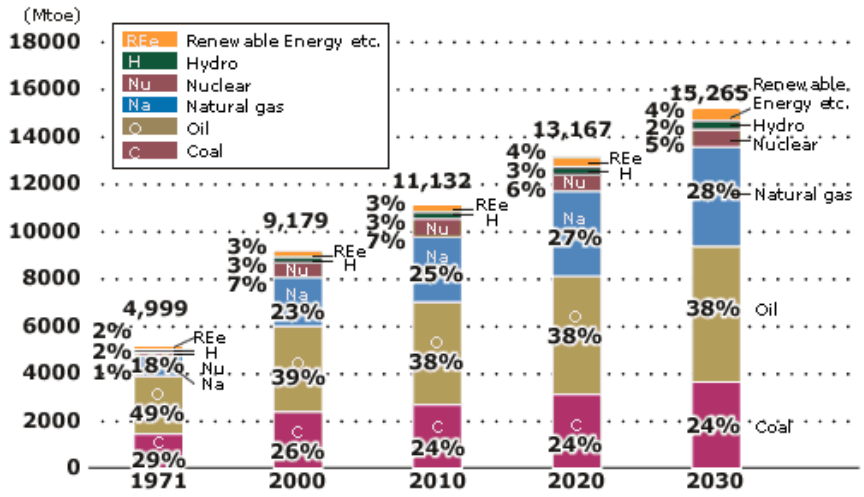

Figure 1.1: Prediction of energy demand and its production with respect to different fuels (Source: IEA/World Energy Outlook)

3. Using renewable energy sources

Around 41% of the energy demand increase is used for electricity generation and about 7% of the electricity produced is lost during the transmission and distribution as waste. Further, there is a lot of research going on to make the electric energy supply more sustainable. A common solution to all the problems mentioned above can be Distributed Generation (DG) which should use primary energy as efficiently as possible, with the least possible environmental impact whilst ensuring that energy supply is secure, safe and supplied at a competitive cost. Typically, the small scale generators connected at several entry points to the distribution grid are termed DG. The deregulation and unbundling of electricity markets in many countries worldwide bring new perspectives for small business specializing in energy generation. As yet, the distribution generation comprise a relatively small fraction of the total capacity; however, it is expected that in near future the situation will change in favour of DG. The efficiency of different technologies is given in Table 1.1.

Various technologies are being used in DG applications with variable degree of success. Among those are: wind turbines, small scale hydro power

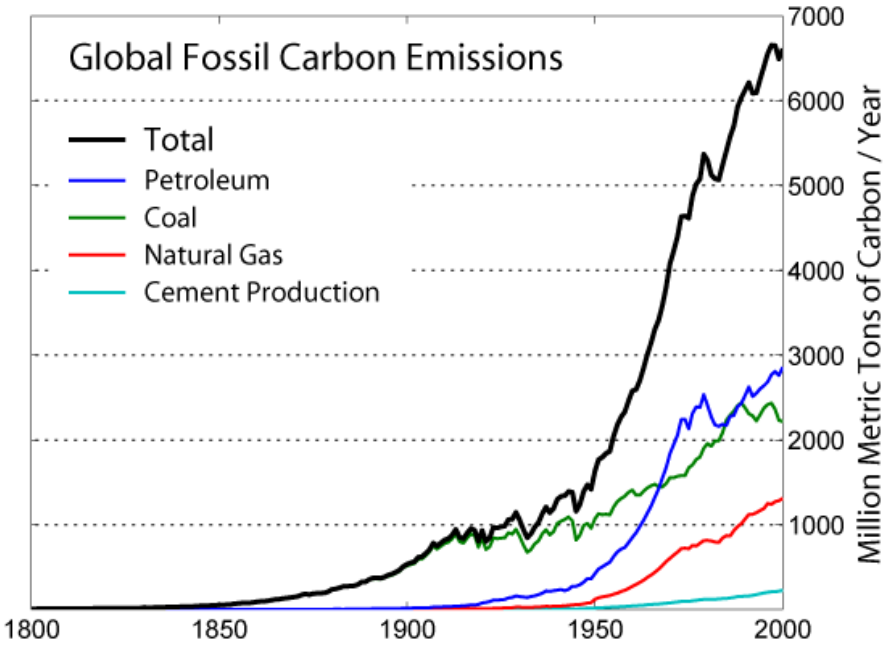

Figure 1.2: Global carbon emission by fuel type (Source: Carbon Dioxide Information Analysis Center)

Table 1.1: Power plant efficiencies of different systems

Technology	Efficiency
Fuel cell	40%-60%
Diesel engines	30%-50%
Steam and gas turbines	30%-60%
Otto motors	10%-40%

plants, biomass, micro turbines, and fuel cells. Recent advances in fuel cell technology significantly improved the technical and economical characteristics of this technology. Environmental friendliness, practically noise free operation and very high efficiency combined with the forecasted shift to gaseous fuels make fuel cells a very sound competitor on the future electricity markets. In addition it should be noted that fuel cell based generators possess other important properties such as compact size, modularity and controllability.

1.2 Fuel cells

A fuel cell is an electrochemical device that converts the chemical energy of a fuel directly into electrical energy [10]. Immediate conversion of the fuel to thermal and mechanical energy is not required. All fuel cells consist of two electrodes (anode and cathode) and an electrolyte. They operate much like a battery except that the reactants are not stored, but continuously fed to the cell. Unlike ordinary combustion, fuel (hydrogen-rich) and oxidant (typically air) are delivered to the fuel cell separately. The fuel and oxidant streams are separated by an electrode-electrolyte system. Fuel is fed to the anode (negative electrode) and an oxidant is fed to the cathode (positive electrode). Electrochemical oxidation and reduction reactions take place at the electrodes to produce electric current. The primary product of fuel cell reactions is water.

A single fuel cell produces less than one volt of electrical potential. To produce higher voltages, fuel cells are stacked on top of each other and connected in series. The number of cells in a stack depends on the desired power output and individual cell performance; stacks range in size from a few (less than 1 kW) to several hundred (250 plus kW).

Currently, there are at least six different fuel cell types in varying stages of development. In general, electrolyte and operating temperature differentiate the various cells. Listed in order of increasing operating temperature, the four fuel cell technologies currently being developed are listed in Table 1.2.

Advantages of fuel cells can be summarized as follows:

- Due to high efficiencies and lower fuel oxidation temperatures, fuel cells emit less carbon dioxide and nitrogen oxides per kilowatt of power generated.

Table 1.2: Fuel cell types

Fuel cell	Operating temperature
Proton exchange membrane fuel cell (PEMFC)	$80°C$
Phosphoric acid fuel cell (PAFC)	$200°C$
Molten carbonate fuel cell (MCFC)	$650°C$
Solid oxide fuel cell (SOFC)	$1000°C$

- Since fuel cells have no moving parts (except for the pumps, blowers etc. that are a necessary part of any power producing system), noise and vibration are practically nonexistent. Noise from a fuel cell power plant is as low as 55 dB. This makes them easier to site in urban or suburban locations. The lack of moving parts also makes for high reliability and low maintenance.

- Another advantage of fuel cells is that their efficiency is high at part-load conditions, unlike gas and steam turbines, fans and compressors.

- Fuel cells can use many different types of fuel such as natural gas, propane, landfill gas, diesel, methanol, and hydrogen. This versatility ensures that fuel cells will not become obsolete due to the unavailability of certain fuels.

Fuel cells can be seen as a key technology, enabling clean efficient production of power and heat from a range of power sources. In this work, Solid Oxide Fuel Cells (SOFC) will be focussed in particular in a hybrid configuration where it is combined with a gas turbine.

1.3 Solid Oxide Fuel Cell and hybrid system

The SOFC with its solid state components may in principle be constructed in any configuration. There are two different SOFC geometries being developed: tubular and planar. Tubular designs are more costly than planar geometry SOFCs. Both technologies are making headway, but the tubular design is closer to commercialization. Siemens Westinghouse, the leader in SOFC technology, is pursuing the tubular design since late 1950s. This tubular SOFC was demonstrated at user sites in a complete, operating fuel

cell power plant of nominal 25kW (40 kW maximum) capacity. However, the high costs for tubular designs have helped to stimulate research interest in SOFC planar technology. The tubular design is the most advanced and is designated for large commercial and industrial cogeneration applications and onsite power generation. The planar design will serve smaller markets (less than 300 kW).

SOFCs employ a solid state electrolyte and operate at the highest temperatures (1000°C) of all fuel cell types. The SOFC uses a solid yittra-stabilized zircona ceramic material as the electrolyte layer. In general, the solid phase design is simpler than PAFCs or MCFCs since it requires only two phases (gas-solid) for the charge transfer reactions at the electrolyte-electrode interface. The two phase contact simplifies the design because it eliminates corrosion and electrolyte management concerns commonly associated with the liquid electrolyte fuel cell. During operation, oxidant (usually air) enters the cathode compartment and after the electrode reaction, oxygen ions migrate through the electrolyte layer to the anode where hydrogen is oxidized. The operating temperature of SOFCs is sufficiently high to provide the necessary heat for the endothermic reforming reaction. SOFCs, therefore, are more tolerant of fuel impurities and can operate using hydrogen and carbon monoxide fuels directly at the anode. They don't require costly external reformers or catalysts to produce hydrogen. The relative insensitivity of SOFCs to gas contaminants normally considered "poisons" to lower temperature fuel cells makes them especially attractive for unconventional fuels such as biomass or coal gasification.

The exhaust heat from the SOFC is at very high temperatures (1000°C) and may be used in a bottoming cycle or recovered for the generation of steam for cogeneration purposes which further increases the efficiency. When integrated with a gas turbine (often denoted as SOFC-GTs or hybrid systems), SOFC systems are expected to achieve 70–75% electrical efficiency, representing a significant leap over all other energy technologies. Additionally, developers expect commercial SOFCs to have lifetimes of 10 to 20 years, two to four times longer than other fuel cells.

The disadvantage of the SOFCs high operating temperature is the stringent material requirement for the critical cell components. The materials selected for use in the SOFC are constrained by the chemical stability in oxidizing and/or reducing conditions, the conductivity and the thermo mechanical compatibility in high temperatures. Another restriction on the

cell components is that they must be capable of withstanding thermal cycling. Exotic ceramics, metal-ceramic composites, and high temperature alloys drive up the cost of SOFCs, as do the manufacturing techniques demanded by these materials. Because of the stringent materials requirement and demanding manufacturing techniques, developers are exploring ways to reduce the operating temperature of SOFCs to the 700-900°C range.

Unique among fuel cell types, SOFCs provide a nearly perfect match with small gas turbines. As mentioned, when integrated with these turbines, SOFCs can potentially obtain electrical efficiencies of 70% or greater. These performance and size characteristics give SOFC-GT system a large market potential if cost reduction targets can be obtained. The SOFC technology can span all of the traditional power generating markets (residential, commercial, industrial/onsite generation, and utility) but is likely to penetrate niche markets first, such as small portable generators and remote or premium power applications.

Due to the tight integration between the SOFC and the GT in a hybrid system, dynamic operability (and hence control) of the process is a challenge. It is important not only to design a good control system, but also to choose a process design that together with the appropriate control structure allows satisfying disturbance rejection and part load operation. To be able to design control structures and analyze dynamic behavior, it is very beneficial to have low complexity models of the components of the hybrid system. Such models are also valuable for online optimization. *An aim of this project is to develop a low complexity mechanistic SOFC-GT dynamic model which includes the relevant dynamics.* There are several dynamic, distributed SOFC models reported in the literature. For example, Achenbach [1] developed a three dimensional, dynamic, distributed model for a planar SOFC stack. Chan et al. [5, 4], Thorud et al. [14], Stiller et al. [13] and Magistri et al. [11] all developed distributed, dynamic tubular SOFC models for designs similar to that of Siemens Westinghouse, for use in hybrid systems. In this project, control-relevant models of all the components of the hybrid system are developed within the modular equation-based modeling environment gPROMS [7].

The main objectives of the control-relevant modeling are summarized below:

1. To perform simulations to get better understanding of the process dynamics

2. To design a good control structure which will perform the following tasks:

   (a) Control the total power from the hybrid system according to the need.

   (b) Control the SOFC temperature.

   (c) Make the system insensitive to disturbances.

   (d) Should be able to perform start up, shut down and load shedding operations effectively.

3. The simple models can be used in an online optimization control.

For any process, a control system is necessary to ensure the safe and reliable performance, for the SOFC-GT system this means reliable power generation. The power generation can be autonomous, without connecting the source system to an universal grid, or it can be connected to the grid. The autonomous power system makes the design of the control system more challenging as the control of power should match to the load demand at all times.

In this project, an autonomous power system is studied and a regulatory control structure is designed. As an autonomous power source, the hybrid system should deliver the power according to the load requirement. In doing so, it has to be operated at varying part-loads thereby inducing SOFC temperature changes. These temperature changes during fast dynamic operation may cause the SOFC material to degrade or even crack, if it is not controlled. Hence, these are important consideration when developing a control structure.

Monitoring and control often require the use of state estimator to compute online estimates of unmeasurable states, this may also apply to the SOFC-GT system. This is the motivation for including research in nonlinear state estimation as a part of this thesis.

1.4 Nonlinear state estimation

State estimation plays an important role in the process industries. It is the means to estimate the unmeasured information (and parameters) and/or to

filter noisy measurements. The Kalman Filter (KF) is the most commonly used state estimator for linear dynamic systems. It is the optimal (minimum mean square error) estimator, in the case of linear systems [8].

There are many uncertainties to deal with in process control; model uncertainties, measurement uncertainties and uncertainties in terms of different noise sources acting on the system. In this kind of environment, representing the model state by an (approximated) probability distribution function (pdf) has distinct advantages. State estimation is a means to propagate the pdf of the system states over time in some optimal way. It is most common to use the Gaussian pdf to represent the model state, process and measurement noises. The Gaussian pdf can be characterized by its mean and covariance.

All practical systems posses some degree of nonlinearity. Depending on the type of process and the operating region of the process, some processes can be approximated with a linear model and the KF can be used for state estimation. In some cases the linear approximation may not be accurate enough, and state estimator designs using nonlinear process models are necessary. The most common way of applying the KF to a nonlinear system is in the form of the Extended Kalman Filter (EKF). In the EKF, the nonlinear process is approximated by a linear model around the operating point at each time instant. In doing so, the EKF needs the Jacobian matrices which may be difficult to obtain for higher order systems, especially in the case of time-critical applications. Further, the linear approximation of the system at a given time instant may introduce errors in the state which may lead the state to diverge over time. In other words, the linear approximation may not be appropriate for some systems.

In order to overcome the drawbacks of the EKF, other nonlinear state estimators have been developed such as the Unscented Kalman Filter (UKF) [9], the Ensemble Kalman Filter (EnKF)[6] and high order EKFs. The EnKF is especially designed for large scale systems, for instance, oceanographic models and reservoir models [6]. The UKF seems to be a promising alternative for process control applications [12] [3]. The UKF propagates the pdf in a simple and effective way and it is accurate up to second order in estimating mean and covariance [9]. *The last part of the thesis is focused on using the UKF for nonlinear state estimation in process systems and the performance is evaluated in comparison with the EKF.* A simple method to incorporate state constraints in the UKF is introduced and tested.

1.5 Publications

The work herein has been reported in several papers and talks as listed below.

1.5.1 Journal articles

1. R. Kandepu, L. Imsland, B. Foss, C. Stiller, B. Thorud and O. Bolland, *Modeling and control of a SOFC-GT-based autonomous power system,* Energy, Volume 32, Issue 4, April 2007, Pages 406-417

2. R. Kandepu, L. Imsland, B. Foss, *Applying the Unscented Kalman Filter for Nonlinear State Estimation*, Accepted for publication in Journal of Process Control.

3. C. Stiller, B. Thorud, O. Bolland, R. Kandepu and L. Imsland , *Control strategy for a solid oxide fuel cell and gas turbine hybrid system*, Journal of Power Sources, Volume 158, Issue 1, 14 July 2006, Pages 303-315

1.5.2 Conferences

1. R. Kandepu, L. Imsland, B. A. Foss, C. Stiller, B. Thorud and O. Bolland, *Control-relevant SOFC modeling and model evaluation*, In proceedings of ECOS, Trondheim, Norway, 2005

2. R. Kandepu, L. Imsland, C. Stiller, B. A. Foss, *Control-relevant modeling and simulation of a SOFC-GT hybrid system*, In proceedings of The 46th conference on Simulation and Modeling (SIMS), Trondheim, Norway, October, 2005

3. R. Kandepu, B. A. Foss and L. Imsland, *Integrated modeling and control of a load connected SOFC-GT autonomous power system*, In proceedings of ACC, Minneapolis, June, 2006

4. R. Kandepu, L. Imsland, B. A. Foss, *Modeling and control of a SOFC-GT hybrid system with single shaft configuration*, In proceedings of ICEPAG, Newport beach, USA, September, 2006

5. R. Kandepu, B. Huang, B. A. Foss, L. Imsland, *State estimation of SOFC/GT hybrid system using UKF*, In proceedings of 8th International Symposium on Dynamics and Control of Process Systems (DYCOPS), Cancun, Mexico, June 6-8th, 2007

6. R. Kandepu, B. Huang, L. Imsland and B. A. Foss, *Comparative Study of State Estimation of Fuel Cell Hybrid System using UKF and EKF, Invited paper,* In proceedings of The Sixth IEEE Conference on Control and Automation (ICCA), Guangzhou, China, May30-June 1, 2007

7. R. Kandepu, L. Imsland, B. A. Foss, *Constrained State Estimation Using the Unscented Kalman Filter,* In preparation.

1.5.3 External Seminars

1. R. Kandepu, Talk at SOFC model benchmarking meeting, *Introduction to SOFC modeling and control*, 17-18, February, 2004, Lund, Sweden

2. R. Kandepu, L. Imsland and B. A. Foss, *Modeling and control of a SOFC/GT power plant*, 12th Nordic Process Control Workshop, 19-21, August 2004, Gothenburg, Sweden

3. R. Kandepu, L. Imsland and B. A. Foss, *Modeling and control of a SOFC-GT based autonomous power system*, 13th Nordic Process Control Workshop, 26-27, January 2006, DTU, Lyngby, Denmark

4. R. Kandepu, L. Imsland, B. A. Foss, *Modeling and control of a SOFC-GT based autonomous power system*, Presented to Thermochemical Power Group, University of Genoa, Genoa, Italy, May 18, 2006

5. R. Kandepu, L. Imsland, B. A. Foss, *Modeling and control of a SOFC-GT based autonomous power system*, Presented in a meeting with Alberta Research Council, Edmonton, Canada, July 9, 2006

1.5.4 Technical reports

1. R. Kandepu, *Modeling of SOFC-GT hybrid system components*, Technical report, 2004-9-W, Department of Engineering Cybernetics, NTNU, 2004

1.6 Overview of thesis

This thesis consists of an introductory part in which the thesis' work is put into perspective. It also gives an overview of the research which has been done. The second part consists of 4 chapters, each of them based on a conference or journal article. There will hence be some overlap in these chapters. Two additional papers are included in appendix A. Modeling details of different components are presented in appendix B.

1.6.1 Paper I: Modeling and control of a SOFC-GT-based autonomous power system

This article is published in Journal of Energy (R. Kandepu, L. Imsland, B. Foss, C. Stiller, B. Thorud and O. Bolland, *Modeling and control of a SOFC-GT-based autonomous power system,* Energy, Volume 32, Issue 4, April 2007, Pages 406-417).

This article describes the operational principle of the SOFC-GT hybrid system in detail. A control relevant model of the SOFC is developed using first principles, and the model is evaluated with a detailed model available. It is shown that the developed lumped model can be extended to capture the distributed nature of the variables. The comparison results show that the model developed capture the required dynamics very well and it is concluded that the developed model can be used to develop a control structure. The SOFC-GT hybrid system discussed in the article focusses on a double shaft configuration. All the models of the hybrid system are briefly described. A regulatory control structure is developed and simulation results are presented.

1.6.2 Paper II: Modeling and control of a SOFC-GT hybrid system with single shaft configuration

This article is presented at the ICEPAG conference, 2006 (R. Kandepu, L. Imsland, B. A. Foss, *Modeling and control of a SOFC-GT hybrid system with single shaft configuration*, In proceedings of ICEPAG, Newport beach, USA, September, 2006).

This article focusses on the SOFC-GT hybrid system with single shaft configuration. The work considers the development of a regulatory control

structure. A cascaded control structure is proposed and the simulation results are presented.

1.6.3 Paper III: State estimation of SOFC/GT hybrid system using UKF

This article is presented at the DYCOPS conference, 2007 (R. Kandepu, B. Huang, B. A. Foss, L. Imsland, *State estimation of SOFC/GT hybrid system using UKF*, In proceedings of 8th International Symposium on Dynamics and Control of Process Systems (DYCOPS), Cancun, Mexico, June 6-8th, 2007).

For monitoring and control purposes, state estimation plays an important role. As SOFC-GT is a nonlinear system and operated at variable part-load conditions, a nonlinear state estimator is necessary. The article focusses on designing a state estimator using the UKF. The results show that the UKF estimator performance is satisfactory.

1.6.4 Paper IV: Applying the Unscented Kalman Filter for Nonlinear State Estimation

This article is submitted for journal publication (R. Kandepu, L. Imsland, B. Foss, *Applying the Unscented Kalman Filter for Nonlinear State Estimation*, Submitted to Journal of Process Control.), and is an extended version of an invited paper presented at the ICCA conference, 2007 (R. Kandepu, B. Huang, L. Imsland and B. A. Foss, *Comparative Study of State Estimation of Fuel Cell Hybrid System using UKF and EKF*, *Invited paper,* In proceedings of The Sixth IEEE Conference on Control and Automation (ICCA), Guangzhou, China, May30-June 1, 2007).

In this article, the principles of the EKF and UKF for state estimation are presented and the differences of the two approaches are listed. Four rather different simulation cases are considered to compare the performance of the UKF and EKF. A simple procedure to include state constraints in the UKF is proposed and tested. The overall impression is that the performance of the UKF is better than the EKF in terms of robustness and speed of convergence. The computational load in applying the UKF is comparable to the EKF.

1.7 Contributions

The following are the main claimed contributions:

- Control relevant models for SOFC-GT power systems

  Control relevant models for SOFC-GT power systems are developed. In addition, the SOFC model developed is validated against a state of the art detailed model. Further, control structures are designed for two configurations of the power system.

- Applying the UKF for state estimation in process systems

  The UKF is applied for state estimation of the developed SOFC-GT power system. The UKF performance is compared with the EKF on different systems including the SOFC-GT power system. A constraint handling method is proposed in the UKF algorithm.

1.8 Conclusions

The SOFC-GT power system is a promising technology to overcome the energy challenges. In this project, a control relevant model of the complete power system is developed. The core of the system, the SOFC model is verified and it gave good results. A regulatory control structure is developed systematically by performing controllability analysis. The control structures are designed for two configurations of the SOFC-GT hybrid systems. Both the control structures give satisfactory results from the control point of view.

The second part of the thesis deals with nonlinear state estimation, which is important for monitoring and advanced control design purposes. The UKF state estimator is designed for the SOFC-GT hybrid system and it performs better than the standard EKF. The UKF is then applied to different available literature examples to test its performance and it performs consistently better than the EKF in terms of faster convergence, better nonlinear approximation and robustness to the model errors. A method is proposed to include state constraints in the UKF algorithm. The method is numerically efficient and shows promising performance. Finally, it is concluded that the UKF state estimator is an alternative to the EKF for nonlinear state estimation in process systems.

1.9 Directions for Further Work

The continuation of the work can summarized as below:

- The proposed control structure may be extended with an overall optimizer, e.g., based on Model Predictive Control.
- The proposed control structure may be extended in order to perform the start up, shut down and load shedding operations of the hybrid system.
- The theoretical aspects of the UKF; stability and convergence properties are may be studied.

References

[1] E. Achenbach. Three-dimensional and time-dependent simulation of a planar solid oxide fuel cell stack. *Journal of Power Sources*, 49:333–348, 1994.

[2] I. E. Agency. World energy outlook 2006, summary and conclusions. *http://www.worldenergyoutlook.org/summaries2006/English.pdf*, 2006.

[3] B. Akin, U. Orguner, and A. Ersak. State estimation of induction motor using unscented kalman filter. *IEEE Transactions on Control Applications*, 2:915–919, 2003.

[4] S. H. Chan, H. K. Ho, and Y. Tian. Modelling of a simple hybrid solid oxide fuel cell and gas turbine power plant. *Journal of Power Sources*, 109(1):111–120, 2002.

[5] S. H. Chan, H. K. Ho, and Y. Tian. Multi-level modeling of SOFC-gas turbine hybrid system. *International Journal of Hydrogen Energy*, 28(8):889–900, 2003.

[6] G. Evensen. *Data Assimilation, The Ensemble Kalman Filter*. Springer Berlin, 2007.

[7] gPROMS (2004). gPROMS introductory user guide. *Process Systems Enterprise Ltd.*, 2004.

[8] A. H. S. Jazwinski. Stochastic processes and filtering theory. *Mathematics in Science and Engineering*, 64, 1970.

[9] S. Julier and J. K. Uhlmann. Unscented filtering and nonlinear estimation. *Proceedings of the IEEE*, 92:401–422, 2004.

[10] J. Larminie and A. Dicks. *Fuel Cell Systems Explained*. Wiley, England, 2003.

[11] L. Magistri, F. Trasino, and P. Costamagna. Transient analysis of a Solid Oxide Fuel Cell hybrids part A: fuel cell models. *Journal of Power Sources*, 2004.

[12] A. Romanenko and J. A. A. M. Castro. The unscented filter as an alternative to the ekf for nonlinear state estimation: a simulation case study. *Computer and Chemical Engineering*, 28:347–355, 2004.

[13] C. Stiller, B. Thorud, S. Seljebø, O. Mathisen, H. Karoliussen, and O. Bolland. Finite-volume modeling and hybrid-cycle performance of planar and tubular solid oxide fuel cells. *Journal of Power Sources*, 141:227–240, 2005.

[14] B. Thorud, C. Stiller, T. Weydahl, O. Bolland, and H. Karoliussen. Part-load and load change simulation of tubular SOFC systems. *Proceedings of Fuel Cell Forum, Lucerne, 28 June-2 July*, 2004.

Chapter 2

Modeling and control of a SOFC-GT based autonomous power system

Abstract

In this article, a dynamic, lumped model of a Solide Oxide Fuel Cell (SOFC) is described, as a step towards developing control relevant models for a SOFC combined with a gas turbine (GT) in an autonomous power system. The model is evaluated against a distributed dynamic tubular SOFC model. The simulation results confirm that the simple model is able to capture the important dynamics of the SOFC and hence it is concluded that the simple model can be used for control and operability studies of the hybrid system. Several such lumped models can be aggregated to approximate the distributed nature of important variables of the SOFC. Further, models of all other components of a SOFC-GT based autonomous power system are developed and a control structure for the total system is developed. The controller provides satisfactory performance for load changes at the cost of efficiency.

2.1 Introduction

In the foreseeable future, fossil fuels including natural gas will be a major source of energy. With today's increasing concern about global warming and climate change, there is an incentive to investigate natural gas power processes that operate efficiently, thus emitting less per kWh produced, and also power production processes with CO_2 capture capabilities. It is widely accepted that fuel cells are power sources that will become increasingly important, due to high efficiency, low levels of pollution and noise, and high reliability. One of the most promising fuel cell technologies is the Solid Oxide Fuel Cell (SOFC), due to its solid state design and internal reforming of gaseous fuels, in addition to its high efficiency [8]. The SOFC converts the chemical energy of a fuel directly to electrical energy. The electrical efficiency of a SOFC can reach 55%. Another significant advantage of the SOFC is that since it operates at high temperature and its efficiency increases when pressurized, it naturally lends itself as a heat source for a gas turbine (GT) cycle. The combined (hybrid) cycle can theoretically have an overall electrical efficiency of up to 70% with a power range from a few hundred kWs to a few MWs [8]. Processes based on SOFCs can be used as power processes with CO_2 capture, since the "used fuel" (including water and CO_2) and air exit streams can be kept separated [7]. The main applications of the hybrid system include remote area power supply and distributed power generation.

There are several models available in the literature for SOFC-GT hybrid systems [10],[2],[13],[23]. In [4], a dynamic model of a grid connected SOFC model is developed. However, to the best of authors' knowledge there is no model in the literature with integration of a SOFC-GT hybrid system with a power grid and an electrical load. The reason for developing such an integrated model is to obtain a comprehensive understanding of the operability of the system which has close dynamic interactions between the power generation system and the local grid. Further, the hybrid system consists of tightly integrated dynamic subsystems with strict operating criteria making the control design more challenging in terms of disturbance rejection, part-load operation and in particular start-up, shutdown and load shedding. Suitable system actuation must be chosen, good control structures must be devised, and good controllers must be designed. As a basis for all these tasks, control relevant models must be developed for the subsystems, and for the total system. Such models should have limited complexity to allow for

the necessary analysis, while at the same time should include the important dynamic interactions.

In this paper we present an integrated model of a SOFC-GT hybrid system with a power grid connecting to an electrical load. A control relevant model of the SOFC is developed with no geometric regard and it is evaluated with a detailed model. Further models of all other components of the power system are described including the main underlying assumptions. The system model is subsequently used to perform analysis of system dynamics. A simple control design is proposed and assessed through a set of simulation scenarios.

2.2 Process description

A schematic diagram of the integrated system where the SOFC-GT hybrid system is connected to the load by a bus bar is shown in Figure 2.1. Methane (fuel) is mixed with a part of the anode flue gas and is partially steam reformed in a pre-reformer generating hydrogen. The heat required for endothermic reformation reactions in the pre-reformer is supplied from the SOFC stack through radiation. The gas mixture from the pre-reformer is fed to the anode volume of the SOFC, where the remaining part of the methane is reformed. Compressed atmospheric air is heated in a recuperative heat exchanger and is used as an oxygen source at the cathode side of the SOFC. In the SOFC, electrochemical reactions take place and DC electric power is produced. The rate of the electrochemical reactions depends on the current. A part of the anode flue gas is recycled to supply steam to the pre-reformer. The remaining part of the anode and cathode flue gases is supplied to a combustion chamber where the unused fuel is combusted. In a CO_2 capture setting, mixing of the anode and cathode flue gases should be avoided, but this is not treated herein.

The hybrid system is modeled using both single-shaft and double-shaft configurations. We will however focus on the double-shaft configuration in the simulations as in Figure 2.1. The combusted gas mixture is expanded in a high pressure turbine (HPT) with variable shaft speed driving the compressor. The HPT flue gas is further expanded to atmospheric pressure in a low pressure turbine (LPT) with constant shaft speed, which is coupled to a synchronous generator producing AC electric power. The expanded gas

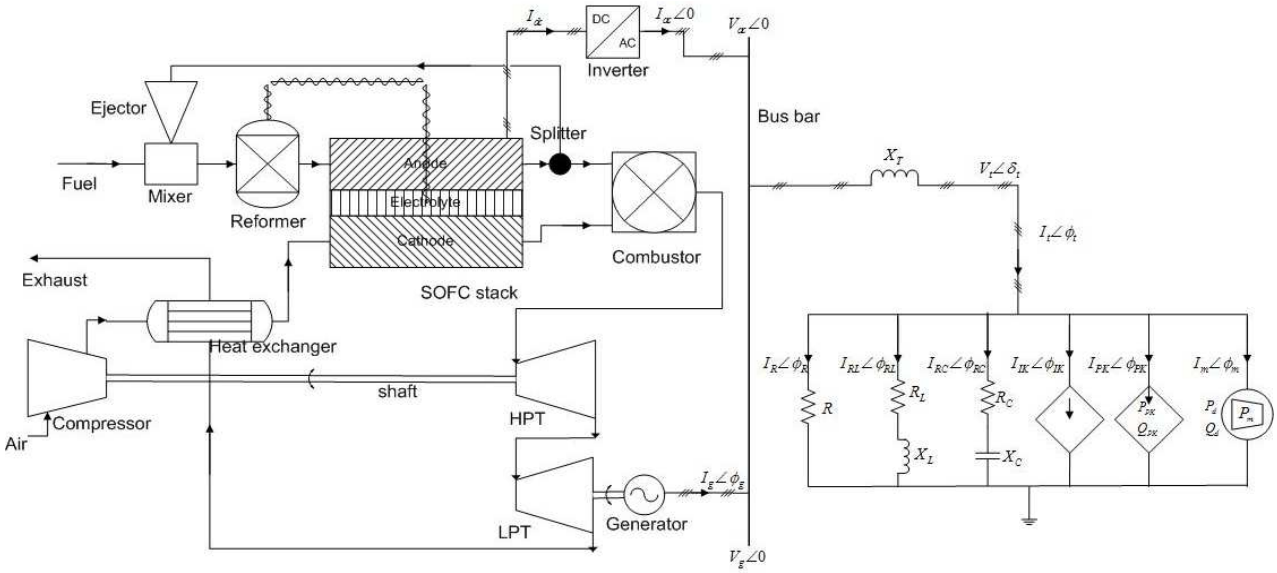

Figure 2.1: SOFC-GT hybrid system integrated with autonomous power system

mixture is used to heat up the compressed air in a heat exchanger. The DC power from the SOFC stack is fed to an inverter which converts DC to AC with a fixed frequency. The inverter and the generator are connected to a local grid, which is connected to a electric load. Both the SOFC stack and the generator supply the electric load demand on the grid. The load sharing between the SOFC stack and the generator cannot be controlled when there is a load change on the grid, even though the load sharing between the SOFC stack and the generator will change. Typically 60-70% of the total power is supplied by the SOFC stack.

2.3 SOFC modeling

2.3.1 SOFC process description

The SOFC is a device which converts chemical energy of a fuel directly into electrical energy [8]. The basic components of the SOFC are anode, cathode and electrolyte as conceptually illustrated in Figure 2.2. Fuel is supplied

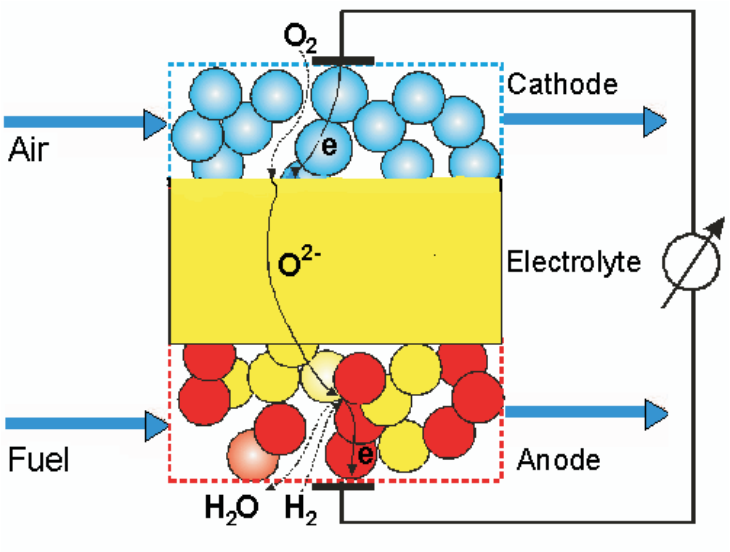

Figure 2.2: SOFC operation

to the anode and air is supplied to the cathode. At the cathode-electrolyte interface, oxygen molecules accept electrons coming from the external circuit to form oxide ions, see Table B.3 for reactions. The electrolyte layer allows only oxide ions to pass through and at the anode-electrolyte interface, hydrogen molecules present in the fuel react with oxide ions to form steam, and electrons get released. These electrons pass through the external circuit and reach the cathode-electrolyte layer, and thus the circuit is closed.

To increase the amount of power generated, a number of cells can be connected in series/parallel. This is known as stacking of cells. Also, there are mainly two types of SOFCs depending on the cell geometry; tubular and planar. The operating pressure can be from one bar to 15 bars. It is found that SOFCs show enhanced performance with increasing cell pressure [8]. The operating temperature of the SOFC is around 800-1000$°C$. The high temperature and pressure operating conditions of the SOFC make it advantageous to combine the SOFC with a gas turbine (GT) to get a hybrid system with an high efficiency [13]. Due to the high operating temperature, several types of fuels can be used. In this paper methane is used as fuel. Because of the electrochemical reactions, there is a production of steam, and partial recirculation of this steam is used to reform methane into hydrogen.

Table 2.1: Reactions at anode and cathode

Anode reaction	Reaction rate (r_j^{an})
H_2+O^{2-}→ $H_2O + 2e^-$	r_1^{an}
CH_4+H_2O ⇔ $CO + 3H_2$	r_2^{an}
$CO + H_2O$ ⇔ CO_2+H_2	r_3^{an}
CH_4+$2H_2O$ ⇔ CO_2+$4H_2$	r_4^{an}
Cathode reaction	Reaction rate (r_j^{an})
$\frac{1}{2}O_2$+$2e^-$→ O^{2-}	r_1^{ca}

Table 2.2: Notation for components

i	1	2	3	4	5	6	7
comp.	N_2	O_2	H_2	CH_4	H_2O	CO	CO_2

Typically, one third of the fuel is reformed, for example in a pre-reformer, before it enters the SOFC and the remaining part is reformed within the SOFC. Table B.3 gives the list of reactions that take place at anode and cathode and the corresponding reaction rates notation.

The dynamic model of a single SOFC is developed using two mass balances; one for anode volume and the other for cathode volume, and one overall energy balance. In all of the streams from/to the SOFC, the following components can be present; Nitrogen (N_2), Oxygen (O_2), Hydrogen (H_2), Methane (CH_4), Steam (H_2O), Carbonmonoxide (CO), and Carbondioxide (CO_2). A number, as shown in Table 2.2, is assigned to each of these components to simplify the notation.

2.3.2 Model assumptions

The following main assumptions are made in developing the model.

1. All the physical variables are assumed to be uniform over one SOFC, resulting in a lumped cell model.

2. There is sufficient turbulence and diffusion within the anode and the cathode for perfect mixing to occur (CSTR).

3. The gas temperatures within the SOFC are assumed to be the same as the solid; i.e. the thermal inertia of the gases is neglected.

4. For the energy balance, pressure changes within the SOFC are neglected.

5. All gases are assumed to be ideal.

6. All cells in the stack are assumed to operate identically.

2.3.3 Mass balance

Two mass balances; one for the anode volume and one for the cathode volume are used:

$$\frac{dN_i^{an}}{dt} = \dot{N}_i^{in,an} - \dot{N}_i^{out,an} + \sum_{j=1}^{n_{rx}^{an}} a_{ij}^{an} r_j^{an}, \quad i = 1, ..., 7, \quad n_{rx}^{an} = 4$$

$$\frac{dN_i^{ca}}{dt} = \dot{N}_i^{in,ca} - \dot{N}_i^{out,ca} + \sum_{j=1}^{n_{rx}^{ca}} a_{ij}^{ca} r_j^{ca}, \quad i = 1, ..., 7, \quad n_{rx}^{ca} = 1$$

The reaction rates corresponding to the electrochemical reactions (r_1^{ca}, r_1^{an}) are directly related by the current,

$$r_1^{an} = I/(2F) = r_1^{ca} \tag{2.1}$$

and the reaction rates corresponding to the reforming reactions are calculated as proposed by Xu [25]

$$\begin{aligned} r_2^{an} &= \frac{k_2}{p_{H_2}^{an\,2.5}} \left(p_{CH_4}^{an} p_{H_2O}^{an} - \frac{p_{H_2}^{an\,3} p_{CO}^{an}}{K_2} \right) /(DEN)^2 \\ r_3^{an} &= \frac{k_3}{p_{H_2}^{an}} \left(p_{CO}^{an} p_{H_2O}^{an} - \frac{p_{H_2}^{an} p_{CO_2}^{an}}{K_3} \right) /(DEN)^2 \\ r_4^{an} &= \frac{k_4}{p_{H_2}^{an\,3.5}} \left(p_{CH_4}^{an} p_{H_2O}^{an\,2} - \frac{p_{H_2}^{an\,4} p_{CO_2}^{an}}{K_4} \right) /(DEN)^2 \end{aligned} \tag{2.2}$$

In (B.6), DEN is given by

$$DEN = 1 + K_{CO}^{ads} p_{CO}^{an} + K_{H_2}^{ads} p_{H_2}^{an} + K_{CH_4}^{ads} p_{CH_4}^{an} + K_{H_2O}^{ads} p_{H_2O}^{an} / p_{H_2}^{an} \tag{2.3}$$

and k_2, k_3 and k_4, the rate coefficients for the reforming reactions, are calculated by

$$k_j = A_{kj} \exp(\frac{-E_j}{RT}), \qquad j = 2, 3, 4 \tag{2.4}$$

The equilibrium constants for the reforming reactions K_2, K_3 and K_4 are given by

$$\begin{aligned} K_2 &= \exp(-26830/T + 30.114) \qquad [bar^2] \\ K_3 &= \exp(4400/T - 4.036) \qquad\quad [-\ ] \\ K_4 &= \exp(-22430/T + 26.078) \qquad [bar^2] \end{aligned} \tag{2.5}$$

In (B.7), $K_{CO}^{ads}, K_{H_2}^{ads}, K_{CH_4}^{ads}$ and $K_{H_2O}^{ads}$ are the adsorption constants, which are calculated by

$$K_i^{ads} = A_{K^{ads}i} \exp(\frac{-\Delta\overline{h}_i^{ads}}{RT}), \quad i = H_2, CH_4, H_2O, CO \tag{2.6}$$

It is assumed that the exhaust flows at the anode and cathode outlets can be described by the choked exhaust flow equation. This means that the mass flow rate of the exhaust flow at the anode (cathode) depends on the pressure difference between the pressure inside the anode (cathode) and the pressure at the outlet [14]:

$$\begin{aligned} \dot{m}_{out,an} &= \sqrt{k_{an}(p_{an} - p_{out,an})} \\ \dot{m}_{out,ca} &= \sqrt{k_{ca}(p_{ca} - p_{out,ca})} \end{aligned} \tag{2.7}$$

The partial pressures, volume, and temperature are assumed to be related by the ideal gas equation, for instance at the anode,

$$p_i^{an} V_{an} = N_i^{an} RT \tag{2.8}$$

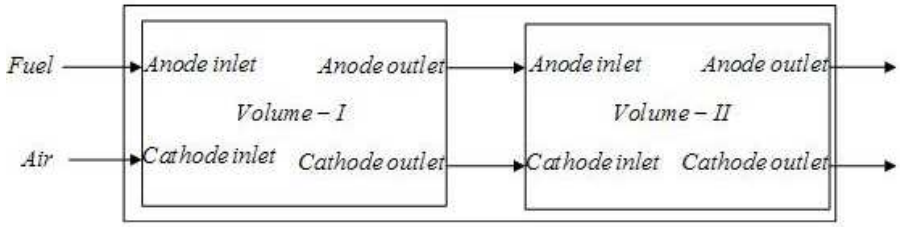

Figure 2.3: Aggregation mechanically

2.3.4 Energy balance

The energy balance accounts for the whole SOFC volume, and is given by [21][9]:

$$C^s \frac{dT}{dt} = \sum_{i=1}^{N} \dot{N}_i^{in,an}(\Delta\overline{h}_i^{in,an} - \Delta\overline{h}_i) + \sum_{i=1}^{N}(\dot{N}_i^{in,ca}(\Delta\overline{h}_i^{in,ca} - \Delta\overline{h}_i) \qquad (2.9)$$
$$- \sum_{j=1}^{M} \Delta\overline{h}_j^{rx} r_j^{an} - P_{DC} - P_{rad} - P_{cond}$$

In this equation, the dynamics of the temperature changes of gases are neglected as they are fast compared to the temperature changes of the solid. Hence the energy balance gives a dynamic equation for the temperature changes of the SOFC solid.

In (B.15), P_{DC} represents the amount of DC power produced by the SOFC, P_{cond} represents the conduction heat loss from SOFC to the surroundings and P_{rad} represents the amount of radiation heat given from the SOFC. As the SOFC operating temperature is higher than that of the surroundings, there is always some loss due to radiation. It can be calculated by [6]

$$P_{rad} = A\delta\varepsilon\sigma(T^4 - T_{sur}^4) \qquad (2.10)$$

In (B.16), A is the surface area, δ is shaping factor, T_{sur} represents the surroundings temperature, ε is the emissivity of the SOFC surface and σ is the *Stefan-Boltzmann constant* ($\sigma = 5.67 \times 10^{-8}\mathrm{W/(m^2.K^4)}$).

The amount of DC power from the SOFC is given by

$$P_{DC} = VI \qquad (2.11)$$

Moreover, Air Utilization (AU) and Fuel Utilization (FU) are defined as

$$\text{AU} = 1 - \frac{\dot{N}_{O_2}^{out}}{\dot{N}_{O_2}^{in}}, \quad \text{FU} \ = 1 - \frac{\dot{N}_{H_2}^{out}}{\dot{N}_{H_2}^{in}}. \tag{2.12}$$

The AU and FU are included in the model as they are identified as important variables in representing the SOFC state [23]. Recycle ratio is defined as the ratio of the fuel flow recycled to the fuel flow at the anode outlet.

2.3.5 Voltage

The operating cell voltage is given by

$$V = E^{OCV} - V_{loss} \tag{2.13}$$

where the open circuit voltage of the cell is given by the *Nernst equation* [8],

$$E^{OCV} = E^o + \frac{RT}{2F} \ln \left(\frac{p_{H_2}^{an} {p_{O_2}^{an}}^{0.5}}{p_{H_2O}^{an}} \right) \tag{2.14}$$

where E^o is the EMF at standard pressure. V_{loss} is the voltage loss. Stiller et al. [20], Thorud et al. [23], Campanari et al. [1], and Magistri et al. [11] used rather complex empirical functions to calculate the voltage loss. In this simple model the voltage loss is approximated by a first order function of cell temperature and current. This function is obtained by curve fitting the simulated data obtained from a distributed model [23]. Thus total voltage loss is calculated by

$$V_{loss} = C_1 I + C_2 T + C_3 \tag{2.15}$$

where C_1, C_2 and C_3 are constants.

2.3.6 Model aggregation

In a real SOFC, temperature and pressure vary over the SOFC volume. The distributed nature cannot be represented by using the "one volume" model. By connecting many volumes in a sequential manner it is possible to approximate the distributed nature of the variables. The whole structure with all the volumes represent a single cell. So, if many volumes are connected,

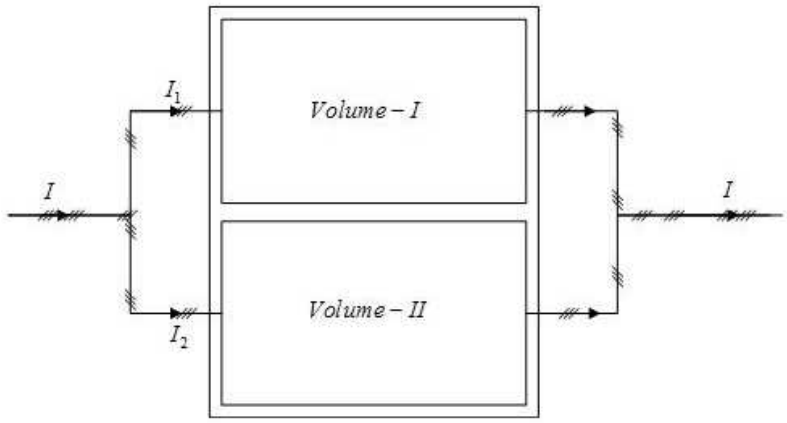

Figure 2.4: Electrical aggregation

each volume can be represented by a scaled-down model. In principle, it is possible to connect any number of volumes, but for simplification, an example is considered where a single SOFC model is obtained by connecting two scaled-down models as shown in Figure B.3. The two volumes are selected such that the first volume is represented by a scaled-down model by scaling down the "one volume" model volume and heat capacity constants by α where $0 < \alpha < 1$ and typically $\alpha = 1/3$. The second volume is represented by a scaled-down model obtained by scaling down the "one volume" model constants by $1-\alpha$. Electrically, the two scaled-down models are connected in parallel (Figure B.4). Ideally, the voltage across each of the volumes should be the same and the total current is divided between the two volumes. Then most of the current is produced from the second volume, as mainly reforming reactions take place in the first volume. In the present work it is assumed that the first volume supplies 1/3rd of the total current and the second volume supplies the remaining current. With this assumption, there is a small voltage difference between the two volumes. Developing a strategy for dividing the currents among the volumes when a SOFC is represented by many volumes is a part of further work. The basic point is to show that it is possible to approximate the distributed nature of the variables by aggregating the scaled-down models.

2.4 Power system modeling

2.4.1 Pre-reformer

A pre-reformer is used to convert methane into hydrogen by steam reforming. It is a fixed volume reactor having two inlets, one for methane and the other for steam and one outlet. The assumptions made in the model development of the pre-reformer are the same as those of the SOFC. The dynamic model is developed using one mass balance and one energy balance. The three reformation reactions considered are given in Table B.3. The reformation is a highly endothermic process, so heat must to be supplied to the reactor. As the SOFC operates at a high temperature, there is radiation from the SOFC stack and this can be supplied to the pre-reformer by using a suitable mechanical design. The operating temperature of the reactor is in the range $500°C - 700°C$.

2.4.2 Heat exchanger

A very simple model of a counter-flow heat exchanger is used, in which the amount of the heat exchanged depends on the heat transfer coefficient of the exchanger wall and also on the average temperature difference between the hot and cold streams. A first order transfer function describes the dynamics of the temperatures of both the streams. The following assumptions were made,

1. The model is lumped. All the physical parameters are assumed to be uniform over the heat exchanger.

2. There is no pressure loss within the heat exchanger.

2.4.3 Combustion chamber

The combustion chamber as shown in Figure 2.1, has 2 inlet streams and one outlet stream. It burns the fuel coming from all the inlet flows in the presence of air. The operating conditions will always be such that there is surplus oxygen available for complete combustion due to the fact that air mass flow rate is much larger than the fuel mass flow rate. In this model,

the fuel can be methane, hydrogen or carbonmonoxide or a mixture of these fuels. The following reactions are being considered during the combustion.

$$\begin{aligned} 2H_2 + O_2 &\rightarrow 2H_2O \\ CH_4 + 2O_2 &\rightarrow 2H_2O + CO_2 \\ 2CO + O_2 &\rightarrow 2CO_2 \end{aligned} \tag{2.16}$$

The following assumptions are made:

1. The pressures of all the inlet flows are the same.
2. As the combustion process is very rapid, it is modeled as an instantaneous process and complete combustion is assumed.
3. The model is a bulk model, i.e. all physical variables are assumed to be uniform over the combustion chamber.
4. There is a 2% pressure loss in the combustor volume.

The following mass and energy balances are used for the control volume:

$$\sum_{k=1}^{n_{in}} \dot{N}_i^{in,k} + \sum_{j=1}^{n_{rx}} a_{ij} r_j = \dot{N}_i^{out}, \quad i = 1...7, \; n_{rx} = 3$$

$$\sum_{k=1}^{n_{in}} \sum_{i=1}^{N} (\dot{N}_i^{in,k} \Delta\overline{h}_i^{in,k} - \sum_{i=1}^{N} \dot{N}_i^{in,k} \Delta\overline{h}_i) - \sum_{j=1}^{M_c} \Delta\overline{h}_j^{rx} r_j = 0$$

where $N = 7$ is the number of components, $M_c = 3$ is the number of reactions as given in (B.36) and n_{in} is the number of inlet streams. Otherwise, the notation is similar to (B.15).

2.4.4 Gas turbine

Compressor and turbine models are based on steady state performance map characteristics [18]. The map is modeled using polynomials of 4th and 5th order for reduced mass flow, pressure and efficiency as functions of reduced shaft speed and operation line. The following are the assumptions made in both the compressor and turbine models:

1. The process has constant isentropic efficiency.

2. The working fluid satisfies the ideal gas equation.

A shaft model accounts for the dynamics of the rotating mass in the gas turbine system which is modeled as

$$\dot{\omega} = P_b/(I\omega) \tag{2.17}$$

where P_b is the power balance across the shaft, I is the moment of inertia of the rotating mass and, ω is the angular velocity of the shaft.

2.4.5 Inverter

A simple model of an inverter is developed with the following assumptions:

1. Power loss is negligible.

2. Pulse Width Modulation (PWM) technique is used to control the AC output voltage and frequency. The controller dynamics are neglected as they are fast compared to the hybrid system dynamics.

3. The inverter supplies AC power at unity power factor.

The power balance on both sides is given by

$$P_{dc} = V_{ac}I_{ac}. \tag{2.18}$$

2.4.6 Synchronous generator

The per-phase equivalent circuit of the synchronous generator is shown in Figure 2.5 taken from [24]. The magnitude of the electro-motive force (EMF) induced in each phase is assumed to be directly proportional to the shaft speed (ω_g) and field current (I_{fg}),

$$E_g = k_g I_{fg} \omega_g \tag{2.19}$$

where k_g is the proportionality constant. The open circuit voltage $V_g\angle 0$, which is taken as the reference in phasor notation, and $E_g\angle\delta_g$ are related as

$$E_g\angle\delta_g = V_g\angle 0 + X_g\angle 90^\circ I_g\angle\phi_g \tag{2.20}$$

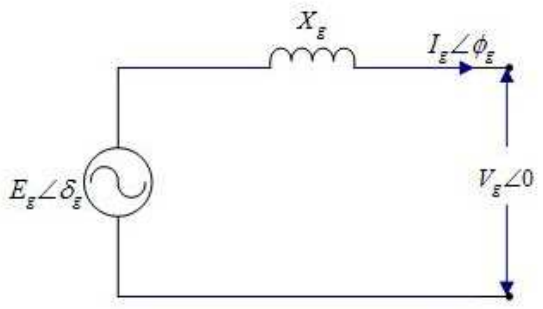

Figure 2.5: Per-phase equivalent circuit of synchronous generator

where $I_g\angle\phi_g$ is the generator current, X_g is the stator per-phase reactance in ohms. It is assumed that there is a 2% power loss in conversion from mechanical to electrical energy which includes rotational loss, copper loss and magnetizing loss. The generator is connected to a power turbine which runs at a constant speed. Hence the frequency of the AC supply from the generator is assumed constant. The real and reactive powers supplied by the generator are given by

$$\begin{aligned} P_g &= V_g I_g \cos\phi_g \\ Q_g &= V_g I_g \sin\phi_g. \end{aligned} \tag{2.21}$$

2.4.7 Autonomous power grid

The integrated SOFC-GT hybrid system with the autonomous power grid is shown in Figure 2.1 [4]. The model of the grid and load is chosen such that the level of complexity is comparable to the SOFC-GT hybrid system models. The bus bar voltage is fixed at $230V$ and is taken as the reference in phasor notation. We assume that the generator field current is controlled such that the generator terminal voltage $V_g\angle 0$ equal to the bus bar voltage $V_{ac}\angle 0$. The bus bar is connected to the load by transmission lines of reactance X_T. The load is represented by six parallel branches with different components in each branch as shown in Figure 2.1. It is categorized into 4 types of loads; constant impedance, constant current, constant power and induction motor load. The constant impedance, constant current and constant power load represent the residential loads such as lights, water heaters, ovens etc. The induction

motor load is considered to represent an industrial load [12]. The constant impedance load is represented by the first three branches with resistive, inductive and capacitive loads. The fourth and fifth branches represent the constant current and constant power loads respectively. The sixth branch represents the induction motor load. The total load current $I_t\angle\phi_t$ is the sum of the currents from the inverter and the synchronous generator,

$$I_t\angle\phi_t = I_{ac}\angle 0 + I_g\angle\phi_g. \tag{2.22}$$

As it is assumed that the inverter supplies power at unity power factor, the generator supplies the load and transmission line reactive power. The load voltage $V_t\angle\delta_t$ is given by

$$V_t\angle\delta_t = V_{ac}\angle 0 - X_T\angle 90^\circ I_t\angle\phi_t. \tag{2.23}$$

The first three branches of the load (R, RL, RC branches) are used to model different constant impedance loads. The currents in these branches are given by

$$\begin{aligned} V_t\angle\delta_t &= RI_R\angle\phi_R \\ V_t\angle\delta_t &= (R_L + X_L\angle 90^\circ)I_{RL}\angle\phi_{RL} \\ V_t\angle\delta_t &= (R_C - X_C\angle 90^\circ)I_{RC}\angle\phi_{RC}. \end{aligned} \tag{2.24}$$

The fourth branch is used to model constant current loads where the current $I_{IK}\angle\phi_{IK}$ is assigned a constant value. The fifth branch is used to model constant power loads where real and reactive powers (P_{PK},Q_{PK}) are assigned constant values and the current $I_{PK}\angle\phi_{PK}$ is calculated by

$$\begin{aligned} P_{PK} &= V_t I_{PK}\cos(\phi_{PK} - \delta_t) \\ Q_{PK} &= V_t I_{PK}\sin(\phi_{PK} - \delta_t). \end{aligned} \tag{2.25}$$

The last branch is used to model induction motor, whose equivalent circuit is shown in Figure 2.6 [5]. Assuming the magnetizing inductance is large, i.e. $X_M \to \infty$, the magnetizing current $I_M\angle\phi_M$ is neglected [5]. The induction

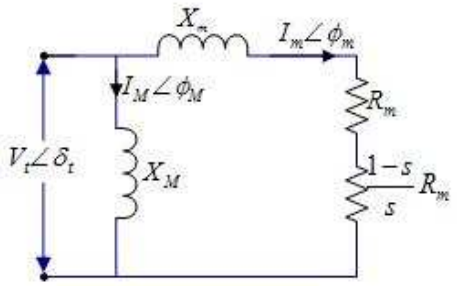

Figure 2.6: Equivalent circuit of induction motor

motor model equations are then given by,

$$\begin{aligned} \frac{ds}{dt} &= \frac{1}{I\omega_o^2}\left(\frac{P_m}{1-s} - P_d\right) \\ V_t\angle\delta_t &= (\frac{R_m}{s} + X_m\angle 90^\circ)I_m\angle\phi_m \\ P_d &= V_t I_m \cos(\phi_m - \delta_t) \\ Q_d &= V_t I_m \sin(\phi_m - \delta_t) \end{aligned} \tag{2.26}$$

where I is moment of inertia of induction motor, ω_o is stator frequency, P_m is mechanical load power on the induction motor, P_d and Q_d are real and reactive power from induction motor, and s is slip given by $s = \frac{\omega_o - \omega_m}{\omega_m}$ where ω_m is induction motor speed.

All the components of the hybrid system and the autonomous power system are modeled in the modular modeling environment gPROMS [3]. The detailed modeling of each component of the system can be found in appendix B.

2.5 SOFC model evaluation

As no experimental data is available to the authors for evaluating the simple model, the model is evaluated with an available detailed model. The detailed model [23] [17] [18] [22] is a quasi two-dimensional dynamic model of a SOFC tube, similar to that of Siemens Westinghouse. It is a discretized model where gas flows are treated as 1D plug flows. The solid structures

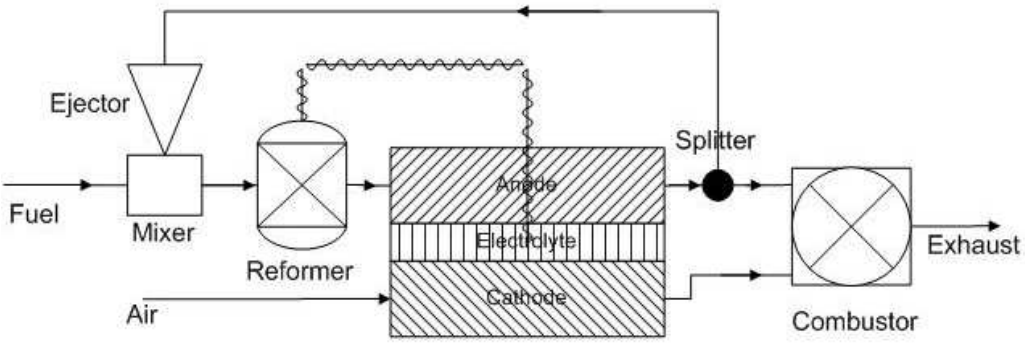

Figure 2.7: SOFC system

Table 2.3: Model parameters

Anode volume	$1.032\times10^{-5}\mathrm{m}^3$
Cathode volume	$4.3\times10^{-5}\mathrm{m}^3$
C^s	800J/K
k_{an}	$1.9\times10^{-3}\mathrm{kg}^2\mathrm{s}^{-2}\mathrm{Pa}^{-1}$
k_{ca}	$4.2\times10^{-3}\mathrm{kg}^2\mathrm{s}^{-2}\mathrm{Pa}^{-1}$

are modeled by a 2D discretization scheme in the axial and radial direction, neglecting effects in the circumferential direction. Both the simple and the detailed models are developed using gPROMS [3]. The detailed model includes about 1300 differential equations, where as the simple model it has 15 differential equations.

To evaluate the SOFC model a part of the system shown in Figure 2.1, as shown in Figure 2.7 is simulated. The results are compared to the detailed model in [23]. The simulations are performed in such a way that the same input conditions are applied to the two SOFC models. The values of some key parameters of the simple model are given in Table 2.3 while the values of some important variables at steady state are given in Table 2.4. Table 2.5 shows the simulation scenarios used for comparing the dynamic behavior of the two models.

Simulations are made for two comparison schemes; first, the simple SOFC model with one volume is compared to the distributed tubular SOFC model [23], and second, the simple SOFC with two volumes is compared to the dis-

Table 2.4: Steady state values

Methane flow rate	4.50×10^{-4}kg/s
Methane inlet temperature	950K
Air flow rate	1.44×10^{-2}kg/s
Air inlet temperature	950K
Current	250A
Anode pressure	3bar
Cathode pressure	3bar
Cell voltage	0.56V
Cell power	141W
Cell temperature	1113K
Air utilization	0.21
Fuel utilization	0.7

Table 2.5: Simulation details

Time(min)	Disturbance
90	Fuel flow is decreased by 20%
180	Fuel flow is increased back to 100%
270	Air flow is decreased by 20%
360	Air flow is increased back to 100%
450	Current is decreased by 20%
540	Current is increased back to 100%

tributed tubular SOFC model. SOFC mean solid temperature, cell voltage and cell power of the simple model and the detailed model are compared in each comparison scheme. Figures 2.8-2.10 show simulation results from the two comparison schemes.

2.5.1 Discussion

One volume SOFC model

Figure 2.8 shows the mean temperatures of the simple and the detailed SOFC models. At nominal steady state there is a temperature difference of about 120K between the two mean SOFC temperatures. This can be explained as follows. For both SOFC models, since inlet massflows and current are the same, the energy balance should ensure that the energy in the outlet massflow (and hence outlet temperature) is approximately[1] the same for both models. In a SOFC, the maximum temperature region is at the outlets of the anode and the cathode. Since the simple model is a bulk model, the exit temperature is equal to the mean temperature. For the detailed model, SOFC temperature is a distributed variable and the mean temperature is certainly less than the exit temperature. It is verified that the maximum temperature of the detailed model at the nominal steady state is approximately equal to the mean temperature of the simple SOFC model. From Figure 2.8, it is clear that both the models exhibit similar dynamics for the disturbances applied during the simulation.

Figure 2.9 shows the voltages of the two models during the simulation. Here also both models show the same dynamic changes in the voltages for all the disturbances applied. Here the simple model has higher voltage than the detailed model which is also mainly because of the higher mean solid temperature of the simple SOFC model. Refering to (B.18), when temperature increases the voltage loss decreases. Hence the simple SOFC voltage given by (B.19) is higher than that of the detailed SOFC model at the nominal steady state.

Figure 2.10 shows a comparison of power production of the two models during the simulation. Since the voltage of the simple SOFC model is higher than that of the detailed model and the current is the same in both models,

[1] A slight difference in voltage and hence produced DC power gives a small temperature difference.

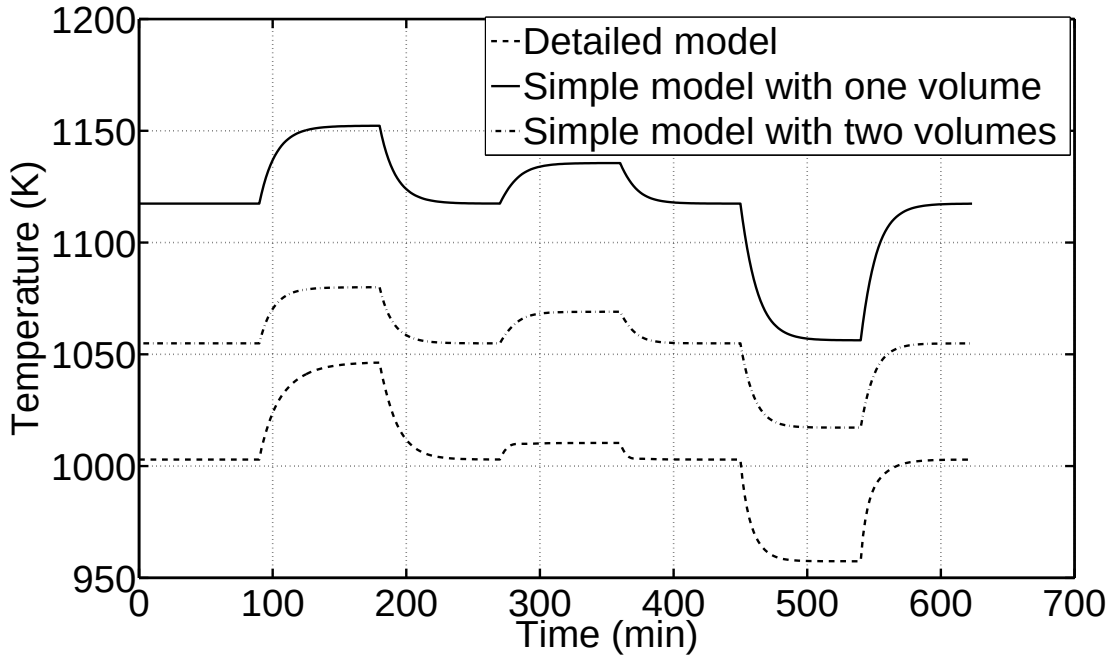

Figure 2.8: Comparison of mean solid temperatures of the simple model with one volume and the detailed model for different disturbances

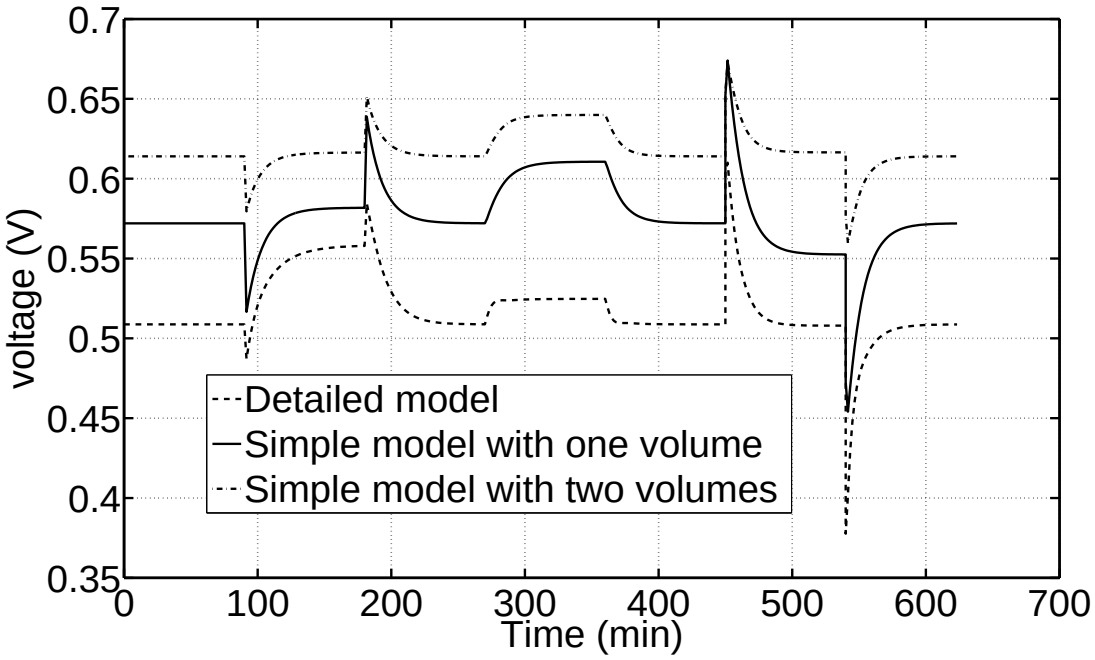

Figure 2.9: Comparison of voltages of the simple model with one volume and the detailed model for different disturbances

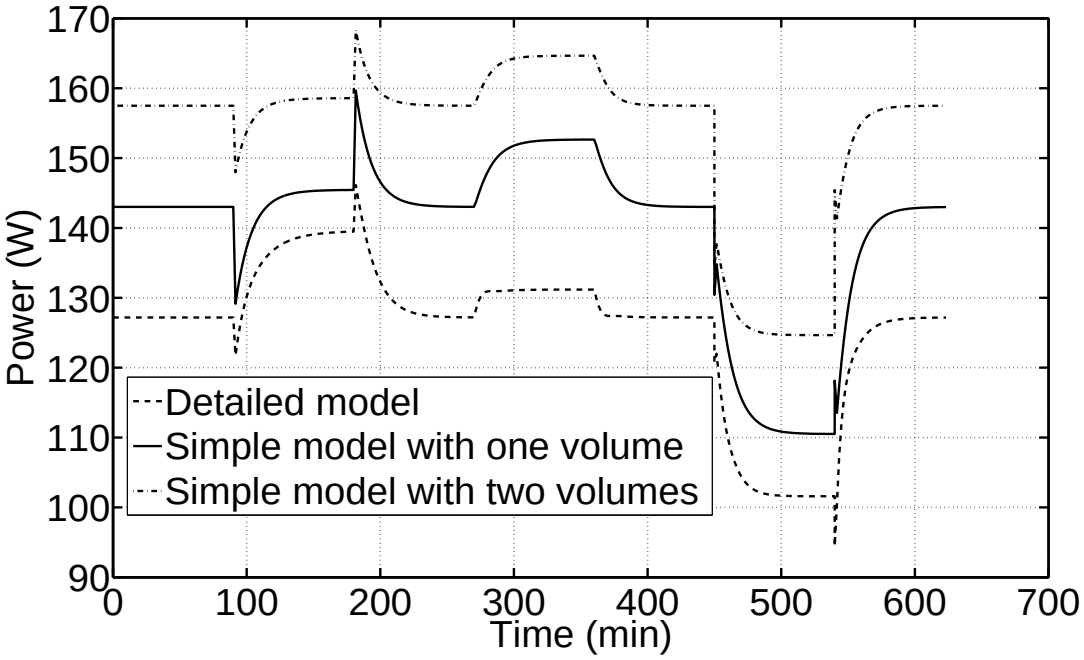

Figure 2.10: Comparison of power production of the simple model with one volume and the detailed model for different disturbances

the power produced by the simple SOFC model is higher.

Two volume SOFC model

Figure 2.8 shows the comparison of the mean temperatures of the two SOFC models. Now, the simple SOFC is represented by aggregation of two volumes. The simple SOFC solid mean temperature is given by the average of the temperatures of the two volumes. The difference between the two mean temperatures at the nominal steady state is reduced to 51K as supposed to 120K. The dynamics of the two volume model is similar to that of the dynamics of the one volume model for all the disturbances. Figures 2.9 and 2.10 show the comparison of the voltages and powers of the two models, for the two volume model the average voltage is plotted. There is a small voltage difference of 0.1V between the two volumes and this is caused by the

somewhat crude approximate distribution of currents between the two volumes. The two-volume model shown here can be taken as a basis to develop a multi-volume model to capture the distributed nature of the variables.

2.6 Hybrid system control and simulation

At first, the integrated open-loop system with double shaft configuration is simulated with a set of nominal, realistic parameters resulting in a nominal state partially shown in Table 3.1. As may be expected, there is a need to design a control system to compensate for load disturbances [17].

As the main source of the power in the hybrid system is the fuel flow, fuel flow must be controlled to match the power demand in case of load changes. Since it is not always possible to know the load in advance, any load change is treated as a disturbance to the controller. As the bus bar voltage is fixed when there is a load change, the current and the FU in SOFC vary. The FU cannot be varied too much since it may cause uneven temperature and voltage distributions inside the cell [19]. Hence, FU is taken as a controlled variable, where it is assumed that FU can be caculated from the measurments available.

A load change can affect the SOFC temperature to change beyond the material constraints [8],[19]. Hence, the SOFC temperature should be controlled during the load changes. As there is no other free manipulated variable available for this purpose, a slight change must be made in the process design. After analyzing three different possible choices for an extra manipulated variable, air blow off at compressor outlet is found to be superior in terms of control authority, compared to air bypass across the heat exchanger and additional fuel to the combustion chamber. The non-linear system is linearized at its nominal state given in Table 3.1, and decentralized PI controllers are tuned according to the rules given in [15]. Further, RGA analysis [16] substantiates the choice of control structure. The proposed control structure is shown in Figure 2.11. The PI controllers are then implemented on the non-linear system.

To evaluate the proposed control structure, the following simulation scenario is used. The system is simulated at the nominal state for one sec. After 5 sec, the following disturbances are applied in a ramp of 5 sec: the mechanical load on the induction motor (P_m) is decreased to 10%, R is in-

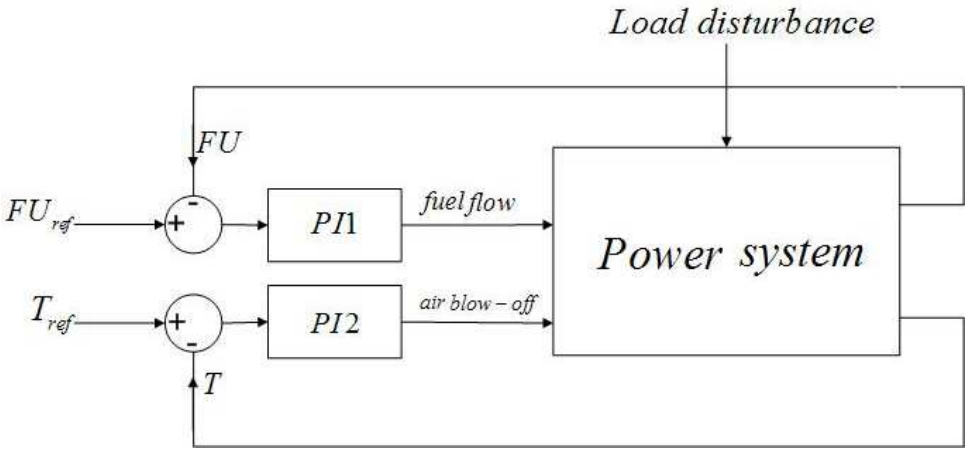

Figure 2.11: Control structure

Table 2.6: Nominal state of the system

Variable	**Value**
SOFC current	250A
Methane flow rate	0.007kg/s
SOFC temperature	1350K
SOFC cell voltage	0.657V
SOFC stack power	191kW
Generator power	87kW
Air mass flow rate	0.445kg/s
AU	0.23
FU	0.85
Recycle ratio	0.54
Reforming degree	0.38
Steam/methane ratio	2
I_t	1248A
V_t	222V
Induction motor slip	0.1

creased by 5 times, I_{IK} is decreased to 10% and P_{PK} is decreased to 10% which constitutes 40% load decrease on the system and the system is simulated at steady state until 20 sec. After 20 secs, the P_m is increased to 50% in a step. The total load change, FU and SOFC solid temperature profiles during the simulation are shown in Figure 2.12. The plant inputs, i.e. fuel flow and air blow-off during the simulation are shown in Figure 2.13.

2.6.1 Discussion

When there is a load decrease, correspondingly the current and amount of fuel utilized in the SOFC are decreased, which decrease the FU. To maintain FU constant at 0.85, the fuel flow rate is decreased as shown in Figure 2.13. When the current decreases in the SOFC, the electrochemical reactions rate is decreased which decreases the SOFC temperature. To maintain the SOFC temperature at a constant value the air mass flow rate through the SOFC should decrease meaning that the air blow-off rate must increase as shown in Figure 2.13. At the nominal state a small non-zero air blow-off rate is chosen to be able to control the SOFC temperature for any small increase in the load at the nominal value. For the 40% load change, the air blow-off rate constitutes about 18% of the total air mass flow rate which may cause a decrease in system efficiency. This is because of the strict control of the SOFC temperature at the nominal value. If the SOFC temperature is chosen to vary within some bounds around the nominal value, the air blow-off utilization can be optimized to a higher system efficiency. However, from the control point of view the proposed control structure gives satisfactory results as seen from Figures 2.12 and 2.13. In Figure 2.12, the SOFC solid temperature profile is shown which is maintained almost constant. Here it is to be noted that we wish to control the SOFC solid temperature, but not the gas temperature, hence the rapid temperature changes are not modeled as thermal inertia of gases are neglected.

It is clear that the control design must be regarded as preliminary, as there are several effects that are not accounted for, e.g. surge in the compressor and constraints on Turbine Inlet Temperature (TIT).

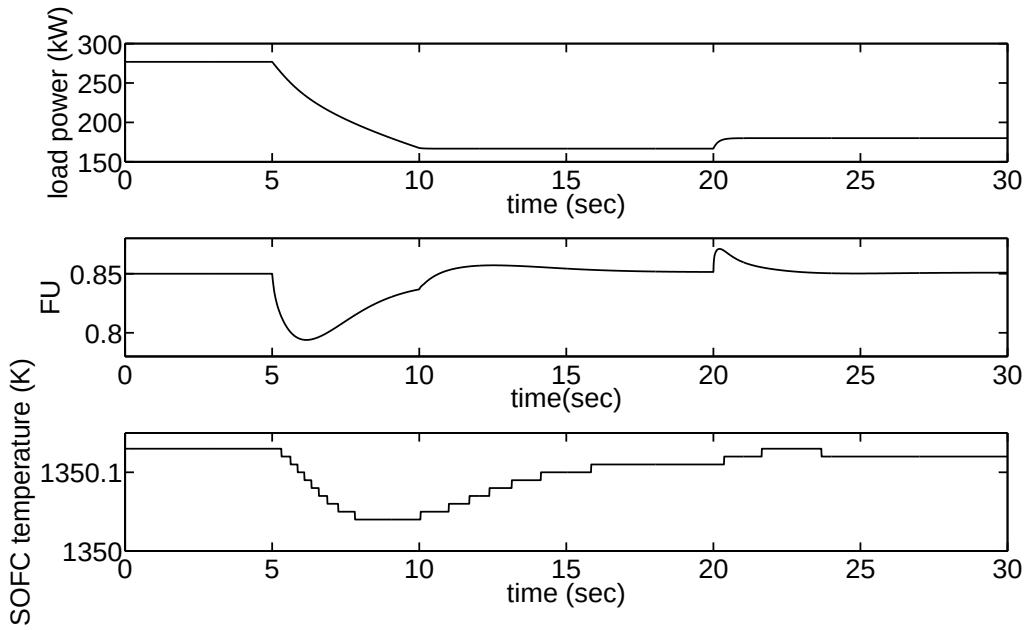

Figure 2.12: Mechanical load change, FU, and SOFC temperature during simulation

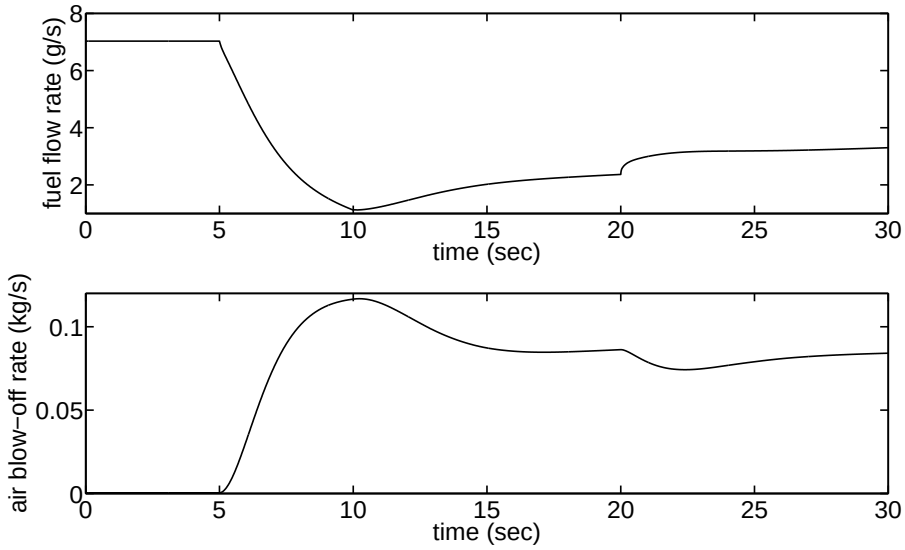

Figure 2.13: Plant inputs during simulation

2.7 Conclusions and further work

From the SOFC model evaluation simulation results, it is quite clear that even though there is some steady state offset, important variables of the simple and the detailed models show similar dynamic behavior during the simulations. It can therefore be concluded that the simple model is able to capture the overall dynamics of the SOFC. This model will hence be used for further studies on control and operability of the hybrid system, i.e. an SOFC integrated in a GT cycle. If the one volume model is too crude, it is possible to aggregate a number of volumes. The results herein however indicate that a one volume model may suffice in many cases.

A model of the complete power system where a SOFC-GT hybrid system is connected to a grid with connected load is developed to include the interactions between the grid and the hybrid system. A control structure with PI controllers shows that satisfactory results can be obtained, but the main disadvantage is that the system efficiency will be reduced with the use of blow-off to control the SOFC temperature during part-load operation.

Future work will focus on optimizing the control design to reduce the air-

blow off utilization to control the SOFC temperature to increase the system efficiency at part load operation, anti-surge and TIT constraints. While the present paper focussed on control design for a two-shaft GT design, a *single-shaft* GT design which poses further challenges for a control design will also be investigated. A single-shaft GT offers the possibility of avoiding air blow-off by controlling shaft speed directly.

2.8 Acknowledgements

Financial support from The Gas Technology Center, NTNU-SINTEF and NFR is acknowledged.

2.9 Nomenclature

a_{ij}	stoichiometric matrix
A	SOFC surface area
A_{k_i}, $A_{K^{ads}}$	pre-exp. factors for k_i
C^s	solid heat capacity
DEN	denominator
E	activation energy
E^o	EMF at standard temperature and pressure
E^{OCV}	open circuit voltage
F	Faraday's constant
I	current
p	pressure
P	power
r_j	reaction rate of reaction j
R	universal gas constant
T	temperature
V_{an}, V_{ca}	volumes
V	voltage
k_2, k_3, k_4	rate coefficients for reforming reactions
k_{an}, k_{ca}	choked flow constants
K_j	equilibrium constant for reaction j
K_i^{ads}	adsorption constant for component i

$\dot{m}$ mass flow rate
n_{rx} number of reactions
N number of moles
$\Delta\overline{h}$ molar specific enthalpy
$\Delta\overline{h}^{rx}$ molar specific enthalpy change of reaction
$\Delta\overline{h}^{ads}$ enthalpy change of adsorption
δ shaping factor

Subscripts and superscripts

i chemical component
j reaction
an anode
ca cathode
in inlet
out outlet
rad radiation
$cond$ conduction

References

[1] S. Campanari. Thermodynamic model and parametric analysis of a tubular SOFC module. *Journal of Power Sources*, 92:26–34, 2004.

[2] S. H. Chan, H. K. Ho, and Y. Tian. Multi-level modeling of SOFC-gas turbine hybrid system. *International Journal of Hydrogen Energy*, 28(8):889–900, 2003.

[3] gPROMS (2004). gPROMS introductory user guide. *Process Systems Enterprise Ltd.*, 2004.

[4] C. J. Hatziadoniu, A. A. Lobo, F. Pourboghart, and M. Daneshdoost. A simplified dynamic model of grid-connected fuel-cell generators. *IEEE Transactions on Power Delivery*, 17(2):467–473, 2002.

[5] D. J. Hill. Nonlinear dynamic load models with recovery for voltage stability studies. *IEEE Transactions on Power Systems*, 8(1):166–176, 1993.

[6] F. P. Incropera and D. P. De Witt. *Fundamentals of Heat and Mass Transfer*. Wiley, USA, 2002.

[7] D. Jensen and J. W. Dijkstra. CO2 capture in SOFC-GT systems. *Proceedings of second annual conference on Carbon Sequestration*, May 2003.

[8] J. Larminie and A. Dicks. *Fuel Cell Systems Explained*. Wiley, England, 2003.

[9] M. D. Lukas, K. Y. Lee, and H. Ghezel-Ayagh. An Explicit Dynamic Model for Direct Reforming Carbonate Fuel Cell Stack. *IEEE Transactions on Energy Conversion*, 16(3), September 2001.

[10] L. Magistri, F. Trasino, and P. Costamagna. Transient analysis of a Solid Oxide Fuel Cell hybrids part A: fuel cell models. *Journal of Power Sources*, 2004.

[11] L. Magistri, F. Trasino, and P. Costamagna. Transient analysis of a Solid Oxide Fuel Cell hybrids part A: fuel cell models. *Journal of Power Sources*, 2004.

[12] I. R. Navarro. *Dynamic power system load - Estimation of parameters from operational data*. Media-Tryck, Lund, 2005.

[13] J. På lsson, A. Selimovic, and L. Sjunnesson. Combined solid oxide fuel cell and gas turbine systems for efficient power and heat generation. *Journal of Power Sources*, 86:442–448, 2000.

[14] J. Padulles, G. W. Ault, and J. R. McDonald. An integrated SOFC dynamic model power systems simulation. *Journal of Power Sources*, 86(1):495–500, 2000.

[15] S. Skogestad. Simple analytic rules for model reduction and PID controller tuning. *Journal of process control*, 13(4):291–309, 2003.

[16] S. Skogestad and I. Postlethwaite. *Multivariable feedback control: Analysis and Design*. Wiley, USA, 1996.

[17] C. Stiller, B. Thorud, and O. Bolland. Safe dynamic operation of a simple SOFC/GT hybrid cycle. *Accepted for publication in the ASME Journal of Engineering for Gas Turbines and Power*, 2005.

[18] C. Stiller, B. Thorud, O. Bolland, R. Kandepu, and L. Imsland. Control strategy for a solid oxide fuel cell and gas turbine hybrid system. *Accepted for publication in the Journal of Power Sources*, 158(1):303–315, 2006.

[19] C. Stiller, B. Thorud, O. Bolland, R. Kandepu, and L. Imsland. Control strategy for a solid oxide fuel cell and gas turbine hybrid system. *Accepted for publication in the Journal of Power Sources*, 158(1):303–315, 2006.

[20] C. Stiller, B. Thorud, S. Seljebø, O. Mathisen, H. Karoliussen, and O. Bolland. Finite-volume modeling and hybrid-cycle performance of planar and tubular solid oxide fuel cells. *Journal of Power Sources*, 141:227–240, 2005.

[21] P. Thomas. *Simulation of Industrial Processes For Control Engineers*. Butterworth-Heinemann, Wobourn, MA, USA, 1999.

[22] B. Thorud. *Dynamic modelling and characterisation of a solid oxide fuel cell integrated in a gas turbine cycle.* Tapir Uttrykk, NTNU, Trondheim, 2005.

[23] B. Thorud, C. Stiller, T. Weydahl, O. Bolland, and H. Karoliussen. Part-load and load change simulation of tubular SOFC systems. *Proceedings of Fuel Cell Forum, Lucerne, 28 June-2 July*, 2004.

[24] L. A. A. Warnes. *Electronic and Electrical Engineering*. Macmillan, London, 1994.

[25] J. Xu and G. F. Froment. Methane Steam Reforming, Methanation and Water-Gas Shift: I. Intrinsic Kinetics. *AIChE Journal*, 35(1):88–96, 1989.

Chapter 3

Modeling and control of a SOFC-GT hybrid system with single shaft configuration

Abstract

This article focuses on issues related to control and operability of a Solid Oxide Fuel Cell (SOFC) - Gas Turbine (GT) hybrid system with single-shaft GT configuration. The models of all the components of the hybrid system are developed and integrated to constitute the hybrid system. An autonomous power grid is modeled as load. The main control objectives considered are control of Fuel Utilization (FU) in the SOFC and SOFC solid temperature during dynamic operation of the hybrid system.

3.1 Introduction

In the foreseeable future, fossil fuels including natural gas will be a major source of energy. With today's increasing concern about global warming and climate change, there is an incentive to investigate natural gas power processes that operate efficiently, thus emitting less per kWh produced, and also power production processes with CO2 capture capabilities. It is widely accepted that fuel cells are power sources that will become increasingly important, due to high efficiency, low levels of pollution and noise, and high

reliability. One of the most promising fuel cell technologies is the Solid Oxide Fuel Cell (SOFC), due to its solid state design and internal reforming of gaseous fuels, in addition to its high efficiency [6]. The SOFC converts the chemical energy of a fuel directly to electrical energy. Since SOFCs operate at high temperatures (about 10000 C), natural gas can be used directly as fuel. The electrical efficiency of a SOFC can reach 55%. Another significant advantage of the SOFC is that since it operates at high temperature and its efficiency increases when pressurized, and it naturally lends itself as a heat source for a gas turbine (GT) cycle. The combined (hybrid) cycle can theoretically have an overall electrical efficiency of up to 70% with a power range from a few hundred kWs to a few MWs. The main applications of the hybrid system include remote area power supply and distributed power generation.

There are several models available in literature for the SOFC-GT hybrid system [7], [1], [8], [13]. In [4], a dynamic model of grid connected SOFC model is developed. However, the SOFC-GT hybrid system with single shaft configuration is integrated in an autonomous power system. The reason for procuring an integrated model is to obtain a comprehensive understanding of the operability of the system which has close dynamic interactions between the power generation system and the local grid. Further, the hybrid system consists of tightly integrated dynamic subsystems with strict operating criteria making the control design more challenging in terms of disturbance rejection, part load operation and in particular startup, shut down and load shedding. Suitable system actuation must be chosen, good control structures must be devised, and good controllers must be designed. As a basis for all these tasks, control relevant models must be developed for the subsystems, and for the total system. Such models should have limited complexity to allow for the necessary analysis, and at the same time should include the important dynamic interactions.

In this paper we present an integrated model of a SOFC-GT hybrid system with a power grid connecting to an electrical load. The process is described on a system level and modeling of each component is discussed briefly. The model is subsequently used to perform analysis of system dynamics and optimize system design. A simple control design is proposed and assessed through a set of simulation scenarios.

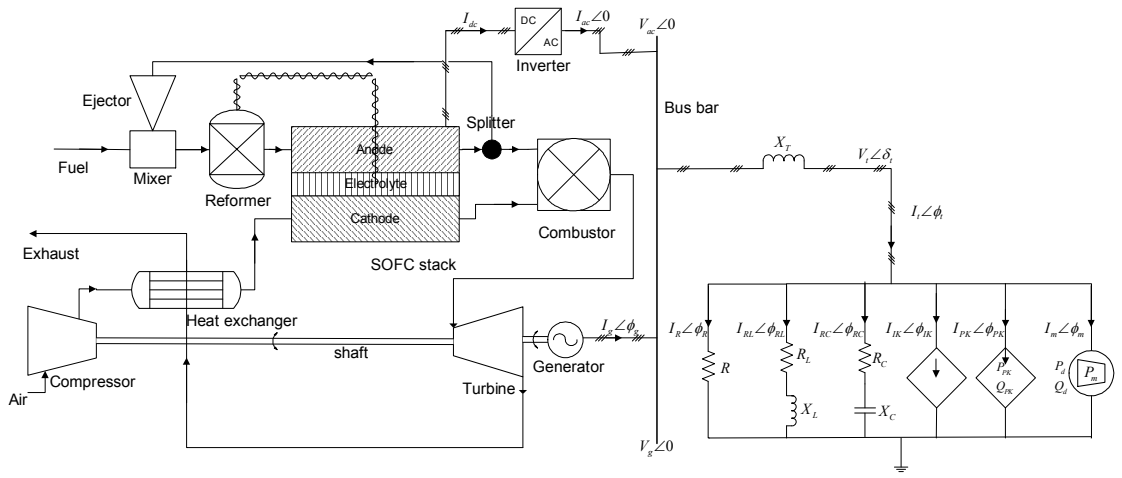

Figure 3.1: SOFC-GT hybrid system with single shaft configuration in an autonomous power system

3.2 Process description

A schematic diagram of the integrated system where the hybrid system is connected to the load by a bus bar is shown in Figure 3.1. Methane (fuel) is mixed with a part of anode flue gas and is partially steam reformed in pre-reformer generating hydrogen. The heat required for endothermic reformation reactions in the pre-reformer is supplied from the SOFC stack through radiation. The gas mixture from the pre-reformer is fed to the anode volume of the SOFC, where the remaining part of the methane is reformed. Compressed atmospheric air is heated in a recuperative heat exchanger and is used as an oxygen source at the cathode side of the SOFC. In the SOFC, electrochemical reactions take place and DC voltage is produced. The rate of the electrochemical reactions depends on the current. A part of the anode flue gas is recycled to supply steam to the pre-reformer. The remaining part of the anode and cathode flue gases is supplied to a combustion chamber where the unused fuel is combusted. The hybrid system considered here uses a single shaft GT configuration. The combusted gas mixture is expanded in a gas turbine which is coupled to a compressor and an alternator through a shaft. The expanded gas mixture is used to heat up the compressed air in a heat exchanger. The DC power from the SOFC stack is fed to an inverter

which converts DC to AC with a fixed frequency. The inverter and the generator are connected to a local grid, which is connected to a six branch electric load. Both the SOFC stack and the generator supply the electric load demand on the grid. The load sharing between the SOFC stack and the generator cannot be controlled when there is a load change on the grid. Typically 60-70% of the total power is supplied by the SOFC stack.

3.3 Modeling

All the models of the system are modeled in the modular modeling environment gPROMS [3]. The detailed modeling of each component of the system can be found in appendix B. A brief description of the each model is presented below.

3.3.1 SOFC stack

It is assumed that all the SOFCs in the stack operate at identical conditions. A zero-dimensional SOFC model is developed with no regard to the geometry of the cell. The model developed is a lumped one, which includes dynamic molar balances of all the species both in anode and cathode volumes separately. It includes an energy balance treating the whole SOFC as a single volume to model the temperature dynamics of the SOFC solid mean temperature. There is a radiation from the SOFC to the pre-reformer. The voltage developed across the cell is modeled using Nernst equation, the operating cell voltage is calculated by considering both ohmic and activation losses.

In [5], the low complexity SOFC model is evaluated against a detailed model developed in [13], [12]. The comparisons indicate that the low complexity model is good enough to approximate the important dynamics of the SOFC and can hence be used for operability and control studies.

3.3.2 Pre-reformer

The pre-reformer is modeled as a Continuously Stirred Tank Reactor (CSTR). Mass balances of all the species are included dynamically and energy balance is implemented to model the pre-reformer temperature dynamics. The steam required for the steam-reforming is provided by the recycle flow of the

anode flue gas. The heat required for the endothermic reforming reaction is obtained by the radiation heat from the SOFC stack.

3.3.3 Combustor

In the combustor, the unused fuel is burnt in presence of oxygen coming from the cathode outlet. The operating conditions will always be such that there is surplus oxygen available for complete combustion due to the fact that air mass flow rate is much larger than the fuel mass flow rate. In the combustor, the fuel can be methane, hydrogen or carbon monoxide or a mixture of these fuels. As the combustion process is rapid it is modeled as an instantaneous process.

3.3.4 Heat exchanger

A very simple model of a counter-flow heat exchanger is used, in which the amount of the heat exchanged depends on the heat transfer coefficient of the exchanger wall and also on the average temperature difference between the hot and cold streams. A first order transfer function describes the dynamics of the temperatures of both the streams.

3.3.5 Gas turbine cycle

The compressor and turbine models are based on steady state performance map characteristics [11]. The map is modeled using polynomials of 4th and 5th order for reduced mass flow, pressure and efficiency as functions of reduced shaft speed and operation line. A shaft model accounts for the dynamics of the rotating mass in the gas turbine system.

3.3.6 Electrical components

A simple model of inverter is used to convert DC electric power from the SOFC stack to AC, which is given to an autonomous grid. The grid side voltage is maintained constant at 230V by using the inverter controllers and the dynamics of these controllers are neglected. An AC-AC frequency converter with 95% efficiency is assumed to be connected to the alternator to convert the varying frequency of the alternator to the grid frequency. The operating

voltage of the alternator is controlled to the grid voltage by controlling the field current in the alternator. The electric load connected to the gird is represented by six parallel branches with different components in each branch. It is categorized into 4 types of loads; constant impedance, constant current, constant power and induction motor load. The constant impedance, constant current and constant power load represent the residential loads such as lights, water heaters, ovens etc. The induction motor load is considered to represent an industrial load. The constant impedance load is represented by the first three branches with resistive, inductive and capacitive loads. The fourth and fifth branches represent the constant current and constant power loads respectively. The sixth branch represents the induction motor load. The total load current is the sum of the currents from the inverter and the alternator.

3.4 Control design

The nominal state of the system is given in Table 3.1. At the steady state if there is any disturbance in any of the variables in the system, then it would disturb the power balance across the shaft in the GT cycle. Further the shaft speed will either accelerate or decelerate depending on the disturbance and it would make the system unstable. In order to make the system stable the shaft speed is to be controlled. The alternator current is manipulated in order to make the power balance satisfied, thus making the system stable. This is accomplished by using Proportional and Integral (PI) controller 1 as shown in Figure 3.2. Generally there are two ways of operating the hybrid system; constant shaft speed operation and variable shaft speed operation. Here variable shaft speed operation is considered as it has got advantages [2].

As the hybrid system is connected to an autonomous power grid, it is to be operated in part load operation, as the electric load changes with time. During the part load operation, the hybrid system has to supply the power exactly needed by the grid. As the main source of the power in the hybrid system is the fuel flow, fuel flow must be controlled to match the power demand in case of any load changes. Since it is not always possible to know the load in advance, any load change is treated as a disturbance. As the bus bar voltage is fixed when there is a load change, the current and the

Table 3.1: Nominal state of the system

Variable	**Value**
SOFC current	263 A
Methane flow rate	0.0072 kg/s
SOFC temperature	1206 K
SOFC cell voltage	0.67 V
SOFC stack power	205 kW
Generator power	76.8 kW
Air mass flow rate	0.462 kg/s
AU	0.235
FU	0.85
Recycle ratio	0.53
Reforming degree	0.29
I_t	1248 A
V_t	222 V
Induction motor slip	0.1

FU in SOFC vary. The FU cannot be varied too much since it may cause uneven temperature and voltage distributions inside the cell [11]. Hence FU is taken as a controlled variable, where it is assumed that a perfect observer is available to estimate FU, as it cannot be measured directly during the dynamic changes. PI controller 2 is designed to control the FU using fuel mass flow as input, in case of any load change as shown in Figure 3.2.

A load change can affect the SOFC temperature to change beyond the material constraints [6] [11]. Hence the SOFC temperature should be controlled during the load changes. The SOFC temperature can be controlled by varying the air mass flow entering the cathode. The air mass flow entering the cathode can be varied by varying the shaft speed. All these things are accomplished using the cascade controller as shown in Figure 3.2. The PI controller 3 is used to control the SOFC temperature to a reference point by varying the shaft speed reference point to the PI controller 2. The PI controller 2 varies the alternator current to make the shaft speed equal to the reference point set by the PI controller 3.

The non-linear system is linearized at its nominal state given in Table 3.1, and decentralized PI controllers are tuned according to the rules given in [9]. Further, RGA analysis [10] substantiates the choice of control structure.

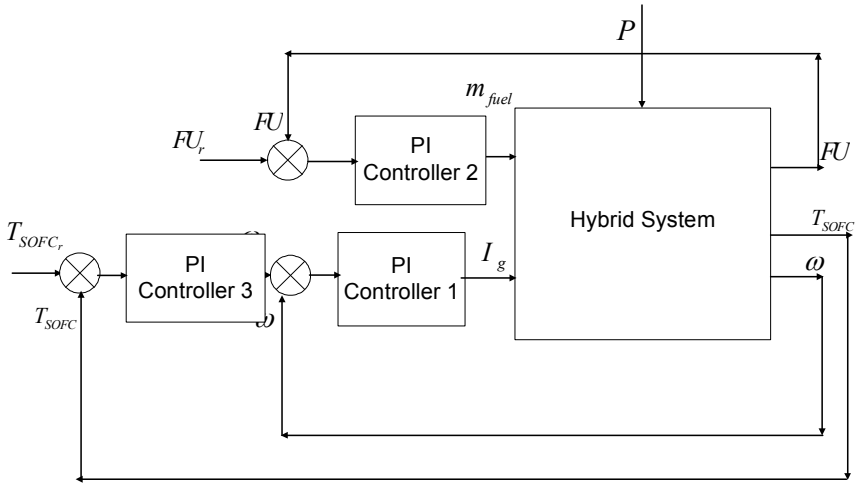

Figure 3.2: Control structure

The PI controllers are then implemented on the non-linear system.

3.5 Simulation

To evaluate the proposed control structure, the following scenario is used. The system is run at steady state for two minutes. After two minutes the following disturbances are given in the different elements of the electric load on the grid is decreased from 100% to 60% in a ramp fashion for 10 sec. duration. After 30 minutes, the load is increased by 8% in a step. During the simulation different power profiles are shown in Figure 3.3. The FU, Air Utilization (AU) and cell voltage profiles during the simulation are shown in Figure 3.4. Also, different temperature profiles during the simulation are shown in Figure 3.5.

When there is a load decrease of 40% from the nominal state, both the SOFC stack and the alternator power are decreased at the new steady state value. From Figure 3.3, it is clear that the stack reacts faster compared to the alternator, as the fuel flow to the stack is decreased by the PI controller 2. At the nominal state the alternator power share is approximately 27.1% in the total power and when the load is decreased, it is maintained at 27%

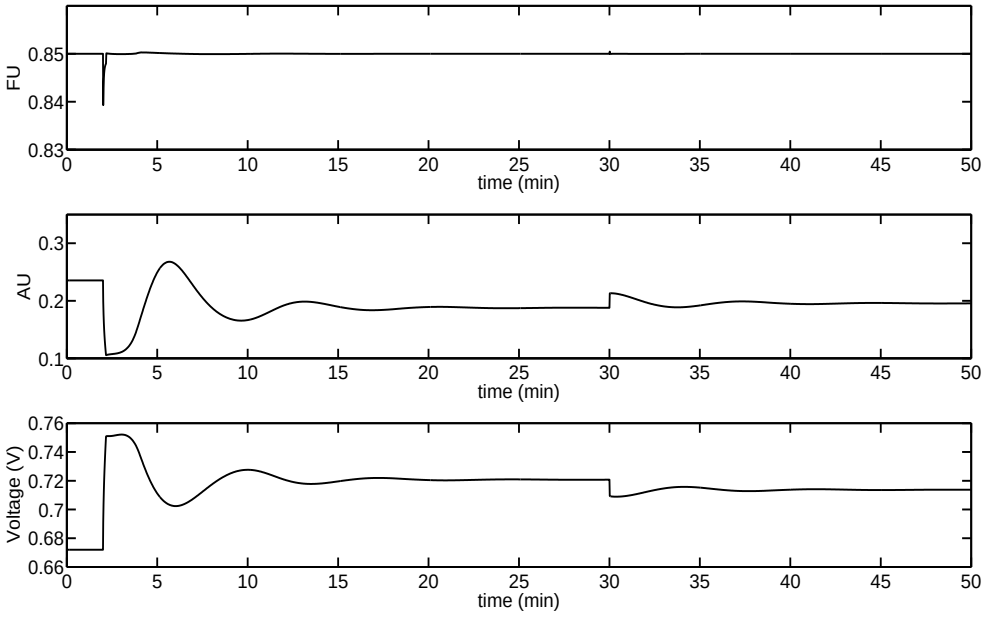

Figure 3.3: Different power profiles during the simulation

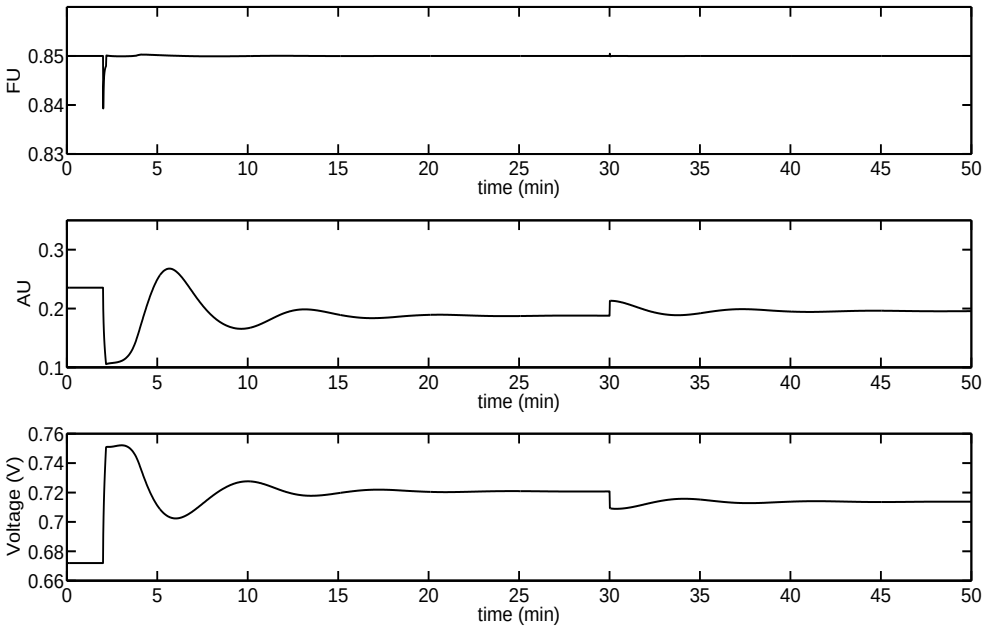

Figure 3.4: FU, AU and voltage profiles during the simulation

at the new steady state as well. When the load decreased, the fuel flow rate is decreased as in Figure 3.5, the current is decreased, hence the number of electrochemical reactions that take place decrease. Hence less oxygen is required and the AU is decreased (see Figure 3.4), even though the air mass flow rate is decreased (see Figure 3.5), as the former effect dominates. The FU is maintained at 0.85 (see Figure 3.4) by the PI controller 2 by manipulating the fuel flow rate, though there is a dip for a small time due to sudden change in the SOFC current due to the load disturbance.

Since the current is decreased, the ohmic loss is reduced. But the open circuit voltage is reduced as the partial pressure of hydrogen is reduced in the cell. As the current is reduced a lot, this effect is dominated and the cell voltage is increased at the new steady state (see Figure 3.4).

As the fuel flow rate is decreased, the quantity of the fuel burnt in the combustor is decreased and TIT is reduced at the new steady state value

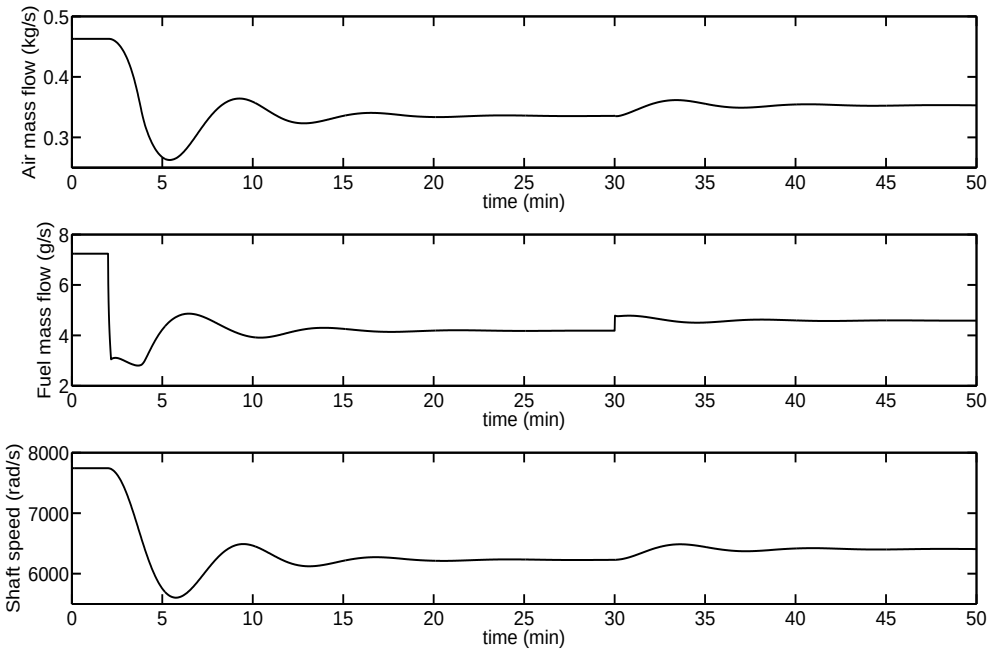

Figure 3.5: Air and fuel mass flow rates and shaft speed profiles during the simulation

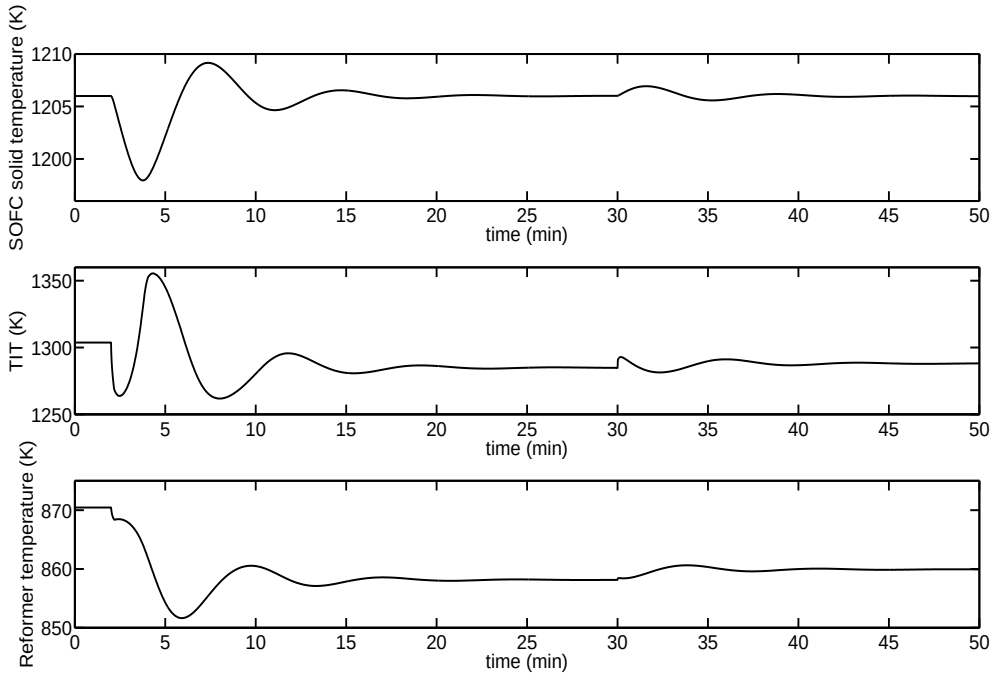

Figure 3.6: Different temperature profiles during the simulation

(see Figure 3.6). When the power is reduced, which will have an effect on SOFC temperature to decrease, and PI controller 3 acts to decrease the air mass flow rate by reducing the shaft speed (see Figure 3.5). The SOFC temperature is varied by only a maximum of $8°C$ during the dynamic change and at the steady state it is controlled at the nominal value.

For a small step increase after 30 minutes, all the variables act in the opposite direction compared to the case where there is decrease in the load.

3.6 Conclusions

An integrated model of a SOFC-GT hybrid system in an autonomous power system is developed with a relatively low complexity, but including the important dynamics required for a control design. A simple control design is proposed which would stabilize the system and includes controls for FU and

SOFC temperature in case of any disturbance in the load connected to the hybrid system.

Future work will focus on the optimization of set points for the all the PI controllers during part load operation by minimizing the fuel input into the system. Also an extension of the proposed control structure for start up and shut down operations of the hybrid system.

3.7 Acknowledgements

Financial support from The Gas Technology Center, NTNU-SINTEF and NFR is acknowledged.

References

[1] S. H. Chan, H. K. Ho, and Y. Tian. Multi-level modeling of SOFC-gas turbine hybrid system. *International Journal of Hydrogen Energy*, 28(8):889–900, 2003.

[2] P. Costamagna, L. Magistri, and A. Massardo. Design and part-load performance of a hybrid system based on a solid oxide fuel cell reactor and a micro gas turbine. *Journal of power sources*, 96:352–368, 2001.

[3] gPROMS (2004). gPROMS introductory user guide. *Process Systems Enterprise Ltd.*, 2004.

[4] C. J. Hatziadoniu, A. A. Lobo, F. Pourboghart, and M. Daneshdoost. A simplified dynamic model of grid-connected fuel-cell generators. *IEEE Transactions on Power Delivery*, 17(2):467–473, 2002.

[5] R. Kandepu, L. Imsland, B. A. Foss, C. Stiller, B. Thorud, and O. Bolland. Control-relevant SOFC modeling and model eveluation. *In the Proceedings of ECOS, the 18th Conference on Efficiency, Cost, Optimization, Simulation and Environmental Impact of Energy Systems, Trondheim, Norway, June, 20-22*, 2005.

[6] J. Larminie and A. Dicks. *Fuel Cell Systems Explained*. Wiley, England, 2003.

[7] L. Magistri, F. Trasino, and P. Costamagna. Transient analysis of a Solid Oxide Fuel Cell hybrids part A: fuel cell models. *Journal of Power Sources*, 2004.

[8] J. På lsson, A. Selimovic, and L. Sjunnesson. Combined solid oxide fuel cell and gas turbine systems for efficient power and heat generation. *Journal of Power Sources*, 86:442–448, 2000.

[9] S. Skogestad. Simple analytic rules for model reduction and PID controller tuning. *Journal of process control*, 13(4):291–309, 2003.

[10] S. Skogestad and I. Postlethwaite. *Multivariable feedback control: Analysis and Design*. Wiley, USA, 1996.

[11] C. Stiller, B. Thorud, O. Bolland, R. Kandepu, and L. Imsland. Control strategy for a solid oxide fuel cell and gas turbine hybrid system. *Accepted for publication in the Journal of Power Sources*, 158(1):303–315, 2006.

[12] C. Stiller, B. Thorud, S. Seljebø, O. Mathisen, H. Karoliussen, and O. Bolland. Finite-volume modeling and hybrid-cycle performance of planar and tubular solid oxide fuel cells. *Journal of Power Sources*, 141:227–240, 2005.

[13] B. Thorud, C. Stiller, T. Weydahl, O. Bolland, and H. Karoliussen. Part-load and load change simulation of tubular SOFC systems. *Proceedings of Fuel Cell Forum, Lucerne, 28 June-2 July*, 2004.

Chapter 4

State estimation of SOFC/GT hybrid system using UKF

Abstract

A description of a Solid Oxide Fuel Cell (SOFC) combined Gas Turbine (GT) hybrid system is given. Modeling of all the components of the hybrid system is briefly presented. A decentralized control structure using PI controllers is designed and is considered as a part of the system. An Unscented Kalman Filter (UKF) is applied to estimate the state vector and the simulation results are presented.

4.1 Introduction

In the foreseeable future, fossil fuels including natural gas will be a major source of energy. With today's increasing concern about global warming and climate change, there is an incentive to investigate natural gas power processes that operate efficiently, thus emitting less per kWh produced, and also power production processes with CO_2 capture capabilities. It is widely accepted that fuel cells are power sources that will become increasingly important, due to high efficiency, low levels of pollution and noise, and high reliability. One of the most promising fuel cell technologies is the Solid Oxide Fuel Cell (SOFC), due to its solid state design and internal reforming of gaseous fuels, in addition to its high efficiency. The SOFC converts the

chemical energy of fuel directly to electrical energy. Since SOFCs operate at high temperatures (about 1000° C), natural gas can be used directly as fuel. The electrical efficiency of a SOFC can reach 55%. Another significant advantage of the SOFC is that since it operates at high temperature, its efficiency increases when pressurized, and it naturally lends itself as a heat source for a gas turbine (GT) cycle. The combined (hybrid) cycle can theoretically have an overall electrical efficiency of up to 70% with a power range from a few hundred kWs to a few MWs. The main applications of the hybrid system include remote area power supply and distributed power generation.

The hybrid system consists of tightly integrated dynamic subsystems with strict operating criteria making the control design more challenging in terms of disturbance rejection, part load operation and in particular start-up, shut down and load shedding. Suitable system actuation must be chosen, good control structures must be devised, and good controllers must be designed. As a basis for all these tasks, control relevant models must be developed for the subsystems, as well as for the total system. Such models should have limited complexity to allow for the necessary analysis, and at the same time should include the important dynamic interactions. In [4], a control relevant model of the hybrid system integrated in an autonomous power system has been developed. Further, control design with PI controllers is proposed, which gives satisfactory results in terms of tracking. It is also concluded that there is a scope to improve the system efficiency by using an advanced control design, for example, Model Predictive Control (MPC).

State estimation plays an important role in developing the MPC and monitoring technologies. The hybrid system is highly nonlinear and it has to be operated under different load conditions, which makes it necessary to design a nonlinear estimator.

Extended Kalman Filter (EKF) is the most widely used estimation algorithm for nonlinear systems. There are some difficulties in applying the EKF such as difficult to implement, difficult to tune, and only reliable for systems that are almost linear on the time scale of updates [3]. Furthermore, it is accurate up to the first order in estimating mean and covariance for a nonlinear probability distribution (pdf) and Jacobian computation is necessary. [3] developed Unscented Kalman Filter (UKF) as a novel extension of Kalman Filter. The UKF is based on the principle that propagation of a pdf through a nonlinear transformation is approximated by the propagation

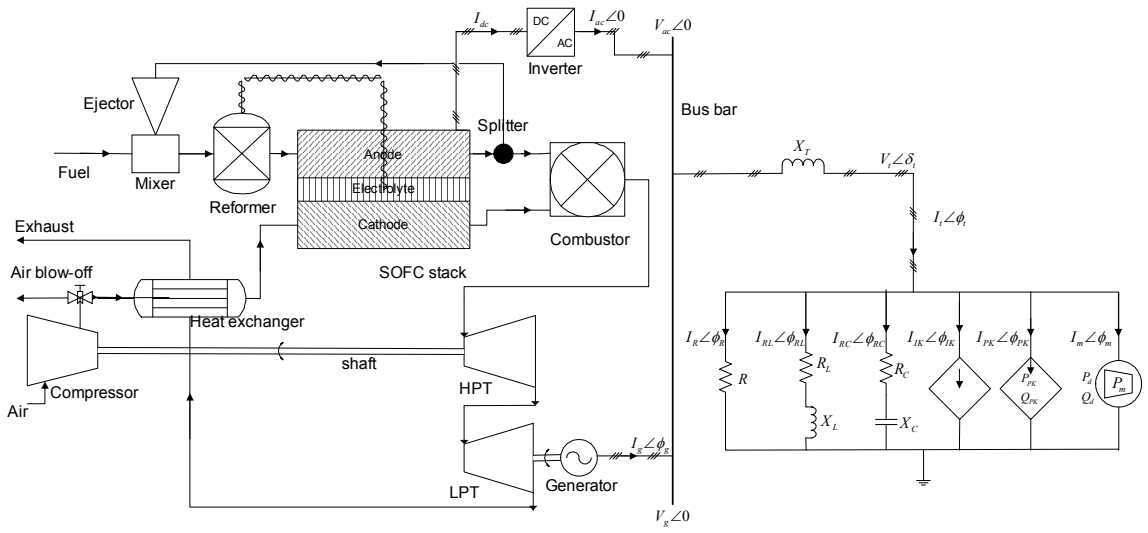

Figure 4.1: SOFC/GT hybrid system integrated in an autonomous power system

of a group of representative samples through the nonlinear transformation ([8], [2]). In EKF, the pdf propagation is approximated by a linear transformation obtained by the linearization of the nonlinear transformation at the present state. Compared to the EKF, the UKF approximates the pdf propagation for a nonlinear system in an efficient way, thus making the UKF estimation accurate up to the second order in estimating the mean and covariance. Furthermore, the computation of the Jacobian is not needed in implementing the UKF. This motivates us to apply the UKF for the state estimation of the hybrid system.

The paper is organized as follows: The SOFC/GT hybrid system is described at the system level. A brief description of modeling of all the components of the system is presented. The developed control structure with PI controllers and the need for MPC are presented. A brief description of UKF principle is explained and simulation results of state estimation are presented.

4.2 Process description

A schematic diagram of the integrated system where the hybrid system is connected to the load by a bus bar is shown in Figure 4.1. Methane (fuel) is mixed with a part of anode flue gas and is partially steam reformed in pre-reformer generating hydrogen. The heat required for endothermic reformation reactions in the pre-reformer is supplied from the SOFC stack through radiation. The gas mixture from the pre-reformer is fed to the anode volume of the SOFC, where the remaining part of the methane is reformed. Compressed atmospheric air is heated in a recuperative heat exchanger and is used as an oxygen source at the cathode side of the SOFC. In the SOFC, electrochemical reactions take place and DC voltage is produced. The rate of the electrochemical reactions depends on the current. A part of the anode flue gas is recycled to supply steam to the pre-reformer. The remaining part of the anode and cathode flue gases is supplied to a combustion chamber where the unused fuel is combusted. The hybrid system considered here uses a double shaft GT configuration. The combusted gas mixture is expanded in a high pressure turbine (HPT) with variable shaft speed driving the compressor. The HPT flue gas is further expanded to atmospheric pressure in a low pressure turbine (LPT) with constant shaft speed, which is coupled to a synchronous generator producing AC electric power. The expanded gas mixture is used to heat up the compressed air in a heat exchanger. The DC power from the SOFC stack is fed to an inverter which converts DC to AC with a fixed frequency. The inverter and the generator are connected to a local grid, which is connected to a six branch electric load. Both the SOFC stack and the generator supply the electric load demand on the grid. The load sharing between the SOFC stack and the generator cannot be controlled when there is a load change on the grid. Typically 60-70% of the total power is supplied by the SOFC stack.

4.3 Modeling

All the models of the system are developed in the modular modeling environment gPROMS [1]. The detailed modeling of each component of the system can be found in appendix B. A brief description of the each model is presented below.

4.3.1 SOFC stack

It is assumed that all the SOFCs in the stack operate at identical conditions along the fuel flow direction. A zero-dimensional SOFC model is developed with no regard to the geometry of the cell. The model developed is a lumped one, which includes dynamic molar balances of all the species both in anode and cathode volumes separately. It includes an energy balance treating the whole SOFC as a single volume to model the temperature dynamics of the SOFC solid phase mean temperature. There is a radiation from the SOFC to the pre-reformer. The voltage developed across the cell is modeled using Nernst equation, the operating cell voltage is calculated by considering both ohmic and activation losses.

In [5], the low complexity, control relevant SOFC model is evaluated against a detailed model developed in [7]. The comparisons indicate that the low complexity model is sufficient to approximate the important dynamics of the SOFC and can hence be used for operability and control studies.

4.3.2 Pre-reformer

The pre-reformer is modeled as a Continuously Stirred Tank Reactor (CSTR). Mass balances of all the species are included dynamically and energy balance is implemented to model the pre-reformer temperature dynamics. The steam required for the steam-reforming is provided by the recycle flow of the anode flue gas. The heat required for the endothermic reforming reaction is obtained by the radiation heat from the SOFC stack.

4.3.3 Combustor

In the combustor, the unused fuel is burnt in presence of oxygen coming from the cathode outlet. The operating conditions will always be such that there is excess oxygen available for complete combustion due to the fact that air mass flow rate is much larger than the fuel mass flow rate. In the combustor, the fuel can be methane, hydrogen or carbon monoxide or a mixture of these fuels. As the combustion process is rapid it is modeled as a steady-state process.

4.3.4 Heat exchanger

A simple model of a counter-flow heat exchanger is used, in which the amount of the heat exchanged depends on the heat transfer coefficient of the exchanger wall and also on the average temperature difference between the hot and cold streams. A first order transfer function describes the dynamics of the temperatures of both the streams.

4.3.5 Gas turbine cycle

The compressor and turbine models are based on steady state performance map characteristics [6]. The map is modeled using polynomials of 4th and 5th order for reduced mass flow, pressure and efficiency as functions of reduced shaft speed and operation line. A shaft model accounts for the dynamics of the rotating mass in the gas turbine system.

4.3.6 Electrical components

A simple model of the inverter is used to convert DC electric power from the SOFC stack to AC, which is given to an autonomous grid. The grid side voltage is maintained constant at 230V by using the inverter controllers and the dynamics of these controllers are neglected. An AC-AC frequency converter with 95% efficiency is assumed to be connected to the alternator to convert the varying frequency of the alternator to the grid frequency. The operating voltage of the alternator is controlled to the grid voltage by controlling the field current in the alternator. The electric load connected to the gird is represented by six parallel branches with different components in each branch. It is categorized into 4 types of loads: constant impedance, constant current, constant power and induction motor load. The constant impedance, constant current and constant power load represent the residential loads such as lights, water heaters, ovens etc. The induction motor load is considered to represent an industrial load. The constant impedance load is represented by the first three branches with resistive, inductive and capacitive loads. The fourth and fifth branches represent the constant current and constant power loads respectively. The sixth branch represents the induction motor load. The total load current is the sum of the currents from the inverter and the alternator.

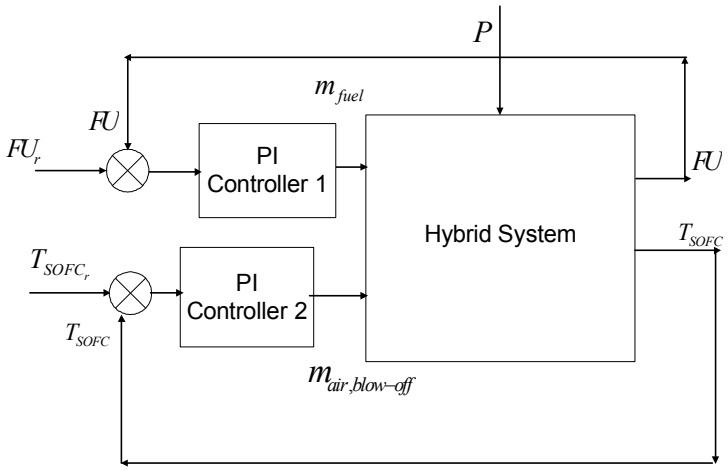

Figure 4.2: De-centralized control structure using PI controllers

4.4 Regulatory controller

Local regulatory control has been considered for the system, and the local control adds additional state to the system. Thus, to design state estimation of the complete system, the local control strategy has to be understood.

A control system is designed for the hybrid system to reject the disturbances; disturbances can be load changes, changes in fuel and air temperatures and pressures, fuel composition etc. Also during the disturbances, the SOFC temperature should also be controlled; otherwise it may lead to a cell break down. A decentralized control scheme with two PI controllers is proposed in [4] to reject the disturbances and to control the SOFC temperature as shown in Figure 4.2.

In Figure 4.2, FU refers to Fuel Utilization, which is defined as the ratio of fuel used in the SOFC and the fuel supplied to the SOFC. It is controlled to the reference value (0.85) by manipulating the fuel flow to the system. The air blow-off flow is manipulated to control the SOFC temperature to the reference value. The controller performs well in terms of tracking (Kandepu, et al., 2006a); the system efficiency can be improved by optimizing the reference values of the controlled variables. Also there are some constraints which are to be taken into account, for example, steam to carbon

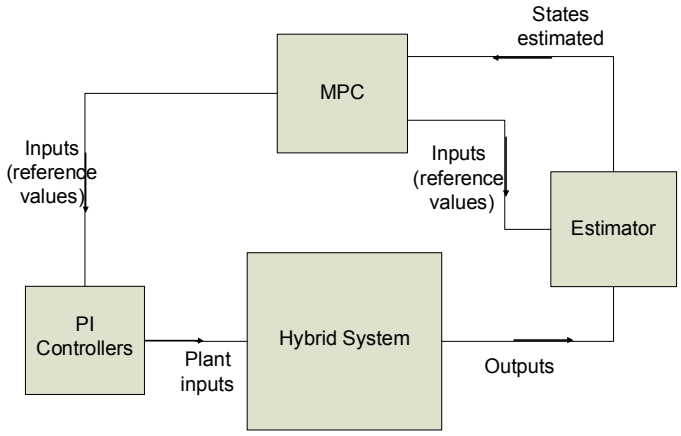

Figure 4.3: Overall control structure

ratio at pre-reformer inlet, differential pressure across anode and cathode, compressor surge etc. To achieve this, MPC is necessary and overall control structure is as shown in Figure 4.3. As a basis to develop the MPC as well as monitoring of the hybrid system, the state estimator is to be designed.

4.5 State estimation using UKF

The principle of the UKF is explained with the following example: let x be a random variable and

$$y = f(x) \tag{4.1}$$

be a nonlinear function. The question is how the UKF approximate the propagation of pdf of x? For example, in the case of Gaussian distribution, how to calculate the mean ($\overline{y}$) and covariance (Σ_y) of y? Consider a set of sigma points $x^{(i)}$, (similar to the random samples of a specific distribution function in Monte Carlo simulations) with each point being associated with a weight $w^{(i)}$. Both the sigma points and the weights are computed deterministically through a set of conditions given in [3]. Then the following steps are involved in approximating the mean and covariance:

1. Propagate each sigma point through the nonlinear function,

$$y^{(i)} = f(x^{(i)}) \tag{4.2}$$

2. Mean is the weighted average of the transformed points,

$$\overline{y} = \sum_{i=0}^{p} w^{(i)} y^{(i)} \tag{4.3}$$

3. The covariance is the weighted outer product of the transformed points,

$$\Sigma_y = \sum_{i=0}^{p} w^{(i)} \left(y^{(i)} - \overline{y}\right) \left(y^{(i)} - \overline{y}\right)^T \tag{4.4}$$

The UKF algorithm is presented below; for the fundamental theory, refer to [8, 2]. Let the system be represented by the following standard discrete time equations:

$$x_k = f(x_{k-1}, v_{k-1}, u_{k-1}) \tag{4.5}$$

$$y_k = h\left(x_k, n_k, u_k\right) \tag{4.6}$$

where x is the system state, v the process noise, n the observation noise, u the input and y the noisy observation of the system. An augmented state at time instant k,

$$x_k^a = \begin{bmatrix} x_k \\ v_k \\ n_k \end{bmatrix} \tag{4.7}$$

is defined. The augmented state variable dimension is,

$$L = L_x + L_v + L_n \tag{4.8}$$

where L_x is the original state dimension, L_v is the process noise dimension and L_n is the observation noise dimension. Similarly, the augmented state covariance matrix is built from the covariance matrices of x, v,and n:

$$P^a = \begin{bmatrix} P_x & 0 & 0 \\ 0 & R_v & 0 \\ 0 & 0 & R_n \end{bmatrix} \tag{4.9}$$

where R_v and R_n are the process and observation noise covariance matrices.

Algorithm:

- *Initialization* :

$$\widehat{x}_0 = E\left[x_0\right], \quad P_{x_0} = E\left[\left(x_0 - \widehat{x}_0\right)\left(x_0 - \widehat{x}_0\right)^T\right] \tag{4.10}$$

$$\widehat{x}_0^a = E\left[x^a\right] = E\left[\widehat{x}_0 \quad 0 \quad 0\right]^T \tag{4.11}$$

$$\begin{aligned} P_0^a &= E\left[\left(x_0^a - \widehat{x}_0^a\right)\left(x_0^a - \widehat{x}_0^a\right)^T\right] \\ &= \begin{bmatrix} P_x & 0 & 0 \\ 0 & R_v & 0 \\ 0 & 0 & R_n \end{bmatrix} \end{aligned} \tag{4.12}$$

- *For* $k = 1, 2, ...\infty$:

1. Calculate sigma-points [8]:

$$\chi_{k-1}^a = \left[\begin{array}{ccc} \widehat{x}_{k-1}^a & \widehat{x}_{k-1}^a + \gamma\sqrt{P_{k-1}^a} & \widehat{x}_{k-1}^a - \gamma\sqrt{P_{k-1}^a} \end{array}\right] \tag{4.13}$$

   where γ is a scaling parameter.

2. Time-update equations:

$$\chi_{k/k-1}^x = f\left(\chi_{k-1}^x, \chi_{k-1}^v, u_{k-1}\right) \tag{4.14}$$

$$\widehat{x}_k^- = \sum_{i=0}^{2L} w_i^{(m)} \chi_{i,k/k-1}^x \tag{4.15}$$

$$P_{x_k}^- = \sum_{i=0}^{2L} w_i^{(c)} \left(\chi_{i,k/k-1}^x - \widehat{x}_k^-\right)\left(\chi_{i,k/k-1}^x - \widehat{x}_k^-\right)^T \tag{4.16}$$

3. Measurement-update equations:

$$y_{k/k-1} = h\left(\chi_{k/k-1}^x, \chi_{k-1}^n\right) \tag{4.17}$$

$$\widehat{y_k^-} = \sum_{i=0}^{2L} w_i^{(m)} y_{i,k/k-1} \tag{4.18}$$

Table 4.1: Inputs

No.	**Input**
1	FU reference point
2	SOFC temperature reference point
3	electric load on the system (measured disturbance)

Table 4.2: Outputs

No.	**Output**
1	Pre-reformer temperature (K)
2	Shaft speed (rad/s)
3	Heat exchanger hot stream temperature (K)
4	Heat exchanger cold stream temperature (K)
5	SOFC outlet temperature (K)
6	Combustor outlet temperature (K)
7	Fuel mass flow rate (kg/s)
8	Anode recycle flow rate (kg/s)
9	Flow to the combustion chamber (kg/s)
10	Air blow-off flow rate (kg/s)
11	Air mass flow rate (kg/s)
12	SOFC current (A)
13	SOFC voltage (V)
14	Generator power (kW)

$$P_{\overline{y}_k} = \sum_{i=0}^{2L} w_i^{(c)} \left(y_{i,k/k-1} - \widehat{y_k^-}\right) \left(y_{i,k/k-1} - \widehat{y_k^-}\right)^T \tag{4.19}$$

$$P_{x_k y_k} = \sum_{i=0}^{2L} w_i^{(c)} \left(\chi_{i,k/k-1}^x - \widehat{x_k^-}\right) \left(y_{i,k/k-1} - \widehat{y_k^-}\right)^T \tag{4.20}$$

$$K_k = P_{x_k y_k} P_{\overline{y}_k}^{-1} \tag{4.21}$$

$$\widehat{x}_k = \widehat{x_k^-} + K_k \left(y_k - \widehat{y_k^-}\right) \tag{4.22}$$

$$P_{x_k} = P_{x_k}^- - K_k P_{\overline{y}_k} K_k^T \tag{4.23}$$

Table 4.3: States

No.	**State**
1	Pre-reformer temperature (K)
2	H_2 concentration in pre-reformer (mol)
3	CH_4 concentration in pre-reformer (mol)
4	H_2O concentration in pre-reformer (mol)
5	CO concentration in pre-reformer (mol)
6	CO_2 concentration in pre-reformer (mol)
7	PI controller 1 integral term
8	Compressor shaft speed (rad/s)
9	PI controller 2 integral term
10	Heat exchanger hot stream temperature (K)
11	Heat exchanger cold stream temperature (K)
12	O_2 concentration in cathode (mol)
13	H_2 concentration in anode (mol)
14	CH_4 concentration in anode (mol)
15	H_2O concentration in anode (mol)
16	CO concentration in anode (mol)
17	CO_2 concentration in anode (mol)
18	SOFC outlet temperature (K)

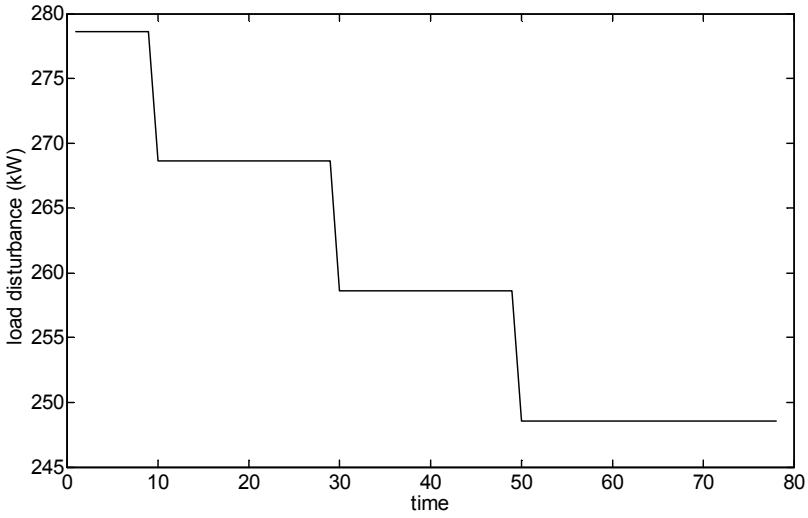

Figure 4.4: Load perturbation on the hybrid system

4.5.1 The SOFC/GT hybrid system description

The SOC/GT hybrid system is modeled in gPROMS [1] modeling environment. It has 3 inputs, 14 measured outputs and 18 states which are listed in Tables 1, 2, and 3 respectively. The hybrid system model in gPROMS is exported to matlab and can be used as function in matlab using the gO:MATLAB package [1].

4.5.2 Simulations and results

Process and observation noises that are applied to the system are white noise with Gaussian distribution. A simulation is done with disturbances in the load as shown in Figure 4.4. The initial state estimate is taken very near to the actual state and the initial state covariance matrix (P_x) is tuned in order to get a satisfactory predicted estimate. The simulation is performed online while applying the load disturbance, process noise and observation noise.

The main challenge in designing the UKF is to tune the state covariance matrix P_x, to be able to get satisfactory results. The simulations results are

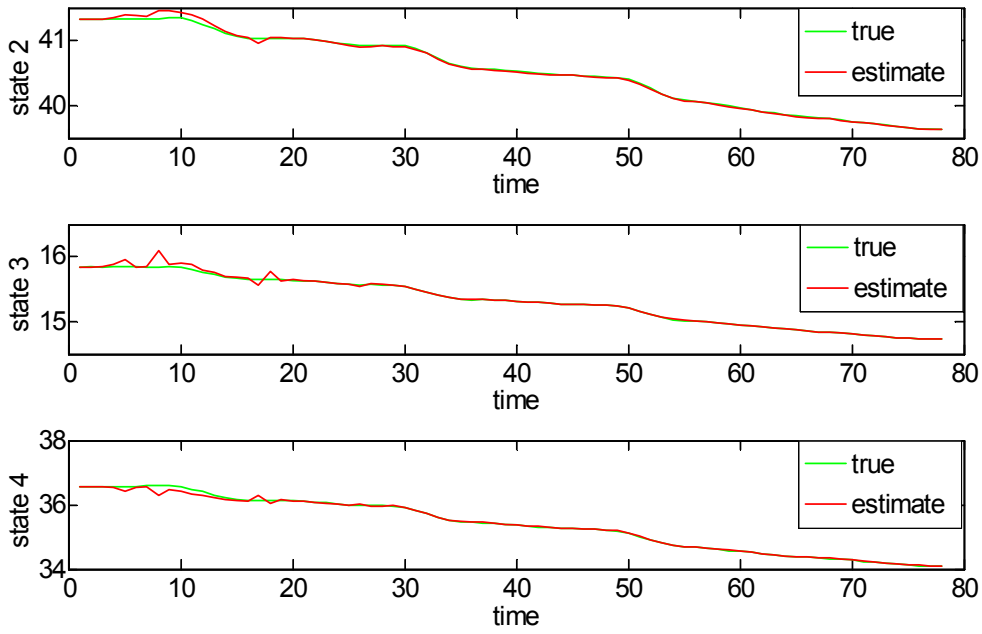

Figure 4.5: State estimation results showing the estimaed and actual states; concentrations of H_2, CH_4 and H_2O in pre-reformer

presented in Figures 4.5, 4.6 and 4.7.

The simulation results (Fig. 4.5, 4.6 and 4.7) show that UKF is promising in tracking the actual state of the SOFC/GT hybrid system. The present results are with the assumption that the initial state estimate is very near to the actual state. This condition has to be met to avoid numerical problems in numerical solver for the nonlinear differential equations. The estimated state from UKF tracks actual state well even in the presence of significant load perturbations plus process and observation noise. Without the numerical issue in the nonlinear equation solution, we expect a good performance to be achieved, even if the initial state estimate is significantly different from the actual state, as the UKF estimate is able to converge in the presence of significant step perturbations in the load according to this simulation.

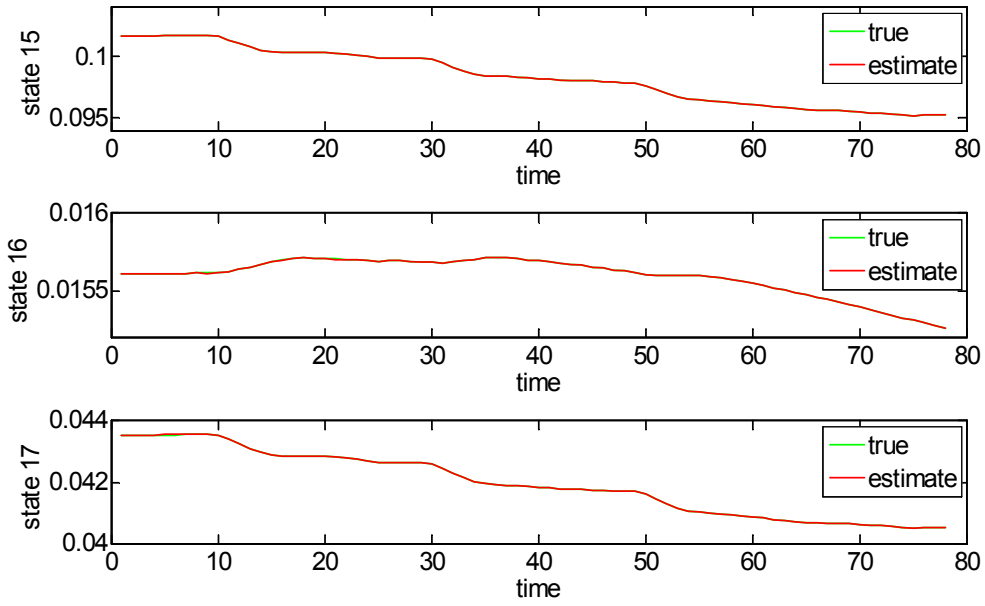

Figure 4.6: State estimation results showing the estimated and actual states; concentrations of H_2O, CO and CO_2 in SOFC anode

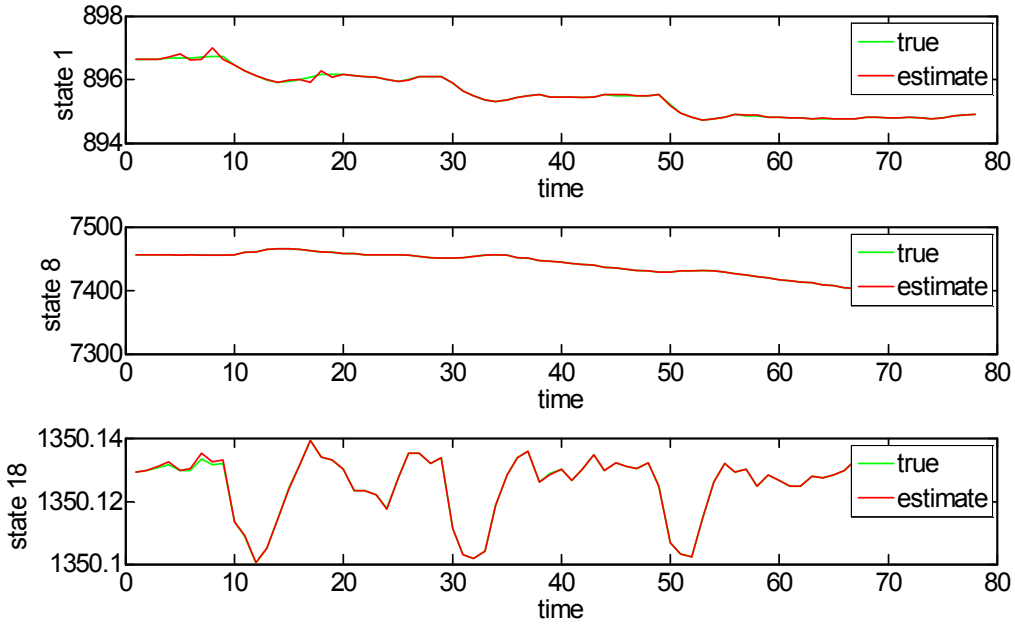

Figure 4.7: State estimation results showing the estimated and actual states; Pre-reformer, SOFC temperatures and compressor shaft speed

4.6 Conclusion and further work

The state estimator is developed for SOFC/GT hybrid system using UKF. The results show that UKF is promising in the state estimation where the system is highly nonlinear with many sub-components being tightly integrated. The implementation of UKF is simpler compared to the EKF, as there is no need of Jacobian matrices.

Further work focuses on resolving numerical issue in the simulation, applying the EKF estimator for the same application and to compare it with the developed UKF estimator. Further, the developed UKF state estimator will be used in designing the MPC for the SOFC/GT hybrid system.

4.7 Acknowledgements

Financial support from The Gas Technology Center, NTNU-SINTEF and NFR is acknowledged. We also acknowledge the funding support from Western Canada Fuel Cell Initiative (WCFCI).

References

[1] gPROMS (2004). gPROMS introductory user guide. *Process Systems Enterprise Ltd.*, 2004.

[2] B. Huang and Q. Wang. Overview of emerging bayesian approach to nonlinear system identification. *Round tables on Non-linear Model Identification, International Workshop on Solving Industrial Control and Optimization Problems, Cramado, Brazil*, 2006.

[3] S. Julier and J. K. Uhlmann. Unscented filtering and nonlinear estimation. *Proceedings of the IEEE*, 92:401–422, 2004.

[4] R. Kandepu, B. Foss, and L. Imsland. Integrated modeling and control of a load-connected sofc-gt autonomous power system. *In proceedings of 2006 American Control COnference, Minneapolis, USA, June 14-16*, pages 3463–3468, 2006.

[5] R. Kandepu, L. Imsland, B. A. Foss, C. Stiller, B. Thorud, and O. Bolland. Control-relevant SOFC modeling and model eveluation. *In the Proceedings of ECOS, the 18th Conference on Efficiency, Cost, Optimization, Simulation and Environmental Impact of Energy Systems, Trondheim, Norway, June, 20-22*, 2005.

[6] C. Stiller, B. Thorud, O. Bolland, R. Kandepu, and L. Imsland. Control strategy for a solid oxide fuel cell and gas turbine hybrid system. *Accepted for publication in the Journal of Power Sources*, 158(1):303–315, 2006.

[7] C. Stiller, B. Thorud, S. Seljebø, O. Mathisen, H. Karoliussen, and O. Bolland. Finite-volume modeling and hybrid-cycle performance of planar and tubular solid oxide fuel cells. *Journal of Power Sources*, 141:227–240, 2005.

[8] R. Van der Merwe. *PhD Thesis - Sigma-Point Kalman Filters for probability inference in dynamic state-space models*. Oregon Health and Science University, 2004.

Chapter 5

Applying the Unscented Kalman Filter for Nonlinear State Estimation

Abstract

Based on presentation of the principles of the EKF and UKF for state estimation, we discuss the differences of the two approaches. Four rather different simulation cases are considered to compare the performance. A simple procedure to include state constraints in the UKF is proposed and tested. The overall impression is that the performance of the UKF is better than the EKF in terms of robustness and speed of convergence. The computational load in applying the UKF is comparable to the EKF.

5.1 Introduction

In the process industries one of the main goals is to make the end product at the lowest possible cost while satisfying product quality constraints. State estimation often play an important role in accomplishing this goal in process control and performance monitoring applications. There are many uncertainties to deal with in process control; model uncertainties, measurement uncertainties and uncertainties in terms of different noise sources acting on the system. In this kind of environment, representing the model state

by an (approximated) probability distribution function (pdf) has distinct advantages. State estimation is a means to propagate the pdf of the system states over time in some optimal way. It is most common to use the Gaussian pdf to represent the model state, process and measurement noises. The Gaussian pdf can be characterized by its mean and covariance. The Kalman Filter (KF) propagates the mean and covariance of the pdf of the model state in an optimal (minimum mean square error) way in case of linear dynamic systems [7].

All practical systems posses some degree of nonlinearity. Depending on the type of process and the operating region of the process, some processes can be approximated with a linear model and the KF can be used for state estimation. In some cases the linear approximation may not be accurate enough, and state estimator designs using nonlinear process models are necessary. The most common way of applying the KF to a nonlinear system is in the form of the Extended Kalman Filter (EKF). In the EKF, the pdf is propagated through a linear approximation of the system around the operating point at each time instant. In doing so, the EKF needs the Jacobian matrices which may be difficult to obtain for higher order systems, especially in the case of time-critical applications. Further, the linear approximation of the system at a given time instant may introduce errors in the state which may lead the state to diverge over time. In other words, the linear approximation may not be appropriate for some systems. In order to overcome the drawbacks of the EKF, other nonlinear state estimators have been developed such as the Unscented Kalman Filter (UKF) [8], the Ensemble Kalman Filter (EnKF)[3] and high order EKFs. The EnKF is especially designed for large scale systems, for instance, oceanographic models and reservoir models [3]. The UKF seems to be a promising alternative for process control applications [14] [2] [11] [19]. The UKF propagates the pdf in a simple and effective way and it is accurate up to second order in estimating mean and covariance [8]. The present paper focuses on using the UKF for nonlinear state estimation in process systems and the performance is evaluated in comparison with the EKF. The paper proposes a simple method to incorporate state constraints in the UKF.

Section 2 describes the principles and algorithms of EKF and UKF. Section 3 introduces a method to incorporate the state constraints in the UKF state estimation and compares it with the EKF. Four examples are studied in section 4 to compare the performances of the UKF and EKF. Discussion

on the differences between the UKF and EKF is presented in section 5 and conclusions are drawn in section 6.

5.2 The EKF and UKF algorithms for nonlinear state estimation

We present the principles and algorithms of the EKF and UKF. At the end of the section, different characteristics of the EKF and UKF are compared.

5.2.1 EKF principle and algorithm

To illustrate the principle behind the EKF, consider the following example. Let $x \in \mathbb{R}^n$ be a random vector and

$$y = g(x) \tag{5.1}$$

be a nonlinear function, $g : \mathbb{R}^n \rightarrow \mathbb{R}^m$. The question is how to compute the pdf of y given the pdf of x? For example, in the case of being Gaussian, how to calculate the mean $(\overline{y})$ and covariance (Σ_y) of y? If g is a linear function and the pdf of x is a Gaussian distribution, then Kalman Filter (KF) is optimal in propagating the pdf. Even if the pdf is not Gaussian, the KF is optimal up to the first two moments in the class of linear estimators [6]. The KF is extended to the class of nonlinear systems termed EKF, by using linearization. In the case of a nonlinear function $(g(x))$, the nonlinear function is linearized around the current value of x, and the KF theory is applied to get the mean and covariance of y. In other words, the mean $(\overline{y}^{EKF})$and covariance (P_y^{EKF}) of y, given the mean $(\overline{x})$ and covariance (P_x) of the pdf of x are calculated as follows:

$$\overline{y}^{EKF} = g(\overline{x}) \tag{5.2}$$

$$P_y^{EKF} = (\nabla g) P_x (\nabla g)^T \tag{5.3}$$

where (∇g) is the Jacobian of $g(x)$ at $\overline{x}$.

Algorithm

Let a general nonlinear system be represented by the following standard discrete time equations:

$$x_k = f(x_{k-1}, v_{k-1}, u_{k-1}) \tag{5.4}$$

$$y_k = h\left(x_k, n_k, u_k\right) \tag{5.5}$$

where $x \in \mathbb{R}^{n_x}$ is the system state, $v \in \mathbb{R}^{n_v}$ the process noise, $n \in \mathbb{R}^{n_n}$ the observation noise, u the input and y the noisy observation of the system. The nonlinear functions f and h are need not necessarily be continuous. The EKF algorithm for this system is presented below:

- *Initialization at* $k = 0$:

$$\begin{aligned}
\widehat{x}_0 &= E\left[x_0\right], \\
P_{x_0} &= E\left[\left(x_0 - \widehat{x}_0\right)\left(x_0 - \widehat{x}_0\right)^T\right] \\
P_v &= E\left[\left(v - \overline{v}\right)\left(v - \overline{v}\right)^T\right] \\
P_n &= E\left[\left(n - \overline{n}\right)\left(n - \overline{n}\right)^T\right]
\end{aligned}$$

- *For* $k = 1, 2, ..\infty$:

  1. Prediction step
     (a) Compute the process model Jacobians:

$$\begin{aligned}
F_{x_k} &= \nabla_x f\left(x, \overline{v}, u_{k-1}\right)|_{x=\widehat{x}_{k-1}} \\
G_v &= \nabla_v f\left(\widehat{x}_{k-1}, v, u_k\right)|_{v=\overline{v}}
\end{aligned}$$

     (b) Compute predicted state mean and covariance (*time update*)

$$\begin{aligned}
\widehat{x}_k^- &= f\left(\widehat{x}_{k-1}, \overline{v}, u_k\right) \\
P_{x_k}^- &= F_{x_k} P_{x_k} F_{x_k}^T + G_v P_v G_v^T
\end{aligned}$$

  2. Correction step
     (a) Compute observation model Jacobians:

$$\begin{aligned}
H_{x_k} &= \nabla_x h\left(x, \overline{n}, u_k\right)|_{x=\widehat{x}_k^-} \\
D_n &= \nabla_n h\left(\widehat{x}_k^-, n, u_k\right)|_{n=\overline{n}}
\end{aligned}$$

     (b) Update estimates with latest observation (*measurement update*)

$$\begin{aligned}
K_k &= P_{x_k}^- H_{x_k}^T \left(H_{x_k} P_{x_k}^- H_{x_k}^T + D_n P_n D_n^T\right)^{-1} \\
\widehat{x}_k &= \widehat{x}_k^- + K_k\left[y_k - h\left(\widehat{x}_k^-, \overline{n}\right)\right] \\
P_{x_k} &= \left(I - K_k H_{x_k}\right) P_{x_k}^-
\end{aligned}$$

5.2.2 UKF principle and algorithm

Consider now the same example as in the previous section. The question is how the UKF compute pdf of y given the pdf of x, in other words, how to calculate the mean $\left(\overline{y}^{UKF}\right)$ and covariance $\left(P_y^{UKF}\right)$ of y, in the case of being Gaussian? Consider a set of points

$$x^{(i)},\ i \in \{1, ..., p\},\ p = 2n + 1,$$

(similar to the random samples of a specific distribution function in Monte Carlo simulations) with each point being associated with a weight $w^{(i)}$. These sample points are termed as sigma points. Then the following steps are involved in approximating the mean and covariance: Propagate each sigma point through the nonlinear function,

$$y^{(i)} = g(x^{(i)})$$

- the mean is approximated by the weighted average of the transformed points,

$$\overline{y}^{UKF} = \sum_{i=0}^{p} w^{(i)} y^{(i)},\quad \Sigma w^{(i)} = 1$$

- and the covariance is computed by the weighted outer product of the transformed points,

$$P_y^{EKF} = \sum_{i=0}^{p} w^{(i)} \left(y^{(i)} - \overline{y}\right) \left(y^{(i)} - \overline{y}\right)^T.$$

  Both the sigma points and the weights are computed deterministically through a set of conditions given in [8].

Algorithm

The UKF algorithm is presented below; for background theory, refer to [20], [8] and [6]. Let the system be represented by (5.4) and (5.5). An augmented state at time instant k,

$$x_k^a \triangleq \begin{bmatrix} x_k \\ v_k \\ n_k \end{bmatrix} \tag{5.6}$$

is defined. The augmented state dimension is,

$$N = n_x + n_v + n_n \tag{5.7}$$

Similarly, the augmented state covariance matrix is built from the covariance matrices of x, v and n,

$$P^a \triangleq \begin{bmatrix} P_x & 0 & 0 \\ 0 & P_v & 0 \\ 0 & 0 & P_n \end{bmatrix} \tag{5.8}$$

where P_v and P_n are the process and observation noise covariance matrices.

- *Initialization at* $k = 0$:

$$\begin{aligned} \widehat{x}_0 &= E[x_0], \quad P_{x_0} = E\left[(x_0 - \widehat{x}_0)(x_0 - \widehat{x}_0)^T\right] \\ \widehat{x}_0^a &= E[x^a] = E[\widehat{x}_0 \quad 0 \quad 0]^T \\ P_0^a &= E\left[(x_0^a - \widehat{x}_0^a)(x_0^a - \widehat{x}_0^a)^T\right] = \begin{bmatrix} P_x & 0 & 0 \\ 0 & P_v & 0 \\ 0 & 0 & P_n \end{bmatrix} \end{aligned}$$

- *For* $k = 1, 2, ...\infty$:

  1. Calculate $2N + 1$ sigma-points based on the present state covariance:

$$\mathbf{X}_{i,k-1}^a \begin{cases} \triangleq \widehat{x}_{k-1}^a, & i = 0 \\ \triangleq \widehat{x}_{k-1}^a + \gamma \mathbf{S}_i, & i = 1, ..., N \\ \triangleq \widehat{x}_{k-1}^a - \gamma \mathbf{S}_i, & i = N+1, ..., 2N \end{cases} \tag{5.9}$$

  where $\mathbf{S}_i$ is the ith column of the matrix,

$$S = \sqrt{P_{k-1}^a}.$$

  In (5.9) γ is a scaling parameter [20],

$$\gamma = \sqrt{N + \lambda}, \quad \lambda = \alpha^2(N + \kappa) - N$$

  where α and κ are tuning parameters. We must choose $\kappa \geq 0$, to guarantee the semi-positive definiteness of the covariance matrix,

a good default choice is $\kappa = 0$. The parameter α, $0 \leq \alpha \leq 1$, controls the size of the sigma-point distribution and it should ideally be a small number [20].

The ith sigma point (augmented) is the ith column of the sigma point matrix,

$$\mathbf{X}^a_{i,k-1} = \begin{bmatrix} \mathbf{X}^x_{i,k-1} \\ \mathbf{X}^v_{i,k-1} \\ \mathbf{X}^n_{i,k-1} \end{bmatrix}$$

where the superscripts x, v and n refer to a partition conformal to the dimensions of the state, process noise and measurement noise respectively.

2. Time-update equations:

Transform the sigma points through the state-update function,

$$\mathbf{X}^x_{i,k/k-1} = f\left(\mathbf{X}^x_{i,k-1}, \mathbf{X}^v_{i,k-1}, u_{k-1}\right), \; i = 0, 1, ..., 2N \tag{5.10}$$

Calculate the apriori state estimate and apriori covariance,

$$\widehat{x}^-_k = \sum_{i=0}^{2N} \left(w^{(i)}_m \mathbf{X}^x_{i,k/k-1}\right) \tag{5.11}$$

$$P^-_{x_k} = \sum_{i=0}^{2N} w^{(i)}_c \left(\mathbf{X}^x_{i,k/k-1} - \widehat{x}^-_k\right)\left(\mathbf{X}^x_{i,k/k-1} - \widehat{x}^-_k\right)^T. \tag{5.12}$$

The weights $w^{(i)}_m$ and $w^{(i)}_c$ are defined as,

$$\begin{aligned} w^{(0)}_m &= \frac{\lambda}{N+\lambda}, \quad i = 0, \\ w^{(0)}_c &= \frac{\lambda}{N+\lambda} + (1 - \alpha^2 + \beta), \quad i = 0, \\ w^{(i)}_m &= w^{(i)}_c = \frac{1}{2(N+\lambda)}, \quad i = 1, ..., 2N, \end{aligned}$$

where β is a non-negative weighting parameter introduced to affect the weighting of the zeroth sigma-point for the calculation of the covariance. This parameter (β) can be used to incorporate knowledge of the higher order moments of the distribution. For a Gaussian prior the optimal choice is $\beta = 2$ [20].

3. Measurement-update equations:

   Transform the sigma points through the measurement-update function,

$$\mathbf{Y}_{i,k/k-1} = h\left(\mathbf{X}^x_{i,k/k-1}, \mathbf{X}^n_{k-1}, u_k\right), \; i = 0, 1, ..., 2N \tag{5.13}$$

   and the mean and covariance of the measurement vector is calculated,

$$\begin{aligned} \widehat{y_k^-} &= \sum_{i=0}^{2N} w_m^{(i)} \mathbf{Y}_{i,k/k-1} \\ P_{\overline{y}_k} &= \sum_{i=0}^{2N} w_c^{(i)} \left(\mathbf{Y}_{i,k/k-1} - \widehat{y_k^-}\right)\left(\mathbf{Y}_{i,k/k-1} - \widehat{y_k^-}\right)^T. \end{aligned}$$

   The cross covariance is calculated according to

$$P_{x_k y_k} = \sum_{i=0}^{2N} w_c^{(i)} \left(\mathbf{X}^x_{i,k/k-1} - \widehat{x_k^-}\right)\left(\mathbf{Y}_{i,k/k-1} - \widehat{y_k^-}\right)^T.$$

   The Kalman gain is given by,

$$K_k = P_{x_k y_k} P_{\overline{y}_k}^{-1},$$

   and the UKF estimate and its covariance are computed from the standard Kalman update equations,

$$\widehat{x}_k = \widehat{x_k^-} + K_k\left(y_k - \widehat{y_k^-}\right), \tag{5.14}$$

$$P_{x_k} = P_{x_k^-} - K_k P_{\overline{y}_k} K_k^T.$$

5.2.3 Discussion

The difference in the principles of state estimation using UKF and EKF is illustrated based the Figure 5.1 by considering the following example,

$$y = g(x) = x^2, \quad x \in \mathbb{R}, \quad \overline{x} = X_{mean} = 6, \quad \Sigma_x = 16.$$

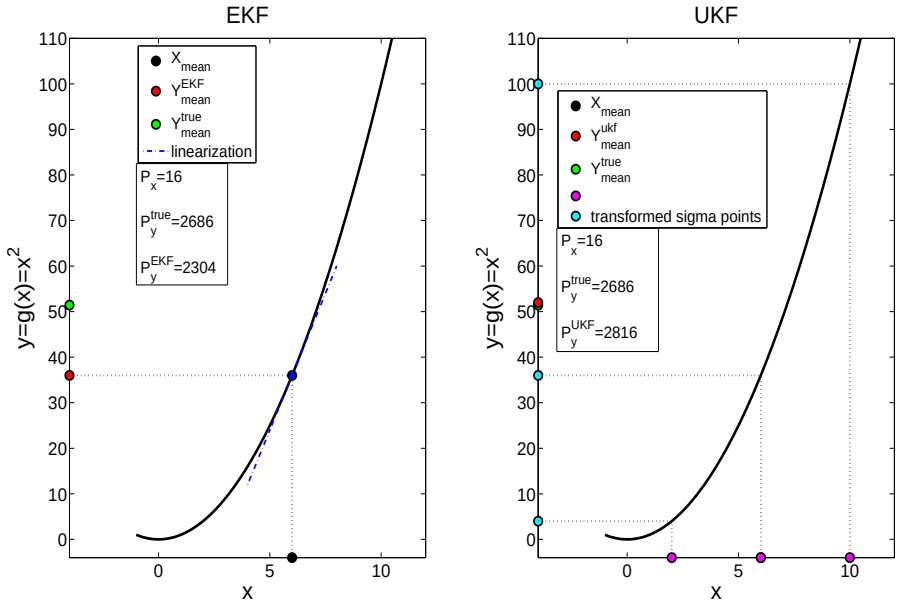

Figure 5.1: Illustration of principle of EKF and UKF

The figure illustrates how the mean and variance of x are propagated to obtain mean and variance of y for EKF and UKF. The true mean and variance are calculated by using the following equations,

$$\begin{aligned} Y_{mean}^{true} &= E\left[g(x)\right] = \int_{-\infty}^{\infty} x^2 . \frac{1}{\sqrt{2\pi}\sigma} e^{-\frac{1}{2}\left(\frac{x-\overline{x}}{\sigma}\right)^2} dx \\ P_y^{true} &= E\left[\left(g(x) - E\left[g(x)\right]\right)^2\right] \end{aligned}$$

where $\sigma = \sqrt{\Sigma_x}$ is the standard deviation. The true mean and variance are 51.43 and 2686 respectively. The EKF mean is obtained by using (5.2) giving

$$Y_{mean}^{EKF} = 36.00,$$

and the variance is obtained by performing the linearization as shown in the figure and using (5.3),

$$P_y^{EKF} = 2304.$$

For the UKF, three sigma points are propagated through the function, and the mean and variance are calculated accordingly,

$$\begin{aligned} Y_{mean}^{UKF} &= 52.00, \\ P_y^{EKF} &= 2816. \end{aligned}$$

The UKF approximates the propagation of the pdf through the nonlinearity more accurately when compared to the EKF as illustrated by the numbers in the example above.

In the EKF algorithm, during the time-update (prediction) step, the mean is propagated through the nonlinear function, in other words, this introduces an error since in general $\overline{y} \neq g(\overline{x})$. In case of the UKF, during the time-update step, all the sigma points are propagated through the nonlinear function which makes the UKF a better and more effective nonlinear approximator. The UKF principle is simple and easy to implement as it does not require the calculation of Jacobians at each time step. The UKF is accurate up to second order moments in the pdf propagation where as the EKF is accurate up to first order moment [20].

Later, we will see that it is possible to implement state constraints by proper conditioning of the sigma points. An example (state estimation of a reversible reaction) will be considered to illustrate the constraint handling capability of the UKF.

5.3 State estimation with constraints

Constraints on states to be estimated are important model information that is often not used in state estimation. Typically, such constraints are due to physical limitations on the states; for instance, estimated concentrations should remain positive. In Kalman filter theory, there is no general way of incorporating these constraints into the estimation problem. However, the constraints can be incorporated in the KF by projecting the unconstrained KF estimates onto the boundary of the feasible region at each time step [16] [18]. An other way of nonlinear state estimation with constraints is Moving Horizon Estimation (MHE), in which the constraints can be included in the estimation problem in a natural way [12]. In MHE, the state trajectory is computed taking state constraints into account at the expense of solving a nonlinear programing problem at each time step. The numerical optimization at each time step may be a challenge in time-critical applications. In this section, a new and simple method is introduced to handle state constraints in the UKF and it is compared to the standard way of constraint handling in the EKF, known as 'clipping' [5].

Assume that the state constraints are represented by box constraints,

$$x_L \leq x \leq x_H.$$

We will illustrate the method for $x \in \mathbb{R}^2$. In case of a second order system, the feasible region by the box constraints can be represented by a rectangle as in Figure 5.2. The figure shows the illustration of the steps of constraint handling in case of the EKF and UKF from one time step to the next. At $t = k-1$, the true state (x_k), its estimate ($\widehat{x}_k$) and state covariance are selected as shown in the figure. At $t = k$, the unconstrained EKF estimate ($\widehat{x}_k^{EKF}$) is outside the feasible region and is projected to the boundary of the feasible region to get the constrained EKF estimate ($x_k^{EKF,C}$) as shown in the figure. While projecting the EKF estimate, the covariance of the EKF estimate is not changed and thus the constraints have no effect on the covariance. Hence, the covariance does not include any constraint information. This way of the handling constraints in the EKF is termed as 'clipping' in literature [5].

The constraints information can be incorporated in the UKF algorithm in a simple way during the time-update step. After the propagation of the sigma points from (5.10), the (unconstrained) transformed sigma points which are outside the feasible region can be projected onto the boundary of

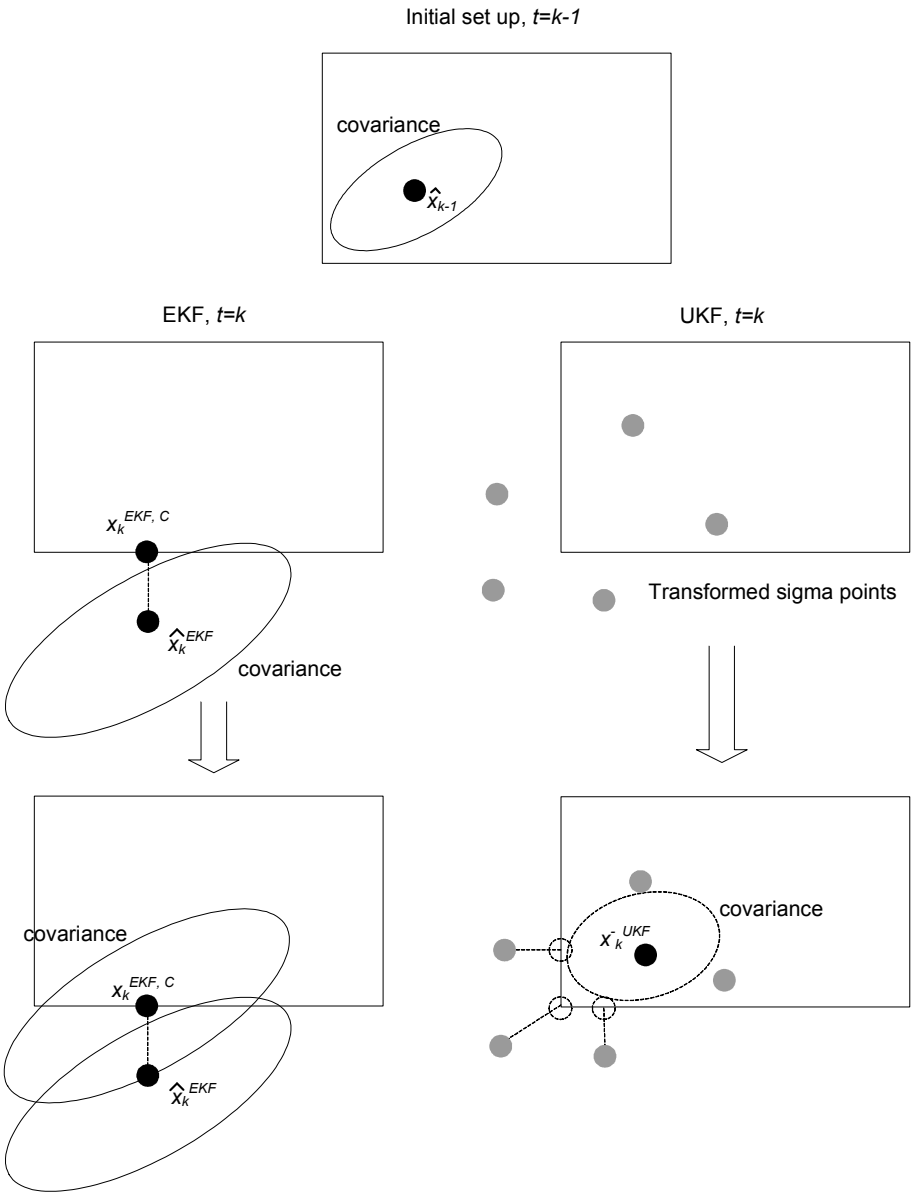

Figure 5.2: Illustration of estimation with state constraints

the feasible region and continue the further steps. In Figure 5.2, at $t = k$ three sigma points which are outside the feasible region are projected onto the boundary (lower right plot in the figure). The mean and covariance with the constrained sigma points now represents the apriori UKF estimate ($x_k^{UKF^-}$) and covariance, and they are further updated in the measurement-update step. The advantage here is that the new apriori covariance includes information on the constraints, which should make the UKF estimate more efficient (accurate) compared to the EKF estimate. An example (reversible reaction) is considered in the next section to illustrate the state estimation with constraints with the proposed method.

Extension of the proposed method to higher dimension is straightforward. Alternative linear constraints. e.g.,

$$Cx \leq d$$

are easily included by projecting the sigma point violating the inequality normally onto the boundary of feasible region. It is observed that the new (constrained) covariance obtained at a time step is lower in size compared to the unconstrained covariance. If, in case, the estimate after the measurement-update (refer (5.14)) is outside the feasible region, the same projection technique can be extended. Further, the technique can be extended to the sigma points from (5.9).

The proposed algorithm is outlined below:

Algorithm (outline)

- *For* $k = 1, 2, ...\infty$:

  1. Calculate $2N + 1$ sigma points based on the present state covariance according to (5.9) and project the sigma points which are outside the feasible region to the boundary to obtain the constrained sigma points,

     $$\mathbf{X}_{i,k-1}^{x,C} = P(\mathbf{X}_{i,k-1}^{x})\ i = 0, 1, ..., 2N$$

     where P refers to the projections.

  2. Time-update equations:
     Transform the sigma points through the state-update function,

     $$\mathbf{X}_{i,k/k-1}^{x} = f\left(\mathbf{X}_{i,k-1}^{x,C}, \mathbf{X}_{i,k-1}^{v}, u_{k-1}\right),\ i = 0, 1, ..., 2N.$$

Again apply the constrains on the transformed sigma points to obtain the constrained transformed sigma points,

$$\mathbf{X}^{x,C}_{i,k/k-1} = P(\mathbf{X}^{x}_{i,k/k-1})\ i = 0, 1, ..., 2N.$$

Calculate the apriori state estimate and apriori covariance as given in (5.11) and (5.12) using the constrained transformed sigma points $\mathbf{X}^{x,C}_{i,k/k-1}$.

3. Measurement-update equations:

   Transform the constrained sigma points through the measurement-update function as in (5.13) and obtain the UKF estimate by following the same steps given in Section 2. If UKF estimate violates the constraints, the same projection technique can be used.

5.4 Simulation studies

Four rather different examples are considered to compare different characteristics of the UKF and the EKF. First, the Van der Pol oscillator is considered to study the behavior of the UKF and also to compare the robustness of the estimator due to model errors with that of the EKF. Second, an estimation problem in an induction machine is chosen to evaluate the performances for a nonlinear system. Third, state estimation of a reversible reaction is studied to illustrate the constraint handling capability of the UKF. Finally, a Solid Oxide Fuel Cell (SOFC) combined Gas Turbine (GT) hybrid system is considered to evaluate the performances in the case of higher order, nonlinear system.

In all the examples, the following assumptions are made:

- The measurement update frequency of the KF coincides with the system discretization sampling frequency.
- The system model and the state estimator model are the same unless otherwise specified.
- Process noise and measurement noise are applied to the system. The noise is Gaussian with zero mean value.

- The tuning parameters (the initial covariance and process and measurement noise covariances) are chosen to be the same for both the EKF and UKF.

- For UKF algorithm, α, β and κ in Section 2.2 are set to the following values,

$$\alpha = 1, \beta = 2 \text{ and } \kappa = 0$$

5.4.1 Van der Pol oscillator

The Van der Pol oscillator is considered as it is a widely used example in the literature. It is highly nonlinear and, depending on the direction of time, it can exhibit both stable and unstable limit cycles [10]. In case of an unstable limit cycle, if the initial state is outside the limit cycle, it diverges and if the initial state is inside the limit cycle, it converges to zero as time progresses. In case of stable limit cycle, any non-zero initial state converges to a stable limit cycle. First, the unstable limit cycle is considered and the initial state is chosen to be just inside the limit cycle and the initial state estimate is considered outside the limit cycle to check the convergence of the UKF and EKF estimates.

Unstable limit cycle

The unstable limit cycle (Van der Pol oscillator in reverse time) is represented by the following state differential equations [10]

$$\begin{aligned} \dot{x}_1 &= -x_2, \\ \dot{x}_2 &= -\mu(1 - x_1^2)x_2 + x_1, \ \mu = 0.2. \end{aligned}$$

The output vector is defined as

$$y = \begin{bmatrix} x_1 & x_2 \end{bmatrix}^T.$$

The system is discretized with a sampling interval of 0.1. Process noise with a covariance of $10^{-3}I_2$ and measurement noise with a covariance of $10^{-3}I_2$ is added to the system states and measurements, respectively. These noise characteristics are used throughout Section. 4.1.

The initial state is chosen as

$$x_0 = \begin{bmatrix} 1.4 & 0 \end{bmatrix}^T,$$

which is just inside the limit cycle. The initial state estimate ($\widehat{x}_0$) is chosen to be outside the limit cycle, and the initial state covariance matrix (P_{x_0}), R_v and R_n are chosen as

$$\widehat{x}_0 = \begin{bmatrix} 0 & 5 \end{bmatrix}^T, \tag{5.15}$$

$$\begin{aligned} P_{x_0} &= k_x I_2, \quad R_v = k_p I_2 \text{ and } R_n = k_n I_2, \\ \text{with} \qquad & k_x = 5, k_p = 10^{-3} \text{ and } k_n = 10^{-3}. \end{aligned} \tag{5.16}$$

The true and estimated states using the UKF and EKF are shown in Figure 5.3. The UKF estimate converges to the true state and stays with it, whereas the EKF estimate could not converge to the true state as the time progresses. Figure 5.4 shows the phase portraits of the UKF and EKF estimates for the first 5 sec. It also includes the corresponding covariances of UKF and EKF estimates at each sec., drawn according to

$$\left\{x | (x - \widehat{x}_k)^T P_{x_k}^{-1} (x - \widehat{x}_k) = 1\right\}.$$

The covariances may also give an idea of the distribution of the sigma points around the mean at a given time instant in the case of the UKF. The covariances of the UKF and the EKF decrease a lot between from t=0 and t=1 sec. Further it may be observed that the later covariances for the EKF are smaller than for the UKF. The choice of P_{x_0} is reasonable here as the initial state estimate is far from the true initial state. The UKF is robust to the choices of the P_{x_0}, R_v and R_n compared to the EKF as is illustrated with the following choices,

$$k_x = 10^{-2}, \; k_p = 10^{-3} \text{ and } k_n = 1. \tag{5.17}$$

Figures 5.5 and 5.6 show the plots and phase portraits corresponding to the choices of a small P_{x_0} and a large R_n. Even though the small P_{x_0} is a bad choice for the considered $\widehat{x}_0$, the UKF estimates are still able to converge to the true states because of the measurement correction and also due to the increase of the size of the covariance until the estimates converge to the true states. On the other hand, the EKF estimate is not converging to the true state as shown in Figure 5.5. The difference can be attributed to the better nonlinear approximation by the UKF at each time step. Compared to figures 5.5 and 5.6, both the UKF and EKF estimates converge very fast

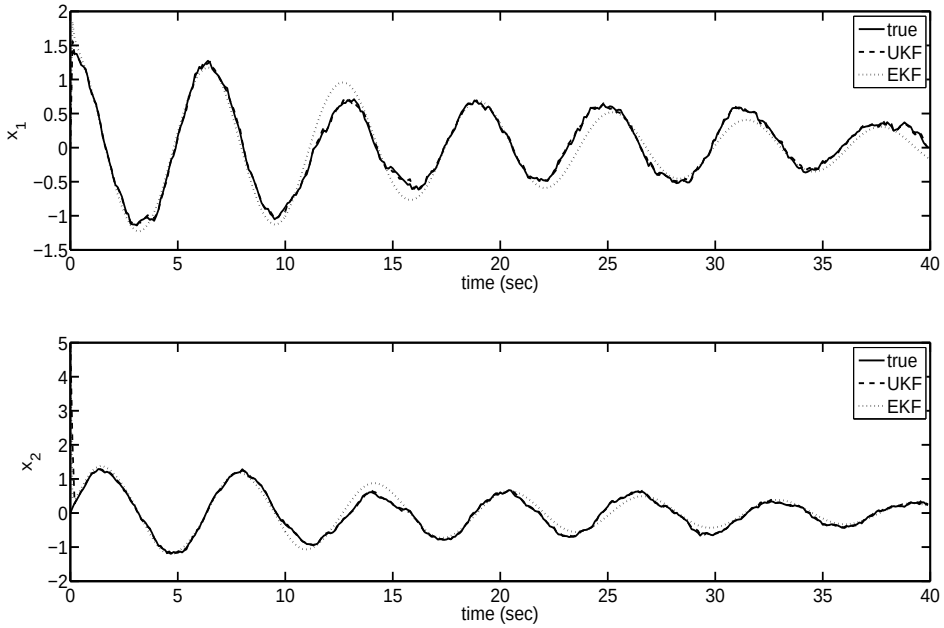

Figure 5.3: Estimated states for the Van der Pol oscillator in reverse time using UKF and EKF with an initial state estimate far from the limit cycle: large initial state covariance and small measurement noise

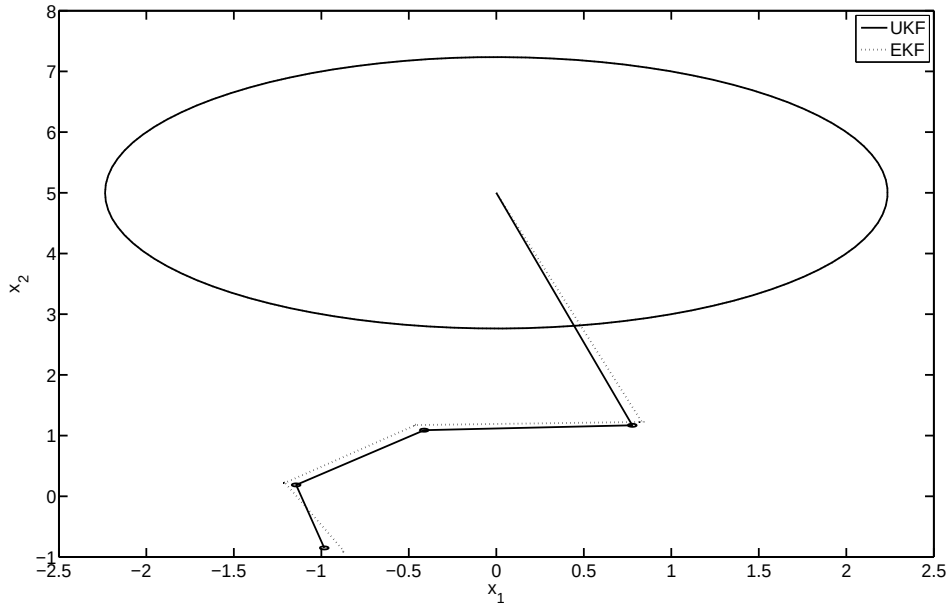

Figure 5.4: Phase portraits of UKF and EKF estimates with an initial state estimate far from limit cycle, large initial state covariance matrix and small measurment noise and with covariances plotted at each sec., until 5 sec.

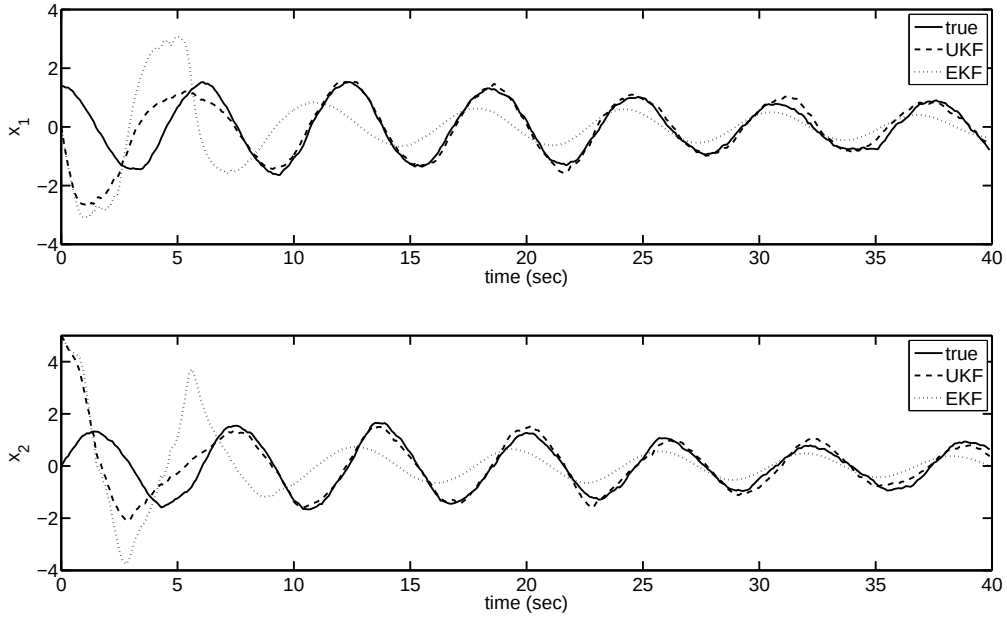

Figure 5.5: Estimated states for Van der Pol equation using UKF with an initial state estimate far from limit cycle, small initial state covariance matrix and large measurment noise covariance

in figures 5.3 and 5.4. The reason is that the assumed measurement noise is less in figures 5.3 and 5.4, and hence the feedback in the measurement-update makes the estimates converge quite fast. In figures 5.5 and 5.6, the assumed measurement noise is higher meaning that the feedback from the measurement-update is less effective.

As the UKF gives a better approximation in time-update step, the UKF estimate is able to converge quite fast, even though the measurement noise is higher and the initial covariance is a bad choice. In addition, the Kalman gain is quite different in the two estimators due to the difference in the covariances as can be observed in Figure 5.6. Hence, it is reasonable to assume that the correction step in the UKF also improves convergence as compared to the EKF.

To verify these results, two Monte Carlo simulations with 100 runs are

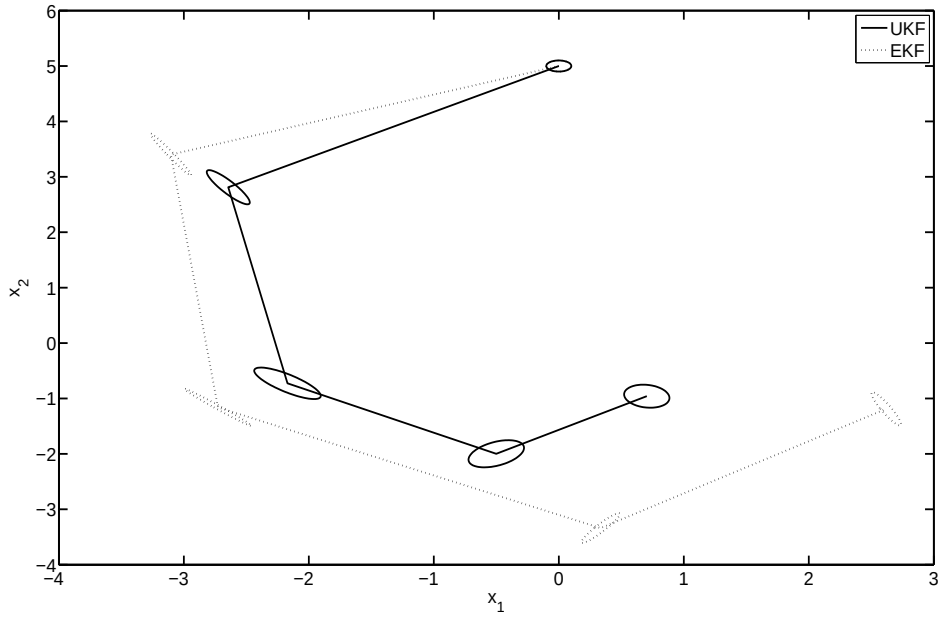

Figure 5.6: Phase portraits of UKF and EKF estimates with an initial state estimate far from limit cycle, small initial state covariance matrix and large measurment noise and with covariances plotted at each sec., until 5 sec.

performed varying the initial state, and the process and measurement noise realizations. In addition the initial state estimate is also varied. Both states of x_0 and $\widehat{x}_0$ were chosen from a normal distribution with zero mean and standard deviation 0.4. The Monte Carlo simulations differ in the choices of the tuning parameters (P_{x_0}, R_v and R_n) as given in (5.16) and (5.17). The corresponding Mean Square Errors (MSE)s of the state estimate errors for the EKF and UKF are 0.18 and 0.02, and 0.23 and 0.09 respectively. The MSEs corresponding to the UKF are considerably lower compared to that of EKF, and hence it can be concluded that the UKF gives improved performance compared to the EKF.

Stable limit cycle - with model error

In [1], it is observed that when there is a significant model error the EKF is not able to converge to the true states in case of the Van der Pol equation with a stable limit cycle. This cycle is considered to evaluate the robustness of the UKF to model errors and it is compared to that of EKF. The state and measurement equations are

$$\begin{aligned} \dot{x}_1 &= x_2, && (5.18)\\ \dot{x}_2 &= \mu(1-x_1^2)x_2 - x_1,\ \mu = 0.2, && (5.19)\\ y &= \begin{bmatrix} x_1 & x_2 \end{bmatrix}^T. && (5.20) \end{aligned}$$

In the state estimator model the value of μ is chosen as 0.5. The system is discretized with sampling interval of 0.1. An initial state is chosen as $x_0 = \begin{bmatrix} 0.5 & 0 \end{bmatrix}^T$. A initial state estimate ($\widehat{x}_0$), and initial state covariance matrix (P_{x_0}), R_v and R_n are chosen as before with the following k_x, k_p and k_n values,

$$\widehat{x}_0 = \begin{bmatrix} 5 & -1 \end{bmatrix}^T, \quad k_x = 1,\ k_p = 10^{-3} \text{ and } k_n = 10^{-3}. \tag{5.21}$$

The estimates states using UKF and EKF are compared in Figure 5.7. The errors in the estimated states in polar coordinates are shown in Figure 5.8. From Figures 5.7 and 5.8, it is clear that the EKF estimates are sensitive to the model error in μ, whereas the UKF shows robust performance to the model error.

5.4.2 State estimation in an induction machine

The UKF and EKF are applied to a highly nonlinear flux and angular velocity estimation problem in an induction machine. To develop high-

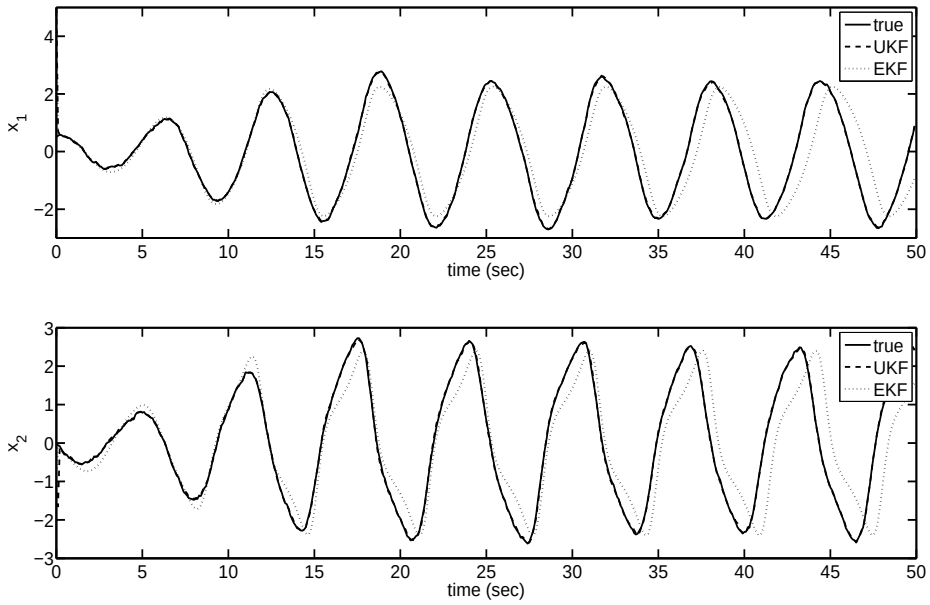

Figure 5.7: Comparison of state estimates using UKF and EKF with a model error

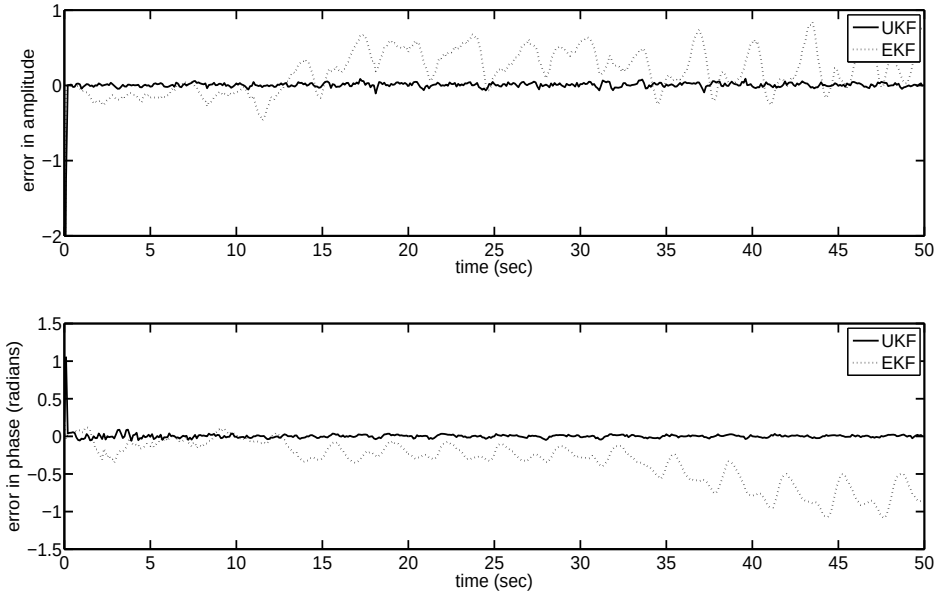

Figure 5.8: Errors in amplitude and phase of the UKF and EKF state estimates

performance induction motor drives, it may be necessary to have rotor flux estimators and rotor time constant identification schemes [15]. In [15] and [13], new EKF-based algorithms are developed for the considered estimation problem as the EKF estimator cannot produce effective results. The state space model for a symmetrical three-phase induction machine is [13],

$$\begin{aligned}
\dot{x}_1 &= k_1 x_1 + z_1 x_2 + k_2 x_3 + z_2 \\
\dot{x}_2 &= -z_1 x_1 + k_1 x_2 + k_2 x_4 \\
\dot{x}_3 &= k_3 x_1 + k_4 x_3 + (z_1 - x_5) x_4 \\
\dot{x}_4 &= k_3 x_2 - (z_1 - x_5) x_3 + k_4 x_4 \\
\dot{x}_5 &= k_5 (x_1 x_4 - x_2 x_3) + k_6 z_3
\end{aligned} \tag{5.22}$$

where x_1, x_2 and x_3, x_4 are the components of the stator and the rotor flux, respectively and x_5 is the angular velocity. All the state variables are normalized. The inputs, the frequency and the amplitude of the stator voltage are denoted by z_1 and z_2 respectively, and the load torque is denoted by z_3. $k_1, ..., k_6$ are parameters depending on the considered drive. The outputs are the normalized stator currents y_1 and y_2. The output equations are given by,

$$\begin{aligned}
y_1 &= k_7 x_1 + k_8 x_3 \\
y_2 &= k_7 x_2 + k_8 x_4
\end{aligned}$$

with parameters k_7 and k_8. For simulation, the model parameters and inputs are set to the values given in Table 5.1. Process noise with a covariance of $10^{-4} I_5$ and measurement noise with a covariance of $10^{-2} I_2$ is added to the system states and measurements, respectively. The model is discretized with a sampling interval of 0.1.

The UKF and EKF are used to estimate the states with the actual initial condition

$$x_0 = \begin{bmatrix} 0.2 & -0.6 & -0.4 & 0.1 & 0.3 \end{bmatrix}^T.$$

The initial estimated state is assumed to be

$$\widehat{x}_0 = \begin{bmatrix} 0.5 & 0.1 & 0.3 & -0.2 & 4 \end{bmatrix}^T.$$

The tuning parameters are selected as,

$P_{x_0} = k_x I_5$, $R_v = k_p I_5$ and $R_n = k_n I_2$, with $k_x = 1$, $k_p = 10^{-4}$ and $k_n = 10^{-2}$.

Table 5.1: Model parameters and inputs

k_1	k_2	k_3	k_4	k_5	k_6	k_7	k_8	z_1	z_2	z_3
-0.186	0.178	0.225	-0.234	-0.081	4.643	-4.448	1	1	1	0

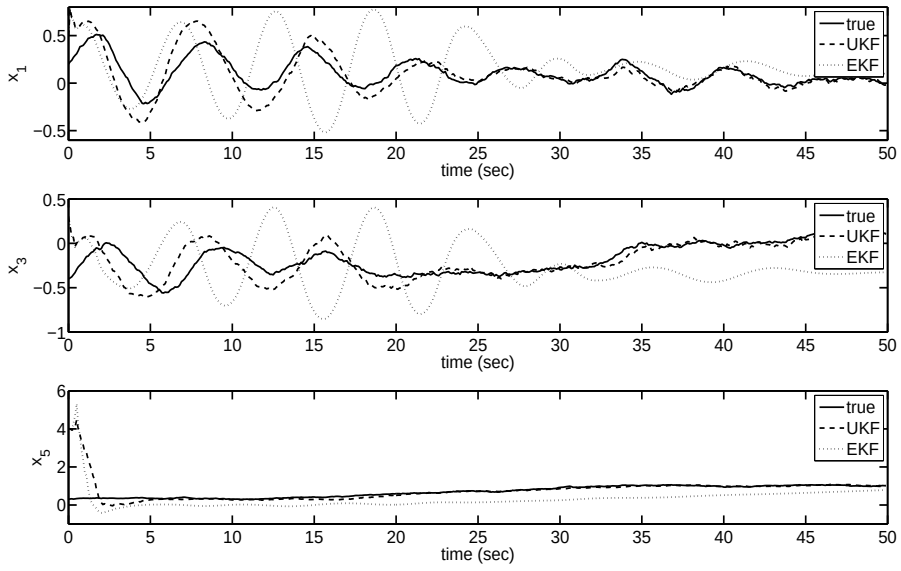

Figure 5.9: Comparison of estimated states: components of stator flux

The state estimation results are shown in Figure 5.9 where the UKF and EKF estimates of states x_1, x_3 and x_5 are compared with the true states. With the initial predicted state far from the actual initial state, the simulation results show that the UKF performs better than the EKF. The reason for the better performance of the UKF is attributed to the better nonlinear approximation at each step. It can be mentioned that the behavior of the EKF is similar to behavior observed in [15].

A Monte Carlo simulation with 100 runs was performed and the MSEs of the EKF and UKF estimates are 0.13 and 0.05 respectively. The MSE corresponding to the UKF is substantially lower compared to those of the EKF. Again the UKF performs significantly better, this time in the case of a highly nonlinear semi-realistic example.

5.4.3 State estimation with constraints: A reversible reaction example

We will here consider an example to illustrate the constraint handling capability of the UKF compared to that of the EKF. Consider the gas-phase, reversible reaction,

$$2A \xrightarrow{\overline{k}} B, \quad \overline{k} = 0.16,$$

with stoichiometric matrix

$$v = \begin{bmatrix} -2 & 1 \end{bmatrix}$$

and reaction rate

$$r = \overline{k} C_A^2.$$

The state and measurement vectors are defined as

$$x = \begin{bmatrix} C_A \\ C_B \end{bmatrix}, \quad y = \begin{bmatrix} 1 & 1 \end{bmatrix} x,$$

where C_j denotes the concentration of species j. It is assumed that the ideal gas law holds and that the reaction occurs in a well-mixed isothermal batch reactor. Then, from first principles, the model for this system is

$$\dot{x} = f(x) = v^T r.$$

The system is discretized with sampling interval of 0.1. The UKF and EKF are used for state estimation, with the following setup as used in [5]:

$$\begin{aligned} x_0 &= \begin{bmatrix} 3 & 1 \end{bmatrix}^T, \widehat{x}_0 = \begin{bmatrix} 0.1 & 4.5 \end{bmatrix}^T \\ P_{x_0} &= \begin{bmatrix} 36 & 0 \\ 0 & 36 \end{bmatrix}, \quad R_v = 10^{-6} \begin{bmatrix} 1 & 0 \\ 0 & 1 \end{bmatrix}, \quad R_n = 10^{-2} \begin{bmatrix} 1 & 0 \\ 0 & 1 \end{bmatrix} \end{aligned}$$

The estimation result for the unconstrained case is shown in Figure 5.10. The result shows that the dynamic performance of the UKF estimates is better compared to that of the EKF. The EKF performance is very similar to the reported results in [5].

However, during the dynamic response, both the UKF and EKF estimates become negative, (meaning negative concentrations) which is not

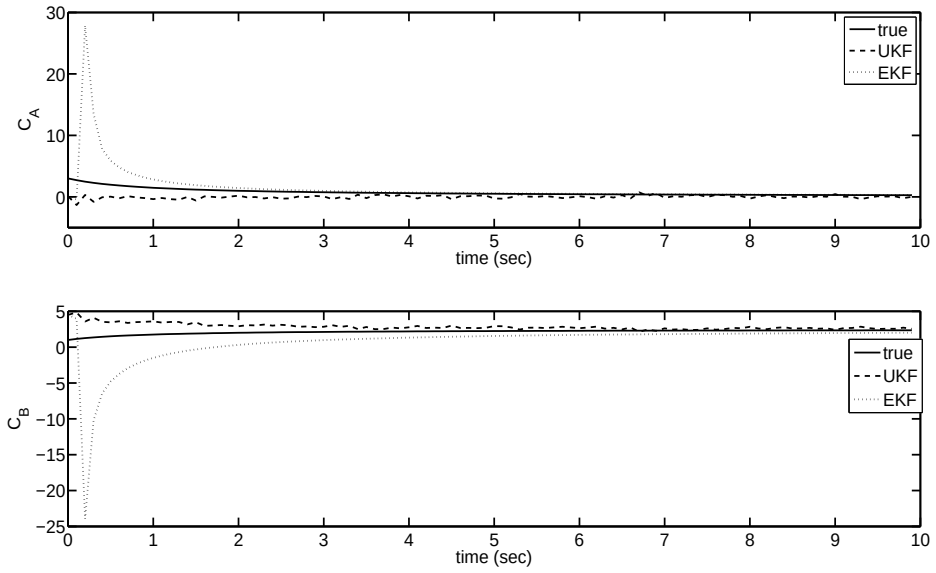

Figure 5.10: Comparison of estimated states: no constraint handling

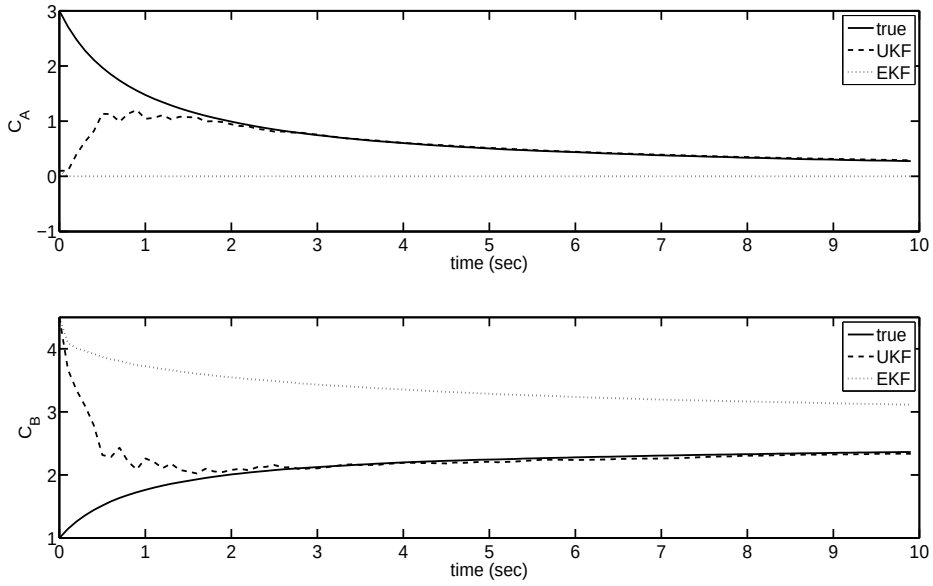

Figure 5.11: Comparison of state estimates: state constraint handling

possible physically. State constraints are incorporated according to the proposed method in section 3 for the UKF and standard "clipping" is used for the EKF. The results are shown in Figure 5.11. From Figure 5.11 the UKF estimates converge to the true states without violating the constraints. Because of the clipping in the EKF, C_A estimate of EKF did not converge to the true state and the estimate of C_B takes much longer time to converge to the true state.

Figure 5.12 shows the phase portraits of the unconstrained and constrained UKF estimates for the first 4 sec. The figure also includes the corresponding covariances plotted at t=0, 1 and 3 seconds. From Figure 5.12, it is clear that it takes longer time for the unconstrained estimate to converge as the corresponding covariances do no include the constraint information. The constrained UKF estimate converges faster as the covariances decrease faster, which include the constraint information. The results from this example confirm that the proposed constraint handling method is

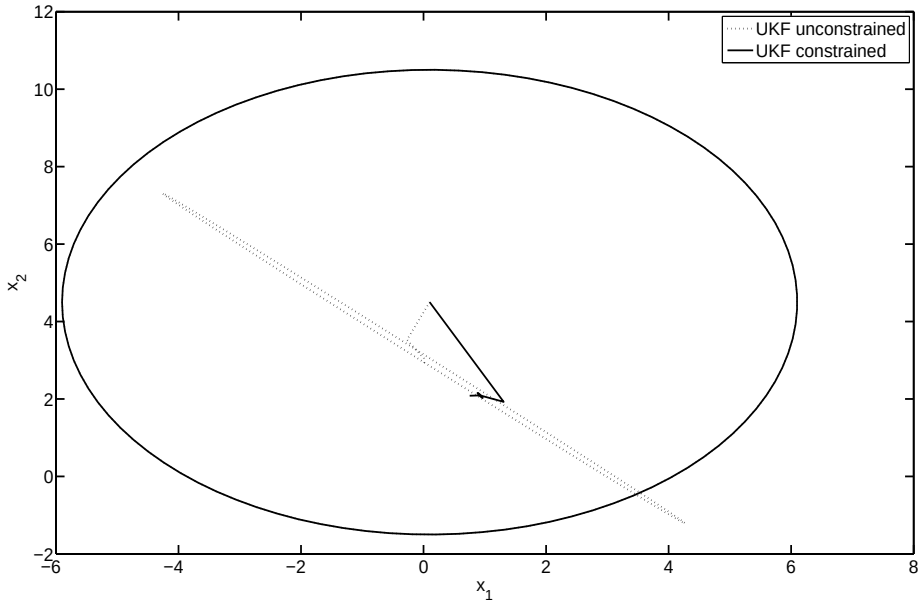

Figure 5.12: Phase portraits of the UKF unconstrained and constrained estimates with covariances

promising.

5.4.4 SOFC/GT hybrid system

The Solid Oxide Fuel Cell (SOFC) stack integrated in a Gas Turbine (GT) cycle, known as SOFC/GT hybrid system, is an interesting power generation system due to its high efficiency in the range of 65-75%. A schematic diagram of the SOFC/GT hybrid system integrated in an autonomous power system is shown in Figure 5.13. The fuel, natural gas (CH_4), is partially steam reformed in a pre-reformer before it enters the SOFC anode. A part of anode flue gas is recycled to supply the necessary steam required for the steam reformation in the pre-reformer. The remaining part of the anode flue gas is supplied to a combustor where the unused fuel is burnt completely in presence of oxygen coming from the cathode flue gas. Air is compressed and preheated in a heat exchanger before entering the SOFC cathode. The

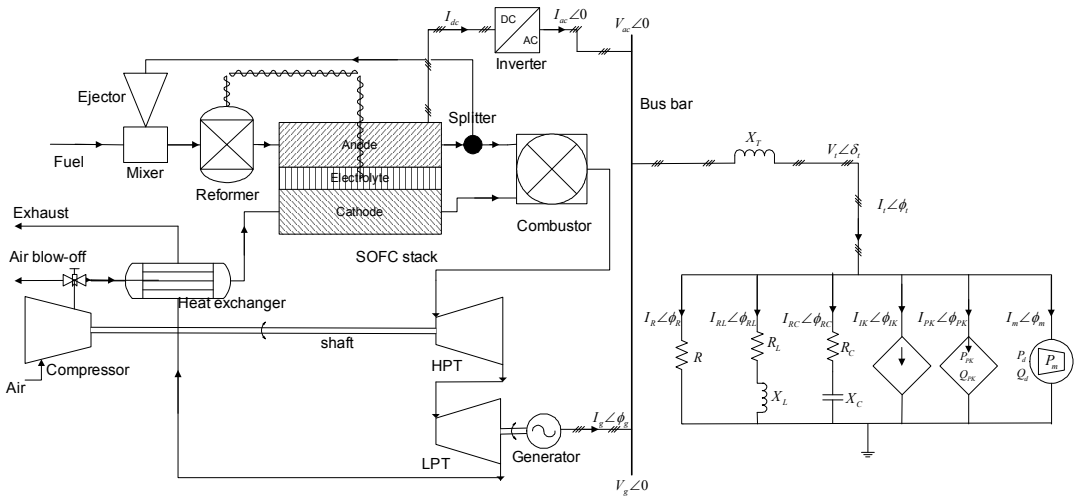

Figure 5.13: SOFC-GT hybrid system integrated in an autonomous power system

hot stream from the combustor is expanded using a High Pressure Turbine (HPT) which drives the compressor. The HPT flue gas is expanded to atmospheric pressure using Low Pressure Turbine (LPT) which drives an alternator. The DC power from SOFC stack is inverted to AC using an inverter. The inverter and the alternator are connected to the electric load through a bus bar. Typically 60-70% of the total power is supplied by the SOFC stack.

All the models of the system are developed in the modular modeling environment gPROMS [4] as reported in [9]. In [9], a low complexity, control relevant SOFC model is evaluated against a detailed model developed in [17]. The comparisons indicate that the low complexity model is sufficient to approximate the important dynamics of the SOFC and can hence be used for operability and control studies. A regulatory control layer is designed and it is included in the model.The purpose of a state estimator is to design an advanced controller and as well for monitoring and fault diagnosis purposes. In this section, EKF and UKF are used to design the state estimator, and their performances and computational load are compared.

The SOFC/GT hybrid system model has 3 inputs, 18 states, and 14 measured outputs which are listed in Table 5.2. A state estimator of the

Table 5.2: Available measurements

No.	Measurement
1	Pre-reformer temperature (K)
2	Shaft speed (rad/s)
3	Heat exchanger hot stream temperature (K)
4	Heat exchanger cold stream temperature (K)
5	SOFC outlet temperature (K)
6	Combustor outlet temperature (K)
7	Fuel mass flow rate (kg/s)
8	Anode recycle flow rate (kg/s)
9	Flow to the combustion chamber (kg/s)
10	Air blow-off flow rate (kg/s)
11	Air mass flow rate (kg/s)
12	SOFC current (A)
13	SOFC voltage (V)
14	Generator power (kW)

hybrid system is designed using both the UKF and EKF, and the simulation results are presented in Figures 5.14 and 5.15. The figures show selected states for a typical run. Both the state estimators are tuned to obtain good performance. In the EKF, the Jacobians are calculated numerically at each time step. The tuning parameters for both the UKF and EKF are the same to ensure a fair comparison.

The initial state estimate is different from the actual initial state and from the simulation results it can be concluded that UKF estimate converges to the true states very fast compared to the EKF estimate. The initial state estimate cannot be chosen too far from the actual state to avoid numerical problems in gPROMS. From this example, it is clear that the UKF can be used to design state estimators for higher order systems and the UKF performance is again favorable. The computational load of the UKF is almost the same as that of the EKF, in addition to providing better performance.

5.5 Discussion

The UKF as a tool for state estimation has been compared to the standard method for nonlinear state estimation; the EKF. The state estimation methods have been compared using the same tuning parameters to make the comparative study as credible as possible. Four different examples have been tested. The UKF shows consistently improved performance as compared to the EKF. In several cases the improvement is substantial, both in the convergence rate as well as in the long term state estimation error. Monte Carlo simulations have also been run with different initial states. These runs reinforced the hypothesis that the UKF is indeed an interesting alternative to the EKF.

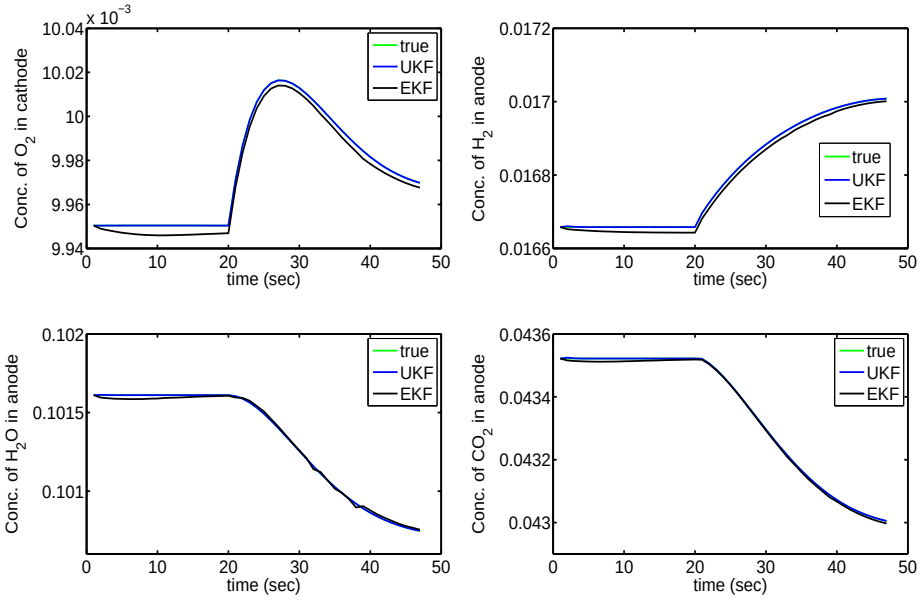

Figure 5.14: Comparison of state estimation using UKF and EKF: concentration of O2 in cathode and concentrations of H2, H2O and CO2 in anode of SOFC

A method for constraint handling in UKF is proposed in Section 3. The results albeit for one example are promising. An important feature of the

proposed constraint handling method is the fact that it adjusts the covariance in addition to the state estimates themselves. This is quite different from the EKF where 'clipping' usually is performed without adjusting the state estimate covariance. A rationale for using the MHE is often attributed to its constraint handling ability. Our results indicate that the UKF with the proposed constraint handling may be an interesting alternative to MHE. Furthermore, it is very simple to implement the proposed method to incorporate the constraints in the UKF compared to the MHE.

The improved performance of the UKF compared to the EKF is due to two factors, the increased time-update accuracy and the improved covariance accuracy. The covariance estimation can be quite different for the two filters as shown in Figure 6. This again makes a difference in terms of different Kalman gains in the measurement-update equation and hence the efficiency of the measurement-update step.

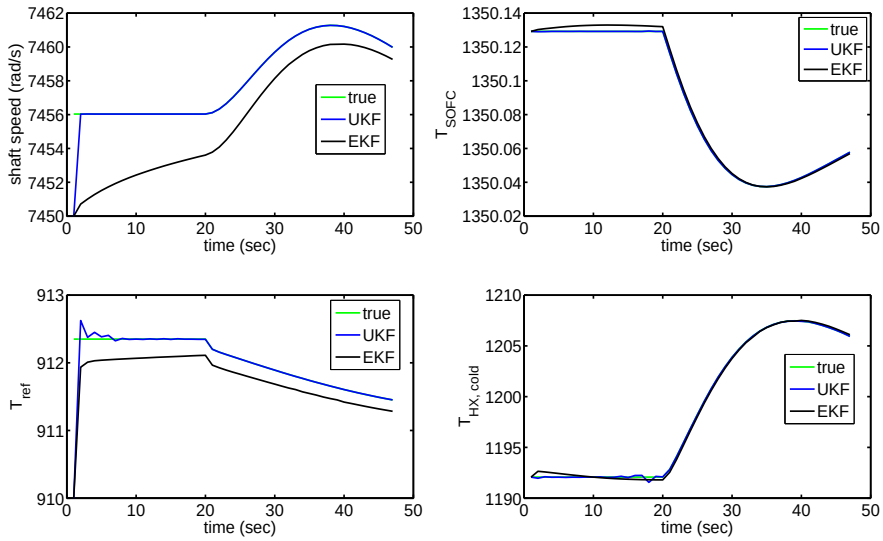

Figure 5.15: Comparison of state estimation using UKF and EKF: Compressor shaft speed and SOFC, pre-reformer and heat exchanger cold stream temperatures

There is usually a price to pay for improved performance. In this case the computational load increases when moving from the EKF to the UKF

if the Jacobians are computed analytically. In many cases, particularly for higher order systems, the Jacobians for the EKF are computed using finite differences. In this case the computational load for the UKF is comparable to the EKF. The latter implies that the computational load using the UKF is significantly lower than what can be expected for the MHE.

5.6 Conclusions

This paper shows that the UKF is an interesting option to the EKF because of improved performance. Further, due to the proposed constraint handling method it may also be an interesting alternative to the MHE. The proposed method is much simpler to implement compared to the MHE. The computational load for the UKF is comparable to the EKF for the typical case, where the Jacobians are computed numerically.

5.7 Acknowledgements

The authors are grateful to Professor Biao Huang for discussions on the UKF. The financial support from The Gas Technology Center, NTNU-SINTEF and Norwegian Research Council is acknowledged.

References

[1] M. S. Ahmed and S. H. Riyaz. Design of dynamic numerical observers. *IEE Proceedings in Control Theory Applications*, 147(3):257–266, 2000.

[2] B. Akin, U. Orguner, and A. Ersak. State estimation of induction motor using unscented kalman filter. *IEEE Transactions on Control Applications*, 2:915–919, 2003.

[3] G. Evensen. *Data Assimilation, The Ensemble Kalman Filter*. Springer Berlin, 2007.

[4] gPROMS (2004). gPROMS introductory user guide. *Process Systems Enterprise Ltd.*, 2004.

[5] E. L. Haseltine and J. B. Rawlings. A critical evaluation of extended kalman filtering and moving horizon estimation. *Technical report, Texas-Wisconsin Modeling and Control Consortium (TWMCC)*, 2003.

[6] B. Huang and Q. Wang. Overview of emerging bayesian approach to nonlinear system identification. *Round tables on Non-linear Model Identification, International Workshop on Solving Industrial Control and Optimization Problems, Cramado, Brazil*, 2006.

[7] A. H. S. Jazwinski. Stochastic processes and filtering theory. *Mathematics in Science and Engineering*, 64, 1970.

[8] S. Julier and J. K. Uhlmann. Unscented filtering and nonlinear estimation. *Proceedings of the IEEE*, 92:401–422, 2004.

[9] R. Kandepu, L. Imsland, B. A. Foss, C. Stiller, B. Thorud, and O. Bolland. Modeling and control of a SOFC-GT based autonomous power system. *Energy*, 32:406–417, 2007.

[10] H. K. Khalil. *Nonlinear Systems Third Edition.* Prentice Hall, 2000.

[11] W. Li and H. Leung. Simultaneous registration and fusion of multiple dissimilar sensors for cooperative driving. *IEEE Transactions on Intelligent Transportation Systems*, 5:84–98, 2004.

[12] C. V. Rao, J. B. Rawlings, and D. Q. Mayne. Constrained state estimation for nonlinear discrete-time systems: stability and moving horizon approximations. *IEEE Transactions on Automatic Control*, 48:246–258, 2003.

[13] K. Reif, F. Sonnemann, and R. Unbehauen. An EKF-based nonlinear observer with a prescribed degree of stability. *Automatica*, 34(9):1119–1123, 1998.

[14] A. Romanenko and J. A. A. M. Castro. The unscented filter as an alternative to the ekf for nonlinear state estimation: a simulation case study. *Computer and Chemical Engineering*, 28:347–355, 2004.

[15] L. Salvatore, S. Stasi, and L. Tarchioni. A new EKF-based algorithm for flux estimation in induction machines. *IEEE Transactions on Industrial Electronics*, 40(5):496–504, 1993.

[16] D. Simon and T. L. Chia. Kalman filtering with state equality constraints. *IEEE Transactions on Aerospace and Electronic Systems*, 38:128–136, 2002.

[17] C. Stiller, B. Thorud, S. Seljebø, O. Mathisen, H. Karoliussen, and O. Bolland. Finite-volume modeling and hybrid-cycle performance of planar and tubular solid oxide fuel cells. *Journal of Power Sources*, 141:227–240, 2005.

[18] S. Ungarala, E. Dolence, and K. Li. Constrained extended kalman filter for nonlinear state estimation. *In proceedings of 8th International IFAC Symposium on Dynamics and Control Process Systems, Cancun, Mexico*, 2:63–68, 2007.

[19] P. Vachhani, S. Narasimhan, and R. Rengaswamy. Robust and reliable estimation via unscented recursive nonlinear dynamic data reconciliation. *Journal of Process Control*, 16:1075–1086, 2006.

[20] R. Van der Merwe. *PhD Thesis - Sigma-Point Kalman Filters for probability inference in dynamic state-space models.* Oregon Health and Science University, 2004.

Appendix A

Additional articles

In this appendix, two additional conference articles are included. The first article is presented at American Control Conference (ACC) 2006, Minneapolis, June, 2006. The second article is an invited article and presented at the Sixth IEEE Conference on Control and Automation (ICCA), Guangzhou, China, May30-June 1, 2007.

A.1 Integrated modeling and control of a load connected SOFC-GT autonomous power system

Proceedings of the 2006 American Control Conference
Minneapolis, Minnesota, USA, June 14-16, 2006

ThB19.4

Integrated modeling and control of a load-connected SOFC-GT autonomous power system

Rambabu Kandepu, Bjarne A. Foss and Lars Imsland

Abstract— **In this paper we have developed low complexity, control-relevant models of all the components of the SOFC-GT hybrid system which is connected to a load through a bus bar. A control structure is designed by analyzing the complete system and simulation results are presented.**

I. INTRODUCTION

In the foreseeable future, fossil fuels including natural gas will be a major source of energy. With today's increasing concern about global warming and climate change, there is an incentive to investigate natural gas power processes that operate efficiently, thus emitting less per kWh produced, and also power production processes with CO_2 capture capabilities. It is widely accepted that fuel cells are power sources that will become increasingly important, due to high efficiency, low levels of pollution and noise, and high reliability. One of the most promising fuel cell technologies is the Solid Oxide Fuel Cell (SOFC), due to its solid state design and internal reforming of gaseous fuels, in addition to its high efficiency [8]. The SOFC converts the chemical energy of a fuel directly to electrical energy. Since SOFCs operate at high temperatures (about 1000°C), natural gas can be used directly as fuel. The electrical efficiency of a SOFC can reach 55%. Another significant advantage of the SOFC is that since it operates at high temperature and its efficiency increases when pressurized, it naturally lends itself as a heat source for a gas turbine (GT) cycle. The combined (hybrid) cycle can theoretically have an overall electrical efficiency of up to 70%. with a power range from a few hundred kWs to a few MWs [8]. Processes based on SOFCs can be used as power processes with CO_2 capture, since the "used fuel" (and water) and air exit streams can be kept separated [6]. The main applications of the hybrid system include remote area power supply and distributed power generation.

There are several models available in literature for the SOFC-GT hybrid system [11], [2], [9], [19]. In [4], a dynamic model of grid connected SOFC model is developed. However, to the best of authors' knowledge there is no model in the literature with integration of a SOFC-GT hybrid system with a power grid and an electrical load. The reason for procuring an integrated model is to obtain a comprehensive understanding of the operability of the system which has close dynamic interactions between the power generation system and the local grid. Further, the hybrid system consists of tightly integrated dynamic subsystems with strict operating criteria making the control design more challenging in terms of disturbance rejection, part-load operation and in particular start-up, shutdown and load shedding. Suitable system actuation must be chosen, good control structures must be devised, and good controllers must be designed. As a basis for all these tasks, control relevant models must be developed for the subsystems, and for the total system. Such models should have limited complexity to allow for the necessary analysis, and at the same time should include the important dynamic interactions.

In this paper we present an integrated model of a SOFC-GT hybrid system with a power grid connecting to an electrical load. The process is described on a system level and modeling of each component is discussed including the main underlying assumptions. The model is subsequently used to perform analysis of system dynamics and optimize system design. A simple control design is proposed and assessed through a set of simulation scenarios.

II. PROCESS DESCRIPTION

A schematic diagram of the integrated system where the hybrid system is connected to the load by a bus bar is shown in Figure 1. Methane (fuel) is mixed with a part of anode flue gas and is partially steam reformed in a pre-reformer generating hydrogen. The heat required for endothermic reformation reactions in the pre-reformer is supplied from the SOFC stack through radiation. The gas mixture from the pre-reformer is fed to the anode volume of the SOFC, where the remaining part of the methane is reformed. Compressed atmospheric air is heated in a recuperative heat exchanger and is used as an oxygen source at the cathode side of the SOFC. In the SOFC, electrochemical reactions take place and DC voltage is produced. The rate of the electrochemical reactions depends on the current. A part of the anode flue gas is recycled to supply steam to the pre-reformer. The remaining part of the anode and cathode flue gases is supplied to a combustion chamber where the unused fuel is combusted.

The hybrid system considered here uses a double shaft GT configuration. The combusted gas mixture is expanded in a high pressure turbine (HPT) with variable shaft speed driving the compressor. The HPT flue gas is further expanded to atmospheric pressure in a low pressure turbine (LPT) with constant shaft speed, which is coupled to a synchronous generator producing AC electric power. The expanded gas mixture is used to heat up the compressed air in a heat exchanger. The DC power from the SOFC stack is fed to an inverter which converts DC to AC with a fixed frequency. The inverter and the generator are connected to a local grid, which is connected to a six branch electric load. Both the SOFC stack and the generator supply the electric load

R. Kandepu, B. A. Foss and L. Imsland are with Department of Engineering Cybernetics, Norwegian University of Science and Technology, Trondheim, Norway {Rambabu.Kandepu, Bjarne.A.Foss, Lars.Imsland}@itk.ntnu.no

1-4244-0210-7/06/$20.00 ©2006 IEEE

TABLE I
REACTIONS AT ANODE AND CATHODE

At anode	
Reaction	Reaction rate (r_j^{an})
$H_2+O^{2-} \rightarrow H_2O+2e^-$	r_1^{an}
$CH_4+H_2O \Leftrightarrow CO+3H_2$	r_2^{an}
$CO+H_2O \Leftrightarrow CO_2+H_2$	r_3^{an}
$CH_4+2H_2O \Leftrightarrow CO_2+4H_2$	r_4^{an}
At cathode	
Reaction	Reaction rate (r_j^{an})
$\frac{1}{2}O_2+2e^- \rightarrow O^{2-}$	r_1^{ca}

demand on the grid. The power sharing between the SOFC stack and the generator cannot be controlled directly and it depends on the system dynamics. When there is a load change on the grid, the load sharing between the SOFC stack and the generator will change. Typically 60-70% of the total power is supplied by the SOFC stack.

III. MODELING

A. SOFC stack

There are several dynamic, distributed SOFC models reported in the literature. For example, Achenbach [1] developed a three dimensional, dynamic, distributed model for a planar SOFC stack. Chan et al. [2], Thorud et al. [19], Stiller et al. [17] and Magistri et al. [11] all developed distributed, dynamic tubular SOFC models for designs similar to that of Siemens Westinghouse, for use in hybrid systems. In this work a low complexity SOFC model is developed with no explicit regard to the geometry of the cell.

The SOFC converts the chemical energy of the fuel directly into electrical energy. Fuel is supplied to the anode and air is supplied to the cathode. At the cathode-electrolyte interface, oxygen molecules accept electrons coming from the external circuit to form oxide ions. The electrolyte layer allows only oxide ions to pass through and at the anode-electrolyte interface, hydrogen molecules present in the fuel react with oxide ions to form steam and electrons get released. These electrons pass through the external circuit and reach the cathode-electrolyte layer, and thus the circuit is closed. Table I gives the list of reactions that take place at anode and cathode and the corresponding reaction rates notation.

In practice, a number of cells are connected either in series or in parallel or both, according to the voltage requirement. The number of cells in the stack depends on the power demand. In this paper, we assume that all the SOFCs in the SOFC stack operate at identical conditions and there are 1160 cells in the stack. In addition, the following main assumptions have been made in developing the model.

1) All the physical variables are uniform over the SOFC, resulting in a lumped model.
2) There is sufficient turbulence and diffusion within the anode and the cathode for perfect mixing to occur (CSTR).
3) The gas temperatures within the SOFC are the same as the solid; i.e. the thermal inertia of the gases is neglected.
4) For the energy balance, pressure changes within the SOFC are negligible.
5) All gases are ideal.

The dynamic model of a single SOFC is developed using two mass balances (one each for anode and cathode volumes) and one overall energy balance. The two mass balances are;

$$\frac{dN_i^{an}}{dt} = \dot{N}_i^{in,an} - \dot{N}_i^{out,an} + \sum_{j=1}^{M} a_{ij}^{an} r_j^{an},$$

$$\frac{dN_i^{ca}}{dt} = \dot{N}_i^{in,ca} - \dot{N}_i^{out,ca} + a_{i1}^{ca} r_1^{ca},$$

where $i = 1, ..., 7$, refers to the following components: Nitrogen (N_2), Oxygen (O_2), Hydrogen (H_2), Methane (CH_4), Steam (H_2O), Carbonmonoxide (CO), and Carbondioxide (CO_2) and the reactions at anode ($M = 4$) and at cathode are given in Table I. The reaction rates corresponding to the electrochemical reactions (r_1^{ca}, r_1^{an}) are directly related by the current I as

$$r_1^{an} = I/(2F) = r_1^{ca} \tag{1}$$

where F is Faraday's constant. The reaction rates corresponding to the reforming reactions are calculated as proposed by Xu [21]. a_{ij}^{an} and a_{i1}^{ca} denote stoichiometric constants of a component in anode and cathode respectively. It is assumed that the exhaust flows at the anode and cathode outlets can be described by the choked exhaust flow equation. This means that the mass flow rate of the exhaust flow at the anode (cathode) depends on the pressure difference between the pressure inside the anode (cathode) and the pressure at the outlet [13]. The partial pressures, volume, and temperature both in anode and cathode are assumed to be related by the ideal gas equation. The energy balance accounts for the whole SOFC volume, and is given by [18], [10]:

$$\begin{aligned} C^s \frac{dT}{dt} = & \sum_{i=1}^{N} \dot{N}_i^{in,an} (\Delta\overline{h}_i^{in,an} - \Delta\overline{h}_i) \\ & + \sum_{i=1}^{N} \dot{N}_i^{in,ca} (\Delta\overline{h}_i^{in,ca} - \Delta\overline{h}_i) \\ & - \sum_{j=1}^{M} \Delta\overline{h}_j^{rx} r_j^{an} - P_{DC} - P_{rad} \end{aligned} \tag{2}$$

where P_{DC} is the amount of DC power produced by the SOFC, P_{rad} is the amount of radiation heat given from the SOFC, $\Delta\overline{h}_i$ is the molar specific enthalpy of a component, $\Delta\overline{h}_j^{rx}$ is the molar specific enthalpy change of a reaction j, C^s is the SOFC solid heat capacity, T is SOFC solid temperature, $N = 7$ is the number of components, $\Delta\overline{h}_i^{in,an}$ and $\Delta\overline{h}_i^{in,ca}$ denote molar specific enthalpy of a component at anode cathode inlets, respectively.

In (2), the temperature dynamics of gases are neglected as they are fast compared to the temperature changes of the solid. As the SOFC operating temperature is higher than that of the surroundings, there is always some loss due to radiation. The operating cell voltage is given by (3), where the open circuit voltage (E^{OCV}) of the cell is given by the *Nernst equation* [8], and V_{loss} is the voltage loss

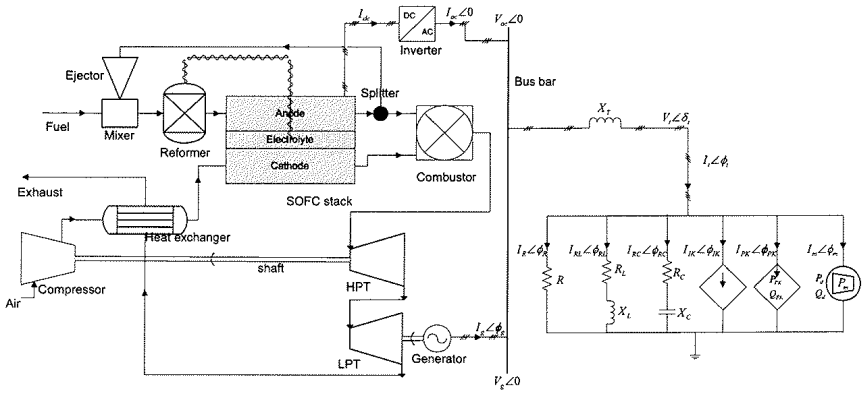

Fig. 1. SOFC-GT hybrid system integrated with autonomous power system

which includes ohmic, concentration and activation losses. Moreover, Air Utilization (AU) and Fuel Utilization (FU) are defined as in (4)

$$V = E^{OCV} - V_{loss} \tag{3}$$

$$\text{AU} = 1 - \frac{\dot{N}^{out}_{O_2}}{\dot{N}^{in}_{O_2}}, \quad \text{FU} = 1 - \frac{\dot{N}^{out}_{H_2}}{\dot{N}^{in}_{H_2}}. \tag{4}$$

The AU and FU are included in the model as they are identified as important variables in representing the SOFC state [19]. Recycle ratio is defined as the ratio of the fuel flow recycled to the fuel flow at the anode outlet.

In [7], the low complexity SOFC model is evaluated against a detailed model developed in [19], [17]. The comparisons indicate that the low complexity model is good enough to approximate the important dynamics of the SOFC and can hence be used for operability and control studies.

B. Reformer

A reformer is used to convert methane into hydrogen by steam reforming. It is a fixed volume reactor having two inlets, one for methane and the other for steam and one outlet. The assumptions made in the model development of the reformer are same as that of the SOFC. The dynamic model is developed using one mass balance and one energy balance. The three reformation reactions considered are given in Table I. The reformation is a highly endothermic process, so heat must to be supplied to the reactor. As the SOFC operates at a high temperature, there is radiation from the SOFC stack and this can be supplied to the reformer by using a suitable mechanical design. The operating temperature of the reactor is in the range $500°C - 700°C$.

C. Heat exchanger

A very simple model of a counter-flow heat exchanger is used, in which the amount of the heat exchanged depends on the heat transfer coefficient of the exchanger wall and also on the average temperature difference between the hot and cold streams. A first order transfer function describes the dynamics of the temperatures of both the streams. The following assumptions were made,

1) The model is lumped. All the physical parameters are assumed to be uniform over the heat exchanger.
2) There is no pressure loss within the heat exchanger.

D. Combustion chamber

The combustion chamber as shown in Figure 1 has $n_{in} = 2$ inlet streams and one outlet stream. It burns the fuel coming from all the inlet flows in the presence of air. The operating conditions will always be such that there is surplus oxygen available for complete combustion due to the fact that air mass flow rate is much larger than the fuel mass flow rate. In this model, the fuel can be methane, hydrogen or carbonmonoxide or a mixture of these fuels. The following reactions are being considered during the combustion.

$$\begin{aligned} 2H_2 + O_2 &\rightarrow 2H_2O \\ CH_4 + 2O_2 &\rightarrow 2H_2O + CO_2 \\ 2CO + O_2 &\rightarrow 2CO_2 \end{aligned} \tag{5}$$

The following assumptions are made:

1) The pressures of all the inlet flows are the same.
2) As the combustion process is very rapid, it is modeled as an instantaneous process and complete combustion is assumed.
3) The model is a bulk model, i.e. all physical variables are assumed to be uniform over the combustion chamber.
4) There is a 2% pressure loss in the combustor volume.

The following mass and energy balances are used for the control volume:

$$\sum_{k=1}^{n_{in}} \dot{N}_i^{in,k} + \sum_{j=1}^{n_{rx}} a_{ij} r_j = \dot{N}_i^{out}, \quad i = 1...7, \; n_{rx} = 3$$

$$\sum_{k=1}^{n_{in}} \sum_{i=1}^{N} (\dot{N}_i^{in,k} \Delta\bar{h}_i^{in,k} - \sum_{i=1}^{N} \dot{N}_i^{in,k} \Delta\bar{h}_i) - \sum_{j=1}^{M_c} \Delta\bar{h}_j^{rx} r_j = 0$$

where $N = 7$ is the number of components, $M_c = 3$ is the number of reactions as given in (5) and the variables notation is similar as in (2) but refer to the combustion chamber.

E. Gas turbine

Compressor and turbine models are based on steady state performance map characteristics [16]. The map is modeled using polynomials of 4th and 5th order for reduced mass flow, pressure and efficiency as functions of reduced shaft speed and operation line. The following are the assumptions made in both the compressor and turbine models:

1) The process has constant isentropic efficiency.
2) The working fluid satisfies the ideal gas equation.

A shaft model accounts for the dynamics of the rotating mass in the gas turbine system which is modeled as

$$\dot{\omega} = P_b/(I\omega) \tag{6}$$

where P_b is the power balance across the shaft, I is the moment of inertia of the rotating mass and ω is the angular velocity of the shaft.

F. Inverter

A simple model of inverter is developed with the following assumptions:

1) Power loss is negligible.
2) Pulse Width Modulation (PWM) technique is used to control the AC output voltage and frequency. The controller dynamics are neglected as they are very fast compared to the hybrid system dynamics.
3) The inverter supplies AC power at unity power factor.

The power balance on both sides is given by

$$P_{dc} = V_{ac} I_{ac}. \tag{7}$$

G. Synchronous generator

The per-phase equivalent circuit of the synchronous generator is shown in Figure 2 taken from [20]. The magnitude of the electro-motive force (EMF) induced in each phase is assumed to be directly proportional to the shaft speed (ω_g) and field current (I_{fg}),

$$E_g = k_g I_{fg} \omega_g \tag{8}$$

where k_g is the proportionality constant. The open circuit voltage $V_g\angle 0$, which is taken as the reference in phasor notation, and $E_g\angle\delta_g$ are related as

$$E_g\angle\delta_g = V_g\angle 0 + X_g\angle 90° I_g\angle\phi_g \tag{9}$$

where $I_g\angle\phi_g$ is the generator current, X_g is the stator per-phase reactance in ohms. It is assumed that there is 2% power loss in conversion from mechanical to electrical form which includes rotational loss, copper loss and magnetizing loss. The generator is connected to a power turbine which runs at a constant speed. Hence the frequency of the AC supply from the generator is assumed constant. The real and reactive powers supplied by the generator are given by

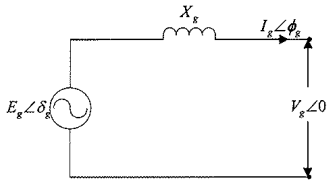

Fig. 2. Per-phase equivalent circuit of synchronous generator

$$\begin{aligned} P_g &= V_g I_g \cos\phi_g \\ Q_g &= V_g I_g \sin\phi_g. \end{aligned} \tag{10}$$

H. Autonomous power grid

The integrated SOFC-GT hybrid system with the autonomous power grid is shown in Figure 1. The model of the grid and load is chosen such that the level of complexity is comparable to the SOFC-GT hybrid system models. The bus bar voltage is fixed at $230V$ and is taken as the reference in phasor notation. We assume that the generator field current is controlled such that the generator terminal voltage $V_g\angle 0$ equal to the bus bar voltage $V_{ac}\angle 0$. The bus bar is connected to the load by transmission lines of reactance X_T. The load is represented by six parallel branches with different components in each branch as shown in Figure 1. It is categorized into 4 types of loads; constant impedance, constant current, constant power and induction motor load. The constant impedance, constant current and constant power load represent the residential loads such as lights, water heaters, ovens etc. The induction motor load is considered to represent an industrial load [12]. The constant impedance load is represented by the first three branches with resistive, inductive and capacitive loads. The fourth and fifth branches represent the constant current and constant power loads respectively. The sixth branch represents the induction motor load. The total load current $I_t\angle\phi_t$ is the sum of the currents from the inverter and the synchronous generator,

$$I_t\angle\phi_t = I_{ac}\angle 0 + I_g\angle\phi_g. \tag{11}$$

As it is assumed that the inverter supplies power at unity power factor, generator supplies the load reactive power and transmission line reactive power. The load voltage $V_t\angle\delta_t$ is given by

$$V_t\angle\delta_t = V_{ac}\angle 0 - jX_T I_t\angle\phi_t. \tag{12}$$

The first three branches of the load (R, RL, RC branches) are used to model different constant impedance loads. The currents in these branches are given by

$$\begin{aligned} V_t\angle\delta_t &= RI_R\angle\phi_R \\ V_t\angle\delta_t &= (R_L + X_L\angle 90°) I_{RL}\angle\phi_{RL} \\ V_t\angle\delta_t &= (R_C - X_C\angle 90°) I_{RC}\angle\phi_{RC}. \end{aligned} \tag{13}$$

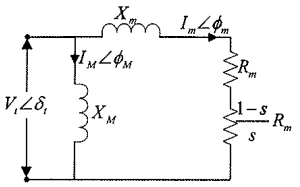

Fig. 3. Equivalent circuit of induction motor

The fourth branch is used to model constant current loads where the current $I_{IK}\angle\phi_{IK}$ is assigned a constant value. The fifth branch is used to model constant power loads where real and reactive powers (P_{PK}, Q_{PK}) are assigned constant values and the current $I_{PK}\angle\phi_{PK}$ is calculated by

$$\begin{aligned} P_{PK} &= V_t I_{PK}\cos(\phi_{PK}-\delta_t) \\ Q_{PK} &= V_t I_{PK}\sin(\phi_{PK}-\delta_t). \end{aligned} \tag{14}$$

The last branch is used to model induction motor, whose equivalent circuit is shown in Figure 3 [5]. Assuming the magnetizing inductance is large, i.e. $X_M \to \infty$, the magnetizing current $I_M\angle\phi_M$ is neglected [5]. The induction motor model equations are then given by,

$$\begin{aligned} \frac{ds}{dt} &= \frac{1}{I\omega_o^2}\left(\frac{P_m}{1-s}-P_d\right) \\ V_t\angle\delta_t &= \left(\frac{R_m}{s}+X_m\angle 90^\circ\right)I_m\angle\phi_m \\ P_d &= V_t I_m\cos(\phi_m-\delta_t) \\ Q_d &= V_t I_m\sin(\phi_m-\delta_t) \end{aligned} \tag{15}$$

where I is moment of inertia of induction motor, ω_o is stator frequency, P_m is mechanical load power on the induction motor, P_d and Q_d are real and reactive power from induction motor, and s is slip given by $s = \frac{\omega_o-\omega_m}{\omega_m}$ where ω_m is induction motor speed.

All the components of the hybrid system and the autonomous power system are modeled in the modular modeling environment gPROMS [3].

IV. CONTROL AND SIMULATION

An integrated open-loop system is simulated with a set of nominal, realistic parameters resulting in a nominal state partially shown in Table II. As may be expected, there is a need to design a control system to compensate for disturbances in the load. The system goes unstable for certain load disturbances which further accentuate the need for a controller design. The open loop simulations further show the importance of including the grid with connected load model since the dynamics and the sensitivity of some important variables of the hybrid system to the load disturbances are different from the situation, when the grid with connected load is represented by a power sink.

As the main source of the power in the hybrid system is the fuel flow, fuel flow must be controlled to match the power demand in case of any load changes. Since it is not always possible to know the load in advance, any load change is treated as a disturbance to the controller. As the bus bar voltage is fixed when there is a load change, the current and the FU in SOFC vary. The FU cannot be varied too much since it may cause uneven temperature and voltage distributions inside the cell [16]. Hence FU is taken as a controlled variable, where it is assumed that a perfect observer is available to estimate FU.

TABLE II
NOMINAL STATE OF THE SYSTEM

Variable	Value
SOFC current	250A
fuel flow rate	0.007kg/s
SOFC temperature	1350K
SOFC cell voltage	0.657V
SOFC stack power	191kW
generator power	87kW
air mass flow rate	0.445kg/s
AU	0.23
FU	0.85
recycle ratio	0.54
reforming degree	0.38
steam/methane ratio	2
I_t	1248A
V_t	222V
Induction motor slip	0.1

A load change can affect the SOFC temperature to change beyond the material constraints [8] [16]. Hence the SOFC temperature should be controlled during the load changes. As there is no other free manipulated variable available for this purpose, a slight change must be made in the process design. After analyzing three different possible choices for the extra manipulated variable, air blow off at compressor outlet is found to be superior in terms of control authority, compared to air bypass across the heat exchanger and additional fuel to the combustion chamber. The control structure is selected from the physical understanding of the process and RGA analysis [15] based on the linearized system confirms it. The non-linear system is linearized at its nominal state given in Table II, and decentralized PI controllers are tuned according to the rules given by Skogestad [14]. The PI controllers are then implemented on the non-linear system.

To evaluate the proposed control structure, the following simulation scenario is used. The system is simulated at the nominal state for one sec. After 5 sec, the following disturbances are applied in a ramp of 5 sec: the mechanical load on the induction motor (P_m) is decreased to 10%, R is increased by 5 times, I_{IK} is decreased to 10% and P_{PK} is decreased to 10% which constitutes 40% load decrease on the system and the system is simulated at steady state until 20 sec. After 20 secs, the P_m is increased to 50% in a step. The total load change, FU and SOFC solid temperature profiles during the simulation are shown in Figure 4. The plant inputs, i.e. fuel flow and air blow-off during the simulation are shown in Figure 5. When there is a load decrease, correspondingly the current and amount of fuel utilized in the SOFC is decreased, which decreases the FU. To maintain FU constant at 0.85, the fuel flow rate is decreased as shown in Figure 5. When the current is decreased in SOFC, the electrochemical reactions rate is decreased which decreases

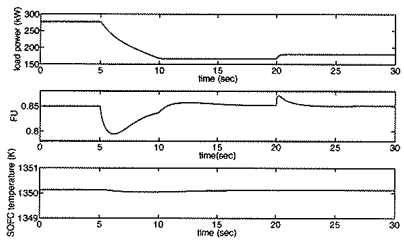

Fig. 4. Mechanical load change, FU, and SOFC temperature during simulation

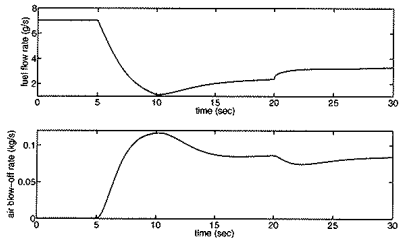

Fig. 5. Plant inputs during simulation

the SOFC temperature. To maintain the SOFC temperature at a constant value the air mass flow rate through the SOFC should decrease meaning that the air blow-off rate must increase as shown in Figure 5. At the nominal state a small non-zero air blow-off rate is chosen to be able to control the SOFC temperature for any small increase in the load at the nominal value. For the 40% load change, the air blow-off rate constitutes about 18% of the total air mass flow rate which may cause a decrease in system efficiency. This is because of the strict control of the SOFC temperature at the nominal value. If the SOFC temperature is chosen to vary in some bounds around the nominal value, the air blow-off utilization can be optimized to a higher system efficiency. However, from the control point of view the proposed control structure gives satisfactory results as seen from Figures 4 and 5.

V. CONCLUSIONS AND FURTHER WORK

A model of complete power system where a SOFC-GT hybrid system is connected to grid with connected load is developed to include the important interactions between the grid and the hybrid system. A control structure with PI controllers shows that satisfactory results can be obtained, but the main disadvantage is that the system efficiency will be reduced with the use of blow-off to control the SOFC temperature during part-load operation.

Future work will focus on optimizing the control design to reduce the air-blow off utilization to control the SOFC temperature to increase the system efficiency at part load operation. While the present paper assumed a two-shaft GT design, we are also looking at integration with a *single-shaft* GT design, which poses further challenge for a control design. A single-shaft GT offers the possibility of avoiding air blow-off by controlling shaft speed directly. It will also be focussed on designing a control structure for start up and shut down operations.

VI. ACKNOWLEDGMENTS

Financial support from The Gas Technology Center, NTNU-SINTEF and NFR is acknowledged. We also thank Dr. Kjetil Uhlen and Dr. Vinay Kariwala for fruitful discussions.

REFERENCES

[1] E. Achenbach. Three-dimensional and time-dependent simulation of a planar solid oxide fuel cell stack. *Journal of Power Sources*, 1994.
[2] S.H. Chan, H.K. Ho, and Y. Tian. Multi-level modeling of SOFC-gas turbine hybrid system. *International Journal of Hydrogen Energy*, 2003.
[3] gPROMS (2004). gPROMS introductory user guide. *Process Systems Enterprise Ltd.*, 2004.
[4] C. J. Hatziadoniu, A. A. Lobo, F. Pourboghart, and M. Daneshdoost. A simplified dynamic model of grid-connected fuel-cell generators. *IEEE transactions on power delivery*, 17(2), April 2002.
[5] D. J. Hill. Nonlinear dynamic load models with recovery for voltage stability studies. *IEEE transactions on power systems*, 8(1), February 1993.
[6] D. Jensen and J. W. Dijkstra. CO2 capture in SOFC-GT systems. *Proceedings of second annual conference on Carbon Sequestration*, May 2003.
[7] R. Kandepu, L. Imsland, B. A. Foss, C. Stiller, B. Thorud, and O. Bolland. Control-relevant SOFC modeling and model eveluation. *Proceedings of ECOS*, 2005.
[8] J. Larminie and A. Dicks. *Fuel Cell Systems Explained.* Wiley, England, 2003.
[9] J. Pålsson, A. Selimovic, and L. Sjunnesson. Combined solid oxide fuel cell and gas turbine systems for efficient power and heat generation. *Journal of Power Sources*, 2000.
[10] M. D. Lukas, K. Y. Lee, and H. Ghezel-Ayagh. An Explicit Dynamic Model for Direct Reforming Carbonate Fuel Cell Stack. *IEEE Transactions on Energy Conversion*, 16(3), September 2001.
[11] L. Magistri, F. Trasino, and P. Costamagna. Transient analysis of a Solid Oxide Fuel Cell hybrids part A: fuel cell models. *Journal of Power Sources*, 2004.
[12] I. R. Navarro. *Dynamic power system load - Estimation of parameters from operational data.* Media-Tryck, Lund, 2005.
[13] J. Padulles, G.W. Ault, and J. R. McDonald. An integrated SOFC dynamic model power systems simulation. *Journal of Power sources*, pages 495–500, 2000.
[14] S. Skogestad. Simple analytic rules for model reduction and PID controller tuning. *Journal of process control*, 2005.
[15] S. Skogestad and I. Postlethwaite. *Multivariable feedback control: Analysis and Design.* Wiley, USA, 1996.
[16] C. Stiller, B. Thorud, O. Bolland, K. Rambabu, and L. Imsland. Control strategy for a solid oxide fuel cell and gas turbine hybrid system. *Submitted to Journal of Power Sources*, 2005.
[17] C. Stiller, B. Thorud, S. Seljebø, Ø. Mathisen, H. Karoliussen, and O. Bolland. Finite-volume modeling and hybrid-cycle performance of planar and tubular solid oxide fuel cells. *Journal of Power Sources, 141, 227-240*, 2005.
[18] P. Thomas. *Simulation of Industrial Processes [F.*
[19] B. Thorud, C. Stiller, T. Weydahl, O. Bolland, and H. Karoliussen. Part-load and load change simulation of tubular SOFC systems. *Proceedings of Fuel Cell Forum, Lucerne, 28 June-2 July*, 2004.
[20] L. A. A. Warnes. *Electronic and Electrical Engineering.* Macmillan, London, 1994.
[21] J. Xu and G. F. Froment. Methane Steam reforming, Methanation and Water-Gas Shift: I. Intrinsic Kinetics. *AIChE Journal*, 1989.

A.2 Comparative Study of State Estimation of Fuel Cell Hybrid System using UKF and EKF

Guangzhou, CHINA - May 30 to June 1, 2007 WeA11.1

Comparative Study of State Estimation of Fuel Cell Hybrid System Using UKF and EKF

(Invited Paper)

Rambabu Kandepu
Dept. of Engineering Cybernetics
Norwegian Univ. of Sci. and Tech.
Trondheim, 7491, Norway
Email: Rambabu.Kandepu@itk.ntnu.no

Biao Huang
Chemical and Materials Engineering
University of Alberta, Canada
Email: Biao.Huang@ualberta.ca

Lars Imsland
SINTEF ICT
Trondheim, Norway
Email: Lars.Imsland@sintef.no

Bjarne Foss
Dept. of Engineering Cybernetics
Norwegian Univ. of Sci. and Tech.
Trondheim, 7491, Norway
Email: Bjarne.Foss@itk.ntnu.no

***Abstract*— The principle of state estimation of a dynamic system using Unscented Kalman Filter (UKF) and Extended Kalman Filter (EKF) is briefly described. Two nonlinear examples are considered to compare the state estimation using UKF and EKF. A Solid Oxide Fuel Cell (SOFC) combined with Gas Turbine (GT) hybrid system is described and system level modeling of the hybrid system is discussed. The state estimation using UKF and EKF is applied to the fuel cell hybrid system.**

I. Introduction

State estimation plays a significant role in control and monitoring. As all the practical systems have some degree of nonlinearity and the nonlinear state estimation has to be taken into consideration for designing an advanced control system and for monitoring purpose. The state estimation is a means to propagate the probability distribution function (pdf) of the state of the system over time and to update the pdf using the measurements from the system. Kalman Filter (KF) is the most commonly used estimator for linear systems. KF is optimal if the system is linear and noises are Gaussian. The Gaussian distribution can be represented by two parameters at a time instant: mean and variance. KF propagates the mean and variance in an optimal (minimum mean square error) way. If the system cannot be approximated by a linear function in its operating region, nonlinear state estimation is necessary for an optimal control design and effective monitoring purpose. The most common way of applying KF for the nonlinear system is in the form of Extended Kalman Filter (EKF). In EKF, the pdf is propagated through a linear approximation of the system around the operating point at that time instant. In doing so, the EKF needs the Jacobian matrices which makes it difficult for higher order systems, for online state estimation. Julier and Uhlmann [3]developed an alternative method for the nonlinear estimation: Unscented Kalman Filter (UKF). The UKF propagates the pdf in a simple and effective way and it is accurate up to second order in estimating mean and covariance [3].

In the foreseeable future, fossil fuels including natural gas will be a major source of energy. With today's increasing concern about global warming and climate change, there is an incentive to investigate natural gas power processes that operate efficiently, thus emitting less per kWh produced, and also investigate power production processes with CO_2 capture capabilities. It is widely accepted that fuel cells are power sources that will become increasingly important due to high efficiency, low levels of pollution and noise, and high reliability. One of the most promising fuel cell technologies is the Solid Oxide Fuel Cell (SOFC) due to its solid state design and internal reforming of gaseous fuels, in addition to its high efficiency. The SOFC converts the chemical energy of fuel directly to electrical energy. Since SOFCs operate at high temperatures (about 1000 °C), natural gas can be used directly as fuel. The electrical efficiency of a SOFC can reach 55%. Another significant advantage of the SOFC is that since it operates at high temperature and its efficiency increases when pressurized, it naturally lends itself as a heat source for a gas turbine (GT) cycle. The combined (hybrid) cycle can theoretically have an overall electrical efficiency of up to 70%. with a power range from a few hundred kWs to a few MWs. Processes based on SOFCs can be used as power sources with CO_2 capture, since the "used fuel" (and water) and air exit streams can be kept separated. The main applications of the hybrid system include remote area power supply and distributed power generation.

The paper is organized as follows: Section II and III explain the principle of UKF and EKF respectively. Section IV applies the UKF and the EKF to two engineering applications and compares the performances of UKF and EKF for the state estimation. Section V describes the SOFC/GT hybrid system and state estimation using UKF and EKF. Section VI gives the conclusions and states future work.

II. State Estimation of Nonlinear Systems

A. UKF

The principle of the UKF is explained with the following example: let x be a random variable and

$$y = f(x) \tag{1}$$

be a nonlinear function. The question is how the UKF approximate the propagation of pdf of x? For example, in the case of Gaussian distribution, how to calculate the mean $(\overline{y})$ and covariance (Σ_y) of y? Consider a set of sigma points $x^{(i)}$, (similar to the random samples of a specific distribution function in Monte Carlo simulations) with each point being associated with a weight $w^{(i)}$. Both the sigma points and the weights are computed deterministically through a set of conditions given in [3]. Then the following steps are involved in approximating the mean and covariance:

1-4244-0818-0/07/$20.00 © 2007IEEE

1) Propagate each sigma point through the nonlinear function,

$$\mathcal{Y}^{(i)} = f(x^{(i)}) \tag{2}$$

2) Mean is the weighted average of the transformed points,

$$\overline{y} = \sum_{i=0}^{p} w^{(i)} y^{(i)} \tag{3}$$

3) The covariance is the weighted outer product of the transformed points,

$$\Sigma_y = \sum_{i=0}^{p} w^{(i)} \left(y^{(i)} - \overline{y}\right)\left(y^{(i)} - \overline{y}\right)^T \tag{4}$$

The UKF algorithm is presented below; for the fundamental theory, refer to [1], [2]. Let the system be represented by the following standard discrete time equations:

$$x_k = f(x_{k-1}, v_{k-1}, u_{k-1}) \tag{5}$$

$$y_k = h(x_k, n_k, u_k) \tag{6}$$

where x is the system state, v the process noise, n the observation noise, u the input and y the noisy observation of the system. An augmented state at time instant k,

$$x_k^a = \begin{bmatrix} x_k \\ v_k \\ n_k \end{bmatrix} \tag{7}$$

is defined. The augmented state variable dimension is,

$$L = L_x + L_v + L_n \tag{8}$$

where L_x is the original state dimension, L_v is the process noise dimension and L_n is the observation noise dimension. Similarly, the augmented state covariance matrix is built from the covariance matrices of x, v,and n:

$$P^a = \begin{bmatrix} P_x & 0 & 0 \\ 0 & R_v & 0 \\ 0 & 0 & R_n \end{bmatrix} \tag{9}$$

where R_v and R_n are the process and observation noise covariance matrices.

1) Algorithm::

- *Initialization* :

$$\widehat{x}_0 = E[x_0], \quad P_{x_0} = E\left[(x_0 - \widehat{x}_0)(x_0 - \widehat{x}_0)^T\right] \tag{10}$$

$$\widehat{x}_0^a = E[x^a] = E[\widehat{x}_0 \quad 0 \quad 0]^T \tag{11}$$

$$P_0^a = E\left[(x_0^a - \widehat{x}_0^a)(x_0^a - \widehat{x}_0^a)^T\right] = \begin{bmatrix} P_x & 0 & 0 \\ 0 & R_v & 0 \\ 0 & 0 & R_n \end{bmatrix} \tag{12}$$

- *For* $k = 1, 2, ...\infty$:
  1) Calculate sigma-points [1]:

$$\chi_{k-1}^a = \left[\begin{array}{ccc} \widehat{x}_{k-1}^a & \widehat{x}_{k-1}^a + \gamma\sqrt{P_{k-1}^a} & \widehat{x}_{k-1}^a - \gamma\sqrt{P_{k-1}^a} \end{array}\right] \tag{13}$$

where γ is a scaling parameter.

2) Time-update equations:

$$\chi_{k/k-1}^x = f\left(\chi_{k-1}^x, \chi_{k-1}^v, u_{k-1}\right) \tag{14}$$

$$\widehat{x_k^-} = \sum_{i=0}^{2L} w_i^{(m)} \chi_{i,k/k-1}^x \tag{15}$$

$$P_{x_k}^- = \sum_{i=0}^{2L} w_i^{(c)} \left(\chi_{i,k/k-1}^x - \widehat{x_k^-}\right)\left(\chi_{i,k/k-1}^x - \widehat{x_k^-}\right)^T \tag{16}$$

3) Measurement-update equations:

$$y_{k/k-1} = h\left(\chi_{k/k-1}^x, \chi_{k-1}^n\right) \tag{17}$$

$$\widehat{y_k^-} = \sum_{i=0}^{2L} w_i^{(m)} y_{i,k/k-1} \tag{18}$$

$$P_{\widetilde{y}_k} = \sum_{i=0}^{2L} w_i^{(c)} \left(y_{i,k/k-1} - \widehat{y_k^-}\right)\left(y_{i,k/k-1} - \widehat{y_k^-}\right)^T \tag{19}$$

$$P_{x_k y_k} = \sum_{i=0}^{2L} w_i^{(c)} \left(\chi_{i,k/k-1}^x - \widehat{x_k^-}\right)\left(y_{i,k/k-1} - \widehat{y_k^-}\right)^T \tag{20}$$

$$K_k = P_{x_k y_k} P_{\widetilde{y}_k}^{-1} \tag{21}$$

$$\widehat{x}_k = \widehat{x_k^-} + K_k\left(y_k - \widehat{y_k^-}\right) \tag{22}$$

$$P_{x_k} = P_{x_k}^- - K_k P_{\widetilde{y}_k} K_k^T \tag{23}$$

2) EKF: Consider the same example discussed in (1). If f is a linear function and the pdf of x is a Gaussian distribution, then Kalman Filter (KF) is optimal in propagating the pdf. Even if the pdf is not Gaussian, the KF is optimal up to the first two moments in the class of linear estimators [2]. The KF is extended to the class of nonlinear systems and it is termed as EKF. In case of a nonlinear function $(f(x))$, the nonlinear function is linearized around the current value of x, and the KF theory is applied to get the mean and variance of y. In other words, the mean $(\overline{y})$and variance (P_y) of y, given the mean $(\overline{x})$ and variance (P_x) of the pdf of x are calculated as follows:

$$\overline{y} = f(\overline{x}) \tag{24}$$

$$P_y = G_x P_x G_x^T \tag{25}$$

where g is the linear approximation of $f((x)$ around $\overline{x}$.

The EKF algorithm is presented below for a general nonlinear system represented by equations (5) and (6) [1].

3) Algorithm:

- *Initialization* :

$$\widehat{x}_0 = E[x_0], \quad (26)$$
$$P_{x_0} = E\left[(x_0-\widehat{x}_0)(x_0-\widehat{x}_0)^T\right] \quad (27)$$
$$R_v = E\left[(v-\overline{v})(v-\overline{v})^T\right] \quad (28)$$
$$R_n = E\left[(n-\overline{n})(n-\overline{n})^T\right] \quad (29)$$

- *For* $k=1,2,..\infty$:
  1) Prediction step
     - Compute the process model Jacobians:

$$F_{x_k} = \nabla_x f(x,\overline{v},u_k)\,|_{x=\widehat{x}_{k-1}} \quad (30)$$
$$G_v = \nabla_v f(\widehat{x}_{k-1},v,u_k)\,|_{v=\overline{v}} \quad (31)$$

     - Compute predicted state mean and covariance (*time update*)

$$\widehat{x}_k^- = f(\widehat{x}_{k-1},\overline{v},u_k) \quad (32)$$
$$P_{x_k}^- = F_{x_k}P_{x_k}F_{x_k}^T + G_vR_vG_v^T \quad (33)$$

  2) Correction step
     - Compute observation model Jacobians:

$$H_{x_k} = \nabla_x h(x,\overline{n},u_k)\,|_{x=\widehat{x}_k^-} \quad (34)$$
$$D_n = \nabla_n h(\widehat{x}_k^-,n,u_k)\,|_{n=\overline{n}} \quad (35)$$

     - Update estimates with latest observation (*measurement update*)

$$K_k = P_{x_k}^-H_{x_k}^T \times\left(H_{x_k}P_{x_k}^-H_{x_k}^T + D_nR_nD_n^T\right)^{-1} \quad (36)$$
$$\widehat{x}_k = \widehat{x}_k^- + K_k\left[y_k - h\left(\widehat{x}_k^-,\overline{n}\right)\right] \quad (37)$$
$$P_{x_k} = (I-K_kH_{x_k})P_{x_k}^- \quad (38)$$

III. Examples

Two examples are considered to compare the state estimation using UKF and EKF.

A. Continuous Stirred Tank Reactors (CSTR) in Series

The system consists of two constant volume reactors cooled by a single coolant stream flowing in a cocurrent fashion. An irreversible, exothermic reaction occurs in the two tanks. The effluent stream from the first reactor serves as the feed stream for the second reactor. The process model consists of four nonlinear ordinary differential equations:

$$\dot{C}_{A1} = \frac{q}{V_1}(C_{Af}-C_{A1}) - k_0C_{A1}\exp\left(-\frac{E}{RT_1}\right) \quad (39a)$$

$$\dot{T}_1 = \frac{q}{V_1}(T_f-T_1) + \frac{(-\Delta H)k_0C_{A1}}{\rho C_p}\exp\left(-\frac{E}{RT_1}\right) + \frac{\rho_cC_{pc}}{\rho C_pV_1}q_c\left[1-\exp\left(-\frac{hA_1}{q_c\rho_cC_{pc}}\right)\right](T_{cf}-T_1) \quad (40)$$

$$\dot{C}_{A2} = \frac{q}{V_2}(C_{A1}-C_{A2}) - k_0C_{A2}\exp\left(-\frac{E}{RT_2}\right) \quad (41)$$

$$\dot{T}_2 = \frac{q}{V_2}(T_1-T_2) + \frac{(-\Delta H)k_0C_{A2}}{\rho C_p}\exp\left(-\frac{E}{RT_2}\right) + \frac{\rho_cC_{pc}}{\rho C_pV_2}q_c\left[1-\exp\left(-\frac{hA_2}{q_c\rho_cC_{pc}}\right)\right] \times\left[T_1-T_2+\exp\left(-\frac{hA_1}{q_c\rho_cC_{pc}}\right)(T_{cf}-T_1)\right] \quad (42)$$

The same notation as in the [7] is being used, where the subscripts $1, 2, c$, and f denote the first reactor, second reactor, coolant stream, and feed stream, respectively. The control objective of the process is to control the effluent composition from the second tank (C_{A2}) by manipulating the coolant flow rate (q_c). The state, output and input variables of the process are defined as follows:

$$x^T = [C_{A1} \quad T_1 \quad C_{A2} \quad T_2], \quad (43)$$
$$y = C_{A2}, \quad (44)$$
$$u = q_c \quad (45)$$

The process is highly nonlinear with the selected input and output variables [7]. The nominal values of all the variables are taken from [7]. The UKF and EKF are used to estimate the states. A white noise with Gaussian distribution is applied on each state and on the output. The simulation results are shown in Figures 1 and 2. The input (q_c) is changed by 50% at 20th sec.

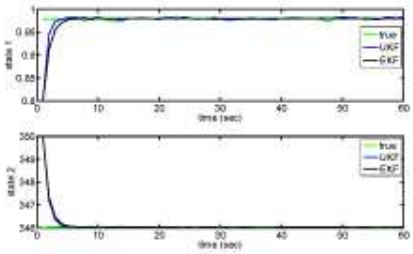

Fig. 1. State estimation of CSTR using UKF and EKF: states 1 and 2

From the simulation results, it is clear that both the UKF and EKF estimates converge even in the presence of process and observation noises, and a large input disturbance, though the UKF estimate converge faster compared to the EKF. For the EKF, the Jacobian matrices are obtained at each time step by numerical linearization.

B. Continuous Fermentor

The process consists of a constant volume reactor in which a single, rate limiting substrate promotes biomass growth and product formation. By assuming constant yields, a process model with three differential equations can be obtained [7].

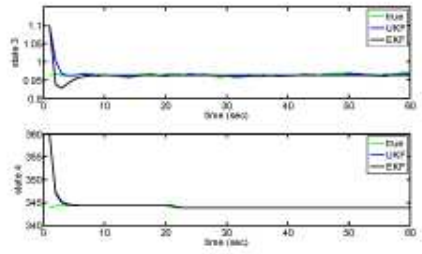

Fig. 2. State estimation of CSTR using UKF and EKF: states 3 and 4

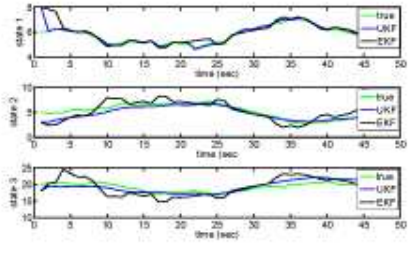

Fig. 3. State estimation of Continuous Fermentor using UKF and EKF: states 1-3

$$\dot{X} = -DX + \mu(S,P)X \tag{46a}$$

$$\dot{S} = D(S_f - S) - \frac{1}{Y_{X/S}}\mu(S,P)X \tag{46b}$$

$$\dot{P} = -DP + [\alpha\mu(S,P) + \beta]X \tag{46c}$$

where X, S and P are the biomass, substrate, and product concentrations, respectively; D is the dilution rate; S_f is the feed substrate concentration; and $Y_{X/S}$, α and β are yield parameters. The specific growth rate μ is modeled as,

$$\mu(S,P) = \frac{\mu_m\left(1 - \frac{P}{P_m}\right)S}{K_m + S + \frac{S^2}{K_i}} \tag{47}$$

where: μ_m is the maximum specific growth rate; and P_m, K_m and K_i are constant parameters. Nominal operating conditions are taken from [7]. For this process D is the manipulated variable and X is the controlled variable:

$$x^T = [X \quad S \quad P], \tag{48}$$

$$y = X, \tag{49}$$

$$u = D \tag{50}$$

A white noise with Gaussian distribution is applied on each state and the output in simulation. The state estimation is performed using both the UKF and EKF and the simulation results are as shown in Figure 3. The input (D) is decreased by a 10% step at 25th sec. The initial estimate of the state is taken different from the actual state. From the simulation results, in the presence of noise, UKF performs better compared to the EKF.

IV. SOFC/GT Hybrid System

A. System Description

A schematic diagram of the SOFC/GT hybrid system integrated in an autonomous power system is shown in Figure 1. Fuel is partially steam reformed in a pre-reformer before it enters the SOFC anode. A part of anode flue gas is recycled to supply the necessary steam required for the steam reformation in the pre-reformer. The remaining part of the anode flue gas is supplied to a combustor where the unused fuel is burnt completely in presence of oxygen coming from the cathode flue gas. Air is compressed and preheated in a heat exchanger before entering the SOFC cathode. The hot stream from the combustor is expanded using a High Pressure Turbine (HPT) which drives the compressor. The HPT flue gas is expanded to atmospheric pressure using Low Pressure Turbine (LPT) which drives an alternator. The DC power from SOFC stack is inverted to AC using an inverter. The inverter and the alternator are connected to the electric load through a bus bar. Typically 60-70% of the total power is supplied by the SOFC stack.

TABLE I
Inputs

No.	Input
1	FU reference point
2	SOFC temperature reference point
3	electric load on the system (measured disturbance)

B. Modeling

All the models of the system are developed in the modular modeling environment gPROMS [6]. The detailed modeling of each component of the system can be found in [4]. A brief description of the SOFC stack model is presented below.

1) SOFC stack: It is assumed that all the SOFCs in the stack operate at identical conditions along the fuel flow direction. A zero-dimensional SOFC model is developed with no regard to the geometry of the cell. The model developed is a lumped one, which includes dynamic molar balances of all the species both in anode and cathode volumes separately. Further, it includes an energy balance treating the whole SOFC as a single volume to model the temperature dynamics of the SOFC solid phase mean temperature. There is a radiation from the SOFC to the pre-reformer. The voltage developed across the cell is modeled using Nernst equation, the operating cell voltage is calculated by considering both ohmic and activation losses.

In [4], the low complexity, control relevant SOFC model is evaluated against a detailed model developed in [5]. The comparisons indicate that the low complexity model is sufficient to approximate the important dynamics of the SOFC and can hence be used for operability and control studies.

C. Regulatory Controller

Local regulatory control has been considered for the system, and the local control adds additional state to the system. Thus,

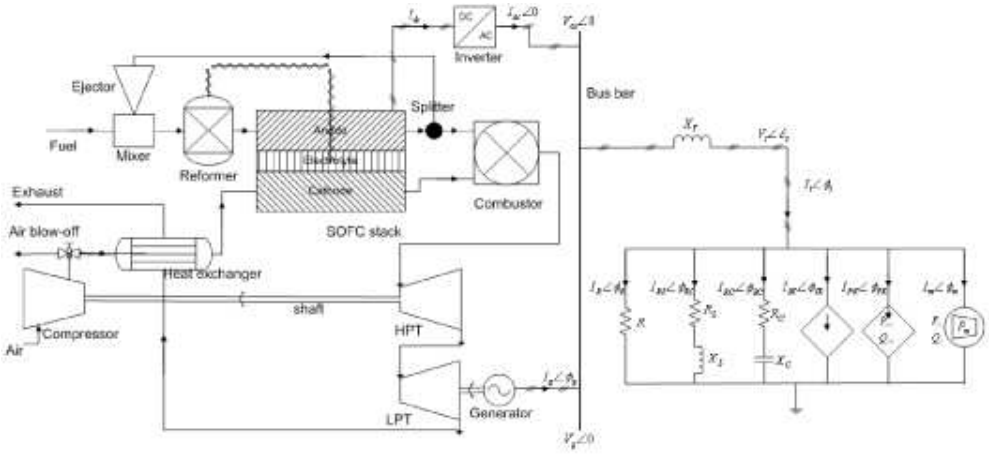

Fig. 4. SOFC-GT hybrid system integrated in an autonomous power system status 1-3

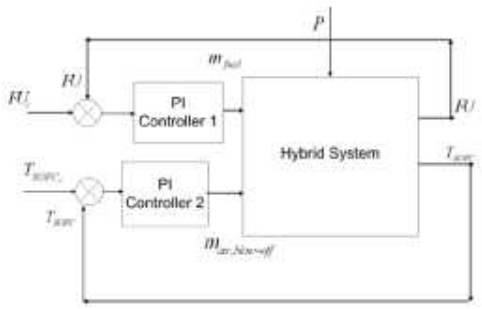

Fig. 5. De-centralized control structure using PI controllers

TABLE II
STATES

No.	State
1	Pre-reformer temperature (K)
2	H_2 concentration in pre-reformer (mol)
3	CH_4 concentration in pre-reformer (mol)
4	H_2O concentration in pre-reformer (mol)
5	CO concentration in pre-reformer (mol)
6	CO_2 concentration in pre-reformer (mol)
7	PI controller 1 integral term
8	Compressor shaft speed (rad/s)
9	PI controller 2 integral term
10	Heat exchanger hot stream temperature (K)
11	Heat exchanger cold stream temperature (K)
12	O_2 concentration in cathode (mol)
13	H_2 concentration in anode (mol)
14	CH_4 concentration in anode (mol)
15	H_2O concentration in anode (mol)
16	CO concentration in anode (mol)
17	CO_2 concentration in anode (mol)
18	SOFC outlet temperature (K)

to design state estimation of the complete system, the local control strategy has to be understood.

A control system is necessary to reject the disturbances such as load changes, fuel and air inlet temperature changes, fuel composition etc. Moreover, during the disturbances, the SOFC temperature should be controlled to prevent cell break down. A decentralized control scheme with two PI controllers is proposed in [4] to reject the disturbances and to control the SOFC temperature. In Figure 5, FU refers to Fuel Utilization, which is defined as the ratio of fuel used in the SOFC and the fuel supplied to the SOFC. It is controlled to the reference value (0.85) by manipulating the fuel flow to the system. The air blow-off flow is manipulated to control the SOFC temperature to the reference value. The controller performs well in terms of tracking [4], the system efficiency can be improved by optimizing the reference values of the controlled variables. Also there are some constraints which are to be taken into account, for example, steam to carbon ratio at pre-reformer inlet, differential pressure across anode and cathode, compressor surge etc. To achieve this, Model Predictive Control (MPC) is necessary and as a basis to develop the MPC as well as monitoring of the hybrid system, the state estimator is to be designed.

D. State Estimation

The SOFC/GT hybrid system is modeled in gPROMS [6] modeling environment. It has 3 inputs, 18 states, and 14 measured outputs which are listed in Tables I, II, and III respectively. The hybrid system model in gPROMS is exported to matlab and is used as function in matlab using the gO:MATLAB package [6]. The state estimator of the hybrid system is designed using both the UKF and EKF and the simulation results are presented in Figures 6 and 7. The initial state estimate is different from the actual initial state and from

TABLE III
OUTPUTS

No.	Output
1	Pre-reformer temperature (K)
2	Shaft speed (rad/s)
3	Heat exchanger hot stream temperature (K)
4	Heat exchanger cold stream temperature (K)
5	SOFC outlet temperature (K)
6	Combustor outlet temperature (K)
7	Fuel mass flow rate (kg/s)
8	Anode recycle flow rate (kg/s)
9	Flow to the combustion chamber (kg/s)
10	Air blow-off flow rate (kg/s)
11	Air mass flow rate (kg/s)
12	SOFC current (A)
13	SOFC voltage (V)
14	Generator power (kW)

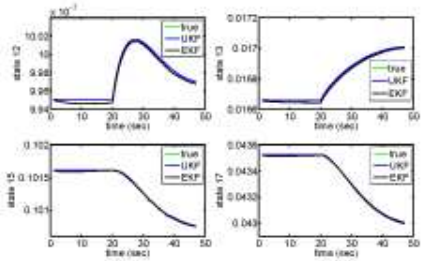

Fig. 6. Comparison of state estimation using UKF and EKF: concentration of O2 in cathode and concentrations of H2, H2O and CO2 in anode of SOFC

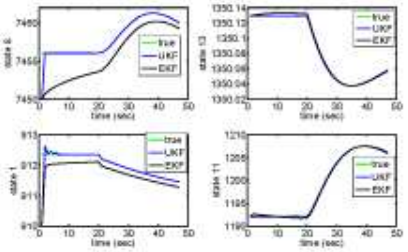

Fig. 7. Comparison of state estimation using UKF and EKF: Compressor shaft speed and SOFC, prereformer and heat exchanger cold stream temperatures

the simulation results it can be concluded that UKF estimate converges to the true states very fast compared to the EKF estimate.

E. Discussion

Some experience is needed in tuning the UKF estimator. The initial covariance matrix should be small in size as it determines the distribution of sigma points around the mean. The state covariance matrix should be positive definite at each iteration and the algorithm doesn't guarantee the positive definiteness of the state covariance matrix. Hence the tuning of the UKF estimator is not straight forward. Further the generated sigma points at each iteration should be feasible for the nonlinear transformation; hence sigma point conditioning may be needed depending on the system.

The EKF needs the Jacobian matrices at each iteration and numerical linearization is performed at each step. The size of the perturbation for the numerical linearization is a tuning factor in addition to the state, process noise and measurement noise covariance matrices. The EKF should be properly tuned otherwise it may result in an unstable state estimator.

Overall, the UKF performs better to EKF in terms of the faster convergence in the considered system. If there is no need of numerical linearization, EKF is faster to UKF in terms of computational load, which is not the case in general for the higher order systems. A fair comparison is done between the two estimators as both the estimators are properly tuned to their best.

V. Conclusions and Future Works

A. Conclusions

The nonlinear estimation using UKF and EKF is performed on two engineering application examples. The results show that the UKF performs better compared to EKF in terms of faster convergence otherwise both the estimators give satisfactory results. The state estimation of SOFC/GT hybrid system is performed using UKF and EKF and the simulation results show that UKF outperforms EKF.

B. Future Works

Future work will be focused on the tuning and positive definite problems mentioned with UKF. The developed estimator will be used to designing a nonlinear MPC.

Acknowledgment

Financial support from The Gas Technology Center, NTNU-SINTEF and NFR is acknowledged. We also acknowledge the funding support from Western Canada Fuel Cell Initiative (WCFCI).

References

[1] R. Van der Merwe, "Sigma-Point Kalman Filters for probability inference in dynamic state-space models" *PhD thesis*, 2004, Oregon Health and Science University.

[2] B. Huang and Q. Wang, "Overview of emerging Bayesian approach to nonlinear system identification", *Round tables on Non-linear Model Identification, International Workshop on Solving Industrial Control and Optimization Problems*, Cramado, Brazil, April 6-7, 2006.

[3] S. Julier and J. K. Uhlmann, "Unscented filtering and nonlinear estimation", *Proceedings of the IEEE*, vol. 92, 2004, pp.401-422.

[4] R. Kandepu, L. Imsland, B. Foss, C. Stiller, B. Thorud and O. Bolland, "Modeling and control of a SOFC-GT based autonomous power system", *Journal of Energy*, 2006, In press.

[5] C. Stiller, B. Thorud, S. Seljebo, H. Karoliussen and O. Bolland "Finite-volume modeling and hybrid-cycle performance of planar and tubular Solid Oxide Fuel Cells", *Journal of power sources*, vol. 141, 2005, pp. 227-240.

[6] gPROMS, "gPROMS introductory user guide", *Process Systems Enterprise Ltd*, 2004.

[7] M. H. Henson, D. E. Seborg, "*Nonlinear Process Control*", Prentice Hall, NJ, Chapter 4, pp. 198-206, 1997.

Appendix B

Modeling report

In this appendix, modeling details of different components of the SOFC-GT power system are presented. The values of the parameters used for developing the models are listed in tables.

B.1 Solid Oxide Fuel Cell (SOFC)

B.1.1 Introduction

The Solid Oxide Fuel Cell (SOFC) is a device which converts chemical energy of a fuel directly into electrical energy [3]. The basic components of the SOFC are anode, cathode and electrolyte. The operation of the SOFC is explained in figure B.1. The electrolyte material is zirconia stabilized with the addition of a small percentage of yttria (Y_2O_3). The anode material is a zirconia cermet. The most common cathode material is strontium-doped lanthanum manganite. Fuel is supplied to the anode and air is the supplied to cathode. At the cathode-electrolyte interface, oxygen molecules accept electrons coming from the external circuit to form oxide ions. The electrolyte layer allows only oxide ions to pass through it and at the anode-electrolyte interface, hydrogen molecules present in the fuel react with oxide ions to form steam and electrons get released. These electrons pass through the external circuit and reach the cathode-electrolyte layer, and thus the circuit is closed. To increase the amount of power generated, a number of cells can be connected in series/parallel. This is known as stacking of cells. Also, there are mainly two types of SOFCs depending on the geometry; tubular and planar. The operating pressure can be from one bar to 15 bars. It is found that SOFCs show enhanced performance with increasing cell pressure [3, Chap.2]. The operating temperature of SOFC is around $1000°C$. Due to the high operating temperature, an advantage is that several types of fuels can be used. In this model, natural gas which mainly consists of methane is used. Because of the electrochemical reactions, there is a production of steam, and this steam is used to reform methane into hydrogen. Typically, one third of the natural gas is reformed (for example, in a pre-reformer) before it enters the SOFC and the remaining part is reformed within the SOFC. The main three reforming reactions that take place during the reformation of methane are

$$\begin{aligned} CH_4 + H_2O &\Leftrightarrow CO + H_2 \\ CO + H_2O &\Leftrightarrow CO_2 + H_2 \\ CH_4 + 2H_2O &\Leftrightarrow CO_2 + 4H_2 \end{aligned} \tag{B.1}$$

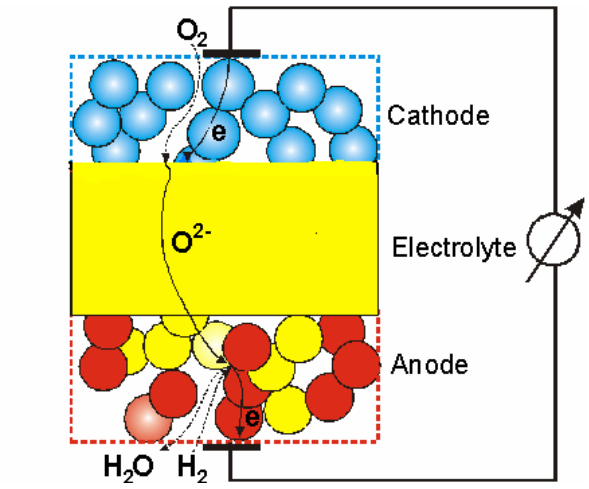

Figure B.1: SOFC operation

The electrochemical reactions that take place in the SOFC are

$$H_2 + O^{2-} \rightarrow H_2O + 2e^- \quad \text{(anode)} \tag{B.2}$$
$$\frac{1}{2}O_2 + 2e^- \rightarrow O^{2-} \quad \text{(cathode)}$$

The main aim here is to get a control relevant model with low complexity which should include the important dynamics from an operating point of view.

B.1.2 Model assumptions

1. All the physical variables vary spatially in the SOFC. Here a bulk model is developed in which it is assumed that all the variables are uniform all over the SOFC. The model is valid for a single SOFC cell. If the "one volume" model is too crude, a sequential model structure can be used, see section *Discretization.*

2. There is sufficient turbulence and diffusion within the fuel cell for perfect mixing to occur [7, Chap.13]. As all the reactants are gases, this assumption can be made without much consideration.

3. As there is a continuous flow of gases across the SOFC, the dynamics of gas components is fast when it is compared with that of solid. As the fast dynamics do not have much effect on the overall SOFC dynamics/performance, they are neglected.

4. The pressure losses are neglected within the SOFC. There can be some friction along the surfaces of the SOFC to the flow of gases, which causes the pressure drop. This pressure loss is small in magnitude, when it is compared with the operating pressure of the SOFC, hence it is neglected.

5. Within the SOFC, all gases are assumed to be ideal, since the temperature is high and pressure is low within the SOFC.

B.1.3 Parameters and variables

Parameters

The parameters used in the model are listed in the Table B.1. In the table, index i refers to component and index j refers to reaction.

Variables

Table B.2 gives the list of all variables used. In the table, index i refers to component and index j refers to reaction.

B.1.4 Interfaces

The interfaces of the SOFC model are shown in figure B.2. The model has four material streams interfaces: Fuel supply to the anode inlet, air supply to the cathode inlet, anode flue gas from anode outlet and cathode flue gas from cathode outlet. And the model has one energy stream interface, which is the heat loss mainly due to the radiation.

Table B.1: SOFC model parameters

Symbol	**Definition**	**Units**	**Value**
R	Universal gas constant	J/(mol·K)	8.3145
F	Faraday's constant	C/mol	96485.3415
E^o	Open circuit voltage	V	1.18
V_{an}	Volume of anode	m^3	
V_{ca}	Volume of cathode	m^3	
mC_p^s	Solid heat capacity	J/K	
a_{ij}^{an}	Stoichiometric matrix for the reactions in anode		
a_{ij}^{ca}	Stoichiometric matrix for the reactions in cathode		
n_{rx}^{an}	Number of reactions at anode		4
n_{rx}^{ca}	Number of reactions at cathode		1
A_{k_2}	Pre-exp. factor for rate coefficient k_2		3.71×10^{17}
A_{k_3}	Pre-exp. factor for rate coefficient k_3		5.43×10^{5}
A_{k_4}	Pre-exp. factor for rate coefficient k_4		2.83×10^{14}
$A_{K_{H_2}^{ads}}$	Pre-exp. factor for adsorption constant of H_2		6.12×10^{-14}
$A_{K_{CH_4}^{ads}}$	Pre-exp. factor for adsorption constant of CH_4		6.65×10^{-9}
$A_{K_{H_2O}^{ads}}$	Pre-exp. factor for adsorption constant of H_2O		1.77×10^{5}
$A_{K_{CO}^{ads}}$	Pre-exp. factor for adsorption constant of CO		8.23×10^{-10}
E_2	Activation energy of the reaction 2 in anode	J/mol	240.1×10^{3}
E_3	Activation energy of the reaction 3 in anode	J/mol	67.13×10^{3}
E_4	Activation energy of the reaction 4 in anode	J/mol	243.9×10^{3}
$-\Delta\overline{h}_{H_2}^{ads}$	Enthalpy change of adsorption of H_2	J/mol	82.9×10^{3}
$-\Delta\overline{h}_{CH_4}^{ads}$	Enthalpy change of adsorption of CH_4	J/mol	38.28×10^{3}
$-\Delta\overline{h}_{H_2O}^{ads}$	Enthalpy change of adsorption of H_2O	J/mol	-88.68×10^{3}
$-\Delta\overline{h}_{CO}^{ads}$	Enthalpy change of adsorption of CO	J/mol	70.65×10^{3}
k_{an}	Constant in the calculation of anode outlet mass flow		
k_{ca}	Constant in the calculation of cathode outlet mass flow		

Table B.2: SOFC model variables

Symbol	Definition	Units
N_i^{an}	Number of moles of component i in anode	mol
N_i^{ca}	Number of moles of component i in cathode	mol
I	Current	A
V	Voltage	V
E	Open circuit voltage	V
V_{act}	Activation voltage	V
V_{conc}	Concentration voltage	V
r	Ohmic resistance	Ω
P_{DC}	Amount of DC power produced by SOFC	W
P_{rad}	Amount of radiation power from SOFC	W
Q	Loss of heat power due to conduction	W
p_{an}	Pressure in anode	Pa
p_i^{an}	Partial pressure of component i in anode	Pa
r_j^{an}	Reaction rate of reaction j in anode	mol/s
r_j^{ca}	Reaction rate of reaction j in cathode	mol/s
$\dot{N}_i^{in,an}$	Molar flow rate of component i at anode inlet	mol/s
$\dot{N}_i^{in,ca}$	Molar flow rate of component i at cathode inlet	mol/s
$\dot{N}_i^{out,an}$	Molar flow rate of component i at anode outlet	mol/s
$\dot{N}_i^{out,ca}$	Molar flow rate of component i at cathode outlet	mol/s
$\dot{m}_{out,an}$	Mass flow rate at anode outlet	kg/s
$\dot{m}_{out,ca}$	Mass flow rate at cathode outlet	kg/s
T	Temperature of SOFC	K
k_2	Rate coefficient for reaction 2 in anode	$\mathrm{mol\,Pa^{0.5}/(kg_{cat}{\cdot}s)}$
k_3	Rate coefficient for reaction 3 in anode	$\mathrm{mol/(kg_{cat}{\cdot}s)}$
k_4	Rate coefficient for reaction 4 in anode	$\mathrm{mol/(kg_{cat}{\cdot}s)}$
$K_{H_2}^{ads}$	Adsorption constant of H_2	$\mathrm{Pa^{-1}}$
$K_{CH_4}^{ads}$	Adsorption constant of CH_4	$\mathrm{Pa^{-1}}$
$K_{H_2O}^{ads}$	Adsorption constant of H_2O	$-$
K_{CO}^{ads}	Adsorption constant of CO	$\mathrm{Pa^{-1}}$
K_j	Equilibrium constants for reforming reaction j	
$\Delta\overline{h}_j^{rx}$	Molar specific enthalpy change of reaction j	J/mol
$\Delta\overline{h}_i$	Molar specific enthalpy of component i	J/mol
$\Delta\overline{h}_i^{in,an}$	Molar specific enthalpy of component i at anode inlet	J/mol
$\Delta\overline{h}_i^{in,ca}$	Molar specific enthalpy of component i at cathode inlet	J/mol
γ_{air}	Air utilization factor	
γ_{fuel}	Fuel utilization factor	
$p_{in,an}$	Anode inlet stream pressure	Pa
$p_{out,an}$	Anode outlet stream pressure	Pa
q_{LHV}	Specific molar low heating value	J/mol
η	Efficiency	
$x_i^{in,an}$	Anode inlet molar fraction of a component	
$\Delta\overline{h}_i^f$	Heat of formation of a component	J/mol

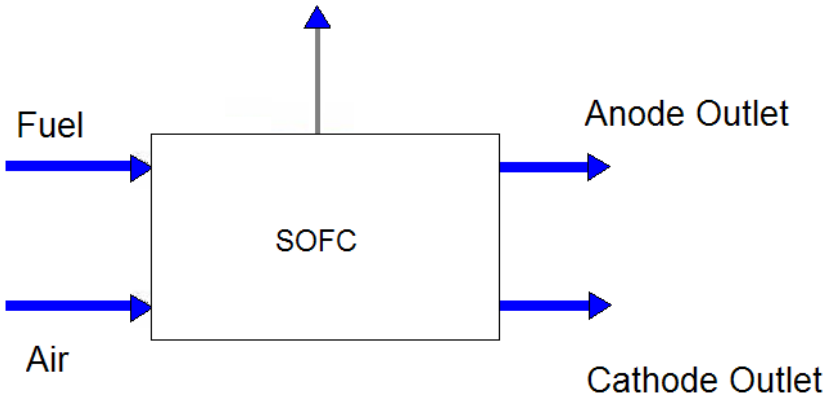

Figure B.2: SOFC interfaces

B.1.5 Equations

Mass balance

We use two mass balances; one for the anode volume and one for the cathode volume:

$$\frac{dN_i^{an}}{dt} = \dot{N}_i^{in,an} - \dot{N}_i^{out,an} + \sum_{j=1}^{n_{rx}^{an}} a_{ij}^{an} r_j^{an}, \quad i = 1, ..., 7, \quad n_{rx}^{an} = 4 \tag{B.3}$$

$$\frac{dN_i^{ca}}{dt} = \dot{N}_i^{in,ca} - \dot{N}_i^{out,ca} + \sum_{j=1}^{n_{rx}^{ca}} a_{ij}^{ca} r_j^{ca}, \quad i = 1, ..., 7, \quad n_{rx}^{ca} = 1$$

In each inlet stream, there can be the following components; Nitrogen (N_2), Oxygen (O_2), Hydrogen (H_2), Methane (CH_4), Steam (H_2O), Carbonmonoxide (CO), and Carbondioxide (CO_2). A number is assigned to each of these components to simplify the notation:

i	1	2	3	4	5	6	7
component	N_2	O_2	H_2	CH_4	H_2O	CO	CO_2

Similarly, each reaction at anode and cathode is assigned with a number, which is given in the Table B.3.

Table B.3: Reactions at anode and cathode

At anode		
Reaction number (j)	**Reaction**	**Reaction rate** (r_j^{an})
1	$H_2 + O^{2-} \rightarrow H_2O + 2e^-$	r_1^{an}
2	$CH_4 + H_2O \Leftrightarrow CO + H_2$	r_2^{an}
3	$CO + H_2O \Leftrightarrow CO_2 + H_2$	r_3^{an}
4	$CH_4 + 2H_2O \Leftrightarrow CO_2 + 4H_2$	r_4^{an}
At cathode		
Reaction number (j)	**Reaction**	**Reaction rate** (r_j^{an})
1	$\frac{1}{2}O_2 + 2e^- \rightarrow O^{2-}$	r_1^{ca}

In (B.3), a_{ij}^{an} represents the stoichiometric matrix for anode reactions,

$$[a_{ij}^{an}] = \begin{bmatrix} 0 & 0 & 0 & 0 \\ 0 & 0 & 0 & 0 \\ -1 & 3 & 1 & 4 \\ 0 & -1 & 0 & -1 \\ 1 & -1 & -1 & -2 \\ 0 & 1 & -1 & 0 \\ 0 & 0 & 1 & 1 \end{bmatrix} \tag{B.4}$$

Similarly, a_{ij}^{ca} is the stoichiometric matrix for the reaction in cathode,

$$[a_{ij}^{ca}] = \begin{bmatrix} 0 \\ -0.5 \\ 0 \\ 0 \\ 0 \\ 0 \\ 0 \end{bmatrix} \tag{B.5}$$

The reaction rates r_1^{an} and r_1^{ca} are related by

$$r_1^{ca} = -I/(2F) = -r_1^{an}$$

and the other reaction rates in the Table B.3, and are calculated by (B.6)

[8].

$$
\begin{aligned}
r_1^{an} &= I/(2F) \\
r_2^{an} &= \frac{k_2}{p_{H_2}^{an^2.5}} \left(p_{CH_4}^{an} p_{H_2O}^{an} - \frac{p_{H_2}^{an^3} p_{CO}^{an}}{K_2} \right) /(DEN)^2 \\
r_3^{an} &= \frac{k_3}{p_{H_2}^{an}} \left(p_{CO}^{an} p_{H_2O}^{an} - \frac{p_{H_2}^{an} p_{CO_2}^{an}}{K_3} \right) /(DEN)^2 \\
r_4^{an} &= \frac{k_4}{p_{H_2}^{an^{3.5}}} \left(p_{CH_4}^{an} p_{H_2O}^{an^2} - \frac{p_{H_2}^{an^4} p_{CO_2}^{an}}{K_4} \right) /(DEN)^2 \\
r_1^{ca} &= -I/(2F) = -r_1^{an}
\end{aligned}
\tag{B.6}
$$

In (B.6), DEN is given by

$$
DEN = 1 + K_{CO}^{ads} p_{CO}^{an} + K_{H_2}^{ads} p_{H_2}^{an} + K_{CH_4}^{ads} p_{CH_4}^{an} + K_{H_2O}^{ads} p_{H_2O}^{an} / p_{H_2}^{an} \tag{B.7}
$$

In (B.6), k_2, k_3 and k_4 are rate coefficients for the reforming reactions are calculated by

$$
k_j = A_{kj} \exp(\frac{-E_j}{RT}), \qquad j = 2, 3, 4 \tag{B.8}
$$

and K_2, K_3 and K_4 are the equilibrium constants for the reforming reactions, given by

$$
\begin{aligned}
K_2 &= \exp(-26830/T + 30.114) \qquad [bar^2] \\
K_3 &= \exp(4400/T - 4.036 \qquad\quad [-\ ] \\
K_4 &= \exp(-22430/T + 26.078) \qquad [bar^2]
\end{aligned}
\tag{B.9}
$$

In (B.7), $K_{CO}^{ads}, K_{H_2}^{ads}, K_{CH_4}^{ads}$ and $K_{H_2O}^{ads}$ are the adsorption constants, which are calculated by

$$
K_i^{ads} = A_{K^{ads}i} \exp(\frac{-\Delta \overline{h}_i^{ads}}{RT}), \qquad i = H_2, CH_4, H_2O, CO \tag{B.10}
$$

It is assumed that the exhaust flows at the anode and cathode outlets can be described by the choked exhaust flow equation. This means the mass flow rate of the exhaust flow at anode (cathode) depends on the pressure

difference between the pressure inside anode (cathode) and the pressure at outlet [5]:

$$\dot{m}_{out,an} = \sqrt{k_{an}(p_{an} - p_{out,an})} \tag{B.11}$$
$$\dot{m}_{out,ca} = \sqrt{k_{ca}(p_{ca} - p_{out,ca})}$$

The pressure, volume, and temperature at anode are assumed to be related by the ideal gas equation,

$$p_{an}V_{an} = \sum_{i=1}^{N}(N_i^{an})RT \tag{B.12}$$

Also, the partial pressure of each component at the anode is calculated by using the ideal gas equation,

$$p_i^{an}V_{an} = N_i^{an}RT \tag{B.13}$$

As no pressure loss within the SOFC is assumed, the pressure in the anode is simply equal to the pressure of the inflow stream,

$$p_{in,an} = p_{an} \tag{B.14}$$

Similarly, all the above pressure related equations are used for the cathode. Since it is assumed that there is perfect mixing within the anode (cathode) volume, the mass fraction of each component within the anode is equal to the mass fraction in the outlet flow.

Energy balance

For the energy balance, the control volume is the whole SOFC [7, Chap.13] and the following energy balance equation (B.15) is used [4].

$$mC_p^s\frac{dT}{dt} = \sum_{i=1}^{N}\dot{N}_i^{in,an}(\Delta\overline{h}_i^{in,an} - \Delta\overline{h}_i) + \sum_{i=1}^{N}\dot{N}_i^{in,ca}(\Delta\overline{h}_i^{in,ca} - \Delta\overline{h}_i) \tag{B.15}$$
$$- \sum_{j=1}^{M}\Delta\overline{h}_j^{rx}r_j^{an} - P_{DC} - P_{rad} - Q$$

In (B.15), P_{DC} represents the amount of DC power developed by the SOFC and P_{rad} represents the amount of radiation power given from SOFC. Also, it is to be noted that the molar specific enthalpy of a component depends on the temperature and pressure of the component. As the SOFC operating temperature is very high when compared with the temperature of surroundings, there is always some loss due to the radiation. It can be calculated by [2, Chap.1],

$$P_{rad} = \varepsilon\sigma(T - T_{sur}^4) \tag{B.16}$$

In (B.16), T_{sur} represents the surroundings temperature, ε is the emissivity of the SOFC surface and σ is the *Stefan-Boltzmann constant* ($\sigma = 5.67 \times 10^{-8}\text{W/m}^2\text{.K}^4$).In (B.15), Q represents the conduction heat loss from SOFC to the surroundings.

Voltage

The open circuit voltage of the cell is given by the *Nernst equation* [3, Chap.2],

$$E = E^o + \frac{RT}{2F}\ln\left(\frac{p_{H_2}^{an} {p_{O_2}^{an}}^{0.5}}{p_{H_2O}^{an}}\right) \tag{B.17}$$

In this equation, E^o is the EMF at standard pressure. When the cell is operated, there are voltage losses coming from different sources; activation losses, concentration losses and ohmic losses [3, Chap.3]. Activation losses are caused by the limited reaction rate on the surface of the electrodes. The ohmic losses are due to the resistance of the electrode material and the various interconnections, as well as the resistance of the electrolyte. The concentration losses result from the change in concentration of the reactants at the surface of the electrodes as the fuel is used. The total voltage loss is calculated by,

$$V_{loss} = V_{act} + rI + V_{conc} \tag{B.18}$$

The operating cell voltage is given by,

$$V = E - V_{loss} \tag{B.19}$$

Power

The amount of DC power from the SOFC is given by,

$$P_{DC} = VI$$

Efficiency

The electrical efficiency is defined as the ratio of the electrical energy produced from the SOFC to the low heating value (LHV) of the fuel,

$$\eta = \frac{P_{DC}}{\left(\sum \dot{N}_i^{in,an}\right) q_{LHV}}$$

q_{LHV} of the fuel is calculated by,

$$q_{LHV} = x_{H_2}^{in,an}(-\Delta\overline{h}_{H_2O}^{f}) + x_{CH_4}^{in,an}(\Delta\overline{h}_{CH_4}^{f} - \Delta\overline{h}_{CO_2}^{f} - 2\Delta\overline{h}_{H_2O}^{f}) + x_{CO}^{in,an}(\Delta\overline{h}_{CO}^{f} - \Delta\overline{h}_{CO_2}^{f})$$

Fuel and air utilization factors

As fuel passes through the cell, the hydrogen will be used and its concentration will be reduced. If all the hydrogen is used up, then in theory the voltage at the exit of the cell would be zero. Hence, in practice, not all the fuel or air that is fed to the fuel cell can be used [3, Chap.7]. The fuel utilization factor (γ_{fuel}) is defined as below:

$$\gamma_{fuel} = \frac{\text{mass of } H_2 \text{ utilized}}{\text{mass of } H_2 \text{ supplied} + \text{mass of } H_2 \text{ produced}} \tag{B.20}$$

Similarly, air utilization (γ_{air}) factor is defined as follows.

$$\gamma_{air} = \frac{\text{mass of } O_2 \text{ utilized}}{\text{mass of } O_2 \text{ supplied}} \tag{B.21}$$

In general, one would think that for higher efficiency, these factors should be as high as possible. But, it can be shown that the cell voltage and the cell efficiency fall with higher utilizations [3, Chap.2]. So, fuel and air (oxygen) utilization factors need careful optimizing, especially in a high temperature fuel cell such as the SOFC. The selection of these factors is an important aspect of system design.

B.1.6 Discretization

In a physical SOFC, all the variables are distributed in the SOFC volume. Some important variables, for example, the temperature of the SOFC, must

be analyzed during the operation of the SOFC. If there is too much variation in the temperature of the solid geometrically, the solid may not withstand to those variations and there will be crackdowns. So the distributed nature of the solid temperature is to be analyzed for different operating conditions in order to get the safe operation. The bulk model of the SOFC which is presented in the above sections gives only the bulk temperature but not any information regarding the geometric distribution of it.

The distributed nature of the variables can be modeled using this model by connecting it in a sequential manner. A single SOFC model can be obtained by connecting a number of scaled-down models in series mechanically. Connecting the models in series mechanically means that the outlet gases from a model are supplied to the corresponding inlets of the next model. Scaled-down model is the one that is obtained by scaling down the values of the parameters by the amount corresponding to the number of models being used to represent the distributed nature. Depending on the need of the distributed nature to be obtained, the number of the scaled-down models can be chosen. For example, a case where a single SOFC model is obtained by connecting two scaled-down models is explained below.

As an example, two scaled-down models are connected in series mechanically (figure B.3) to get the single SOFC model. From the figure it is clear that the anode outlet gas from the first model is given to the anode inlet of the second model; cathode outlet gas from the first model is supplied to the cathode inlet of the second model,

$$\begin{aligned} \dot{m}^{1}_{out,an} &= \dot{m}^{2}_{in,an} \\ \dot{m}^{1}_{out,ca} &= \dot{m}^{2}_{in,ca} \end{aligned} \tag{B.22}$$

Electrically, the two scaled-down models are connected in parallel (figure B.4). This means the voltage across each of the model is the same and the total current is divided between the two models,

$$\begin{aligned} V &= V_1 = V_2 \\ I &= I_1 + I_2 \end{aligned}$$

To get the better distributed nature of the variables, more number of scaled-down models can connected in this way.

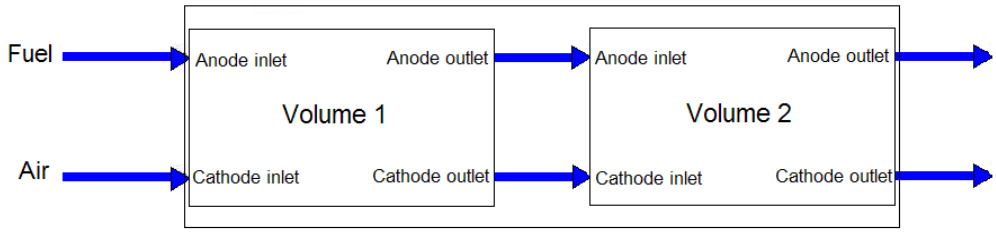

Figure B.3: Composition mechanically

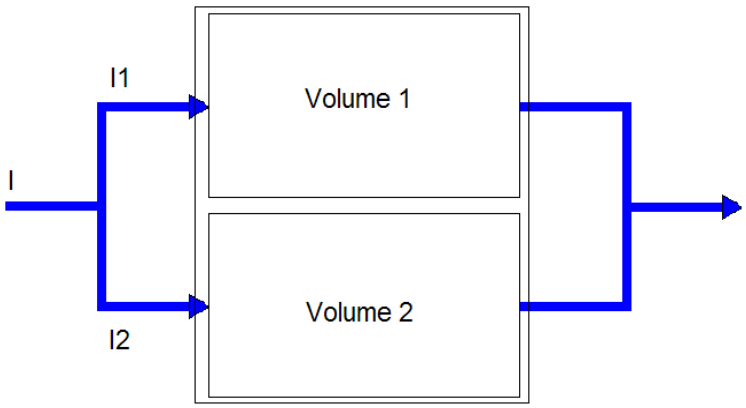

Figure B.4: Composition electrically

B.1.7 SOFC stack

A number of SOFCs are usually connected either in series or in parallel or in both configurations to get the required power. In the stack, it is assumed that all the SOFCs are operating at identical conditions. The fuel and air mass flows at the stack inlet are split into the number of the flows equal to the number of cells in the stack. The split flows are supplied to the cells in parallel. All the anode (cathode) outlet flows from all the cells are mixed at the stack outlet to obtain the stack anode (cathode) outlet flow.

Let n be the number of cells in the stack; $\dot{m}^s_{in,an}, \dot{m}^s_{in,ca}, \dot{m}^s_{out,an}$ and $\dot{m}^s_{out,ca}$ be the stack anode inlet, stack cathode inlet, stack anode outlet and stack cathode outlet flow rates respectively; P^s_{DC} be the stack power, P^s_{rad} be the radiation heat loss from the stack, and Q^s be the conduction heat loss from the stack. The stack variables are related to the each cell variables by the following equations,

$$\begin{aligned}
\dot{m}^s_{in,an} &= n\dot{m}_{in,an} \\
\dot{m}^s_{in,ca} &= n\dot{m}_{in,ca} \\
\dot{m}^s_{out,an} &= n\dot{m}_{out,an} \\
\dot{m}^s_{out,ca} &= n\dot{m}_{out,ca} \\
P^s_{DC} &= nP_{DC} \\
P^s_{rad} &= nP_{rad} \\
Q^s &= nQ
\end{aligned} \tag{B.23}$$

B.2 Reformer

B.2.1 Introduction

The reformer is used to perform steam reforming to convert methane into hydrogen. It is a fixed volume reactor having two inlets; one for methane and the other for steam and one outlet. There are many possible reactions that can take place during the reformation [8]. The following three main

reactions are taken into consideration:

$$\begin{aligned} CH_4 + H_2O &\Leftrightarrow CO + H_2 \\ CO + H_2O &\Leftrightarrow CO_2 + H_2 \\ CH_4 + 2H_2O &\Leftrightarrow CO_2 + 4H_2 \end{aligned} \tag{B.24}$$

The reformation is a highly endothermic process, so heat must to be supplied to the reactor. As the SOFC operates at a high temperature, heat escapes by radiation from the SOFC stack. This heat may be supplied to the reformer by using a suitable mechanical design of the reformer. The operating temperature of the reactor can be in the range $500°C - 700°C$ and the operating pressure can be varied from 2 to 4 bars.

B.2.2 Model assumptions

1. The model is lumped. In practice, a reformer reactor is a tubular reactor [8]. Hence all the variables are distributed. However, all variables are assumed to be uniform over the reactor volume.

2. There is sufficient turbulence and diffusion within reactor for perfect mixing to occur. Since all the reactants are gases, it can be satisfied.

3. The pressure losses are neglected within the reactor.

4. All gases are assumed to obey the ideal gas equation within the reactor volume. At the temperature and pressure conditions the reactor, this assumption can be made.

B.2.3 Parameters and variables

Parameters

The parameters used in the model are listed in Table B.4. In the table, i represents component and j represents reaction.

Variables

Variables used in the model are listed in Table B.5. In the table, i represents component and j represents reaction.

Table B.4: Reformer model parameters

Symbol	**Definition**	**Units**	**Value**
R	Universal gas constant	J/(mol·K)	8.3145
V	Volume of reformer	m^3	
mC_p^s	Solid heat capacity	J/K	
a_{ij}	Stoichiometric matrix for the reactions in reformer		
n_{rx}	Number of reactions		3
A_{k_1}	Pre-exponential factor for rate coefficient k_1		3.71×10^{17}
A_{k_2}	Pre-exponential factor for rate coefficient k_2		5.43×10^{5}
A_{k_3}	Pre-exponential factor for rate coefficient k_3		2.83×10^{14}
$A_{K_{H_2}^{ads}}$	Pre-exponential factor for adsorption constant of H_2		6.12×10^{-14}
$A_{K_{CH_4}^{ads}}$	Pre-exponential factor for adsorption constant of CH_4		6.65×10^{-9}
$A_{K_{H_2O}^{ads}}$	Pre-exponential factor for adsorption constant of H_2O		1.77×10^{5}
$A_{K_{CO}^{ads}}$	Enthalpy change of adsorption of CO		8.23×10^{-10}
E_1	Activation energy of the reaction 1 in reformer	J/mol	240.1×10^{3}
E_2	Activation energy of the reaction 2 in reformer	J/mol	67.13×10^{3}
E_3	Activation energy of the reaction 3 in reformer	J/mol	243.9×10^{3}
$-\Delta\overline{h}_{H_2}^{ads}$	Enthalpy change of adsorption of H_2	J/mol	82.9×10^{3}
$-\Delta\overline{h}_{CH_4}^{ads}$	Enthalpy change of adsorption of CH_4	J/mol	38.28×10^{3}
$-\Delta\overline{h}_{H_2O}^{ads}$	Enthalpy change of adsorption of H_2O	J/mol	-88.68×10^{3}
$-\Delta\overline{h}_{CO}^{ads}$	Enthalpy change of adsorption of CO	J/mol	70.65×10^{3}
k	Constant in calculation of outlet mass flow		

Table B.5: Reformer model variables

Symbol	**Definition**	**Units**
N_i	Number of moles of component i in reactor	mol
p	Pressure in reformer	Pa
p_i	Partial pressure of component i in reactor	Pa
r_j	Reaction rate of reaction j	mol/s
$\dot{N}_i^{in,fuel}$	Molar flow rate of component i at fuel inlet	mol/s
$\dot{N}_i^{in,steam}$	Molar flow rate of component i at steam inlet	mol/s
$\dot{N}_i^{out}$	Molar flow rate of component i at outlet	mol/s
$\dot{m}_{in,fuel}$	Mass flow rate at fuel inlet	kg/s
$\dot{m}_{in,steam}$	Mass flow rate at steam inlet	kg/s
$\dot{m}_{out}$	Mass flow rate at reformer outlet	kg/s
T	Temperature in reactor	K
k_1	Rate coefficient for reforming reaction 1	$mol\, Pa^{0.5}/(kg_{cat} \cdot s)$
k_2	Rate coefficient for reforming reaction 2	$mol/(kg_{cat} \cdot s)$
k_3	Rate coefficient for reforming reaction 3	$mol/(kg_{cat} \cdot s)$
K_i^{ads}	Adsorption constant of component i	
K_j	Equilibrium constant for reforming reaction j	
$\Delta\overline{h}_j^{rx}$	Molar specific enthalpy change of reaction j	J/mol
$\Delta\overline{h}_i$	Molar specific enthalpy of component i in reactor	J/mol
P_{heat}	Amount of heat supplied to the reactor	W
$\Delta\overline{h}_i^{in,fuel}$	Molar specific enthalpy component i at fuel inlet	J/mol
$\Delta\overline{h}_i^{in,steam}$	Molar specific enthalpy component i at steam inlet	J/mol
$\Delta\overline{h}_i^{out}$	Molar specific enthalpy of component i at outlet	J/kg
$p_{in,fuel}$	Fuel inlet stream pressure	Pa
$p_{in,steam}$	Steam inlet stream pressure	Pa
p_{out}	Outlet stream pressure	Pa

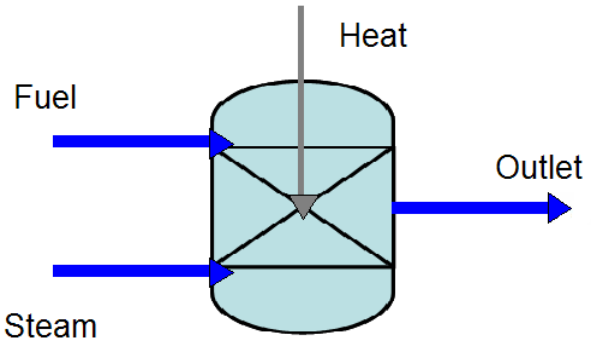

Figure B.5: Reformer interfaces

B.2.4 Interfaces (Ports)

The interfaces of the reformer model are shown in figure B.5. The reformer model has three material streams interfaces; fuel is supplied to one inlet, steam is supplied to the other inlet and the flue gas coming out from the outlet. The model has one energy stream interface: heat to the reformer.

B.2.5 Equations

For modeling, one mass balance and one energy balance are used and are explained as follows.

Mass balance

Mass balance is developed by considering the reformer as a single volume. The mass balance equation is given in (B.25) [7, Chap.13].

$$\frac{dN_i}{dt} = \dot{N}_i^{in,fuel} + \dot{N}_i^{in,steam} - \dot{N}_i^{out} + \sum_{j=1}^{n_{rx}} a_{ij} r_j, \quad i = 1...7,\ n_{rx} = 3 \quad \text{(B.25)}$$

In each inlet stream, there can be the following components; Nitrogen (N_2), Oxygen (O_2), Hydrogen (H_2), Methane (CH_4), Steam (H_2O), Carbonmonoxide (CO), and Carbondioxide (CO_2). A number is assigned to each of these

Table B.6: Reformer reactions

j	**Reaction**	**Reaction rate (r_j)**
1	$CH_4 + H_2O \Leftrightarrow CO + H_2$	r_1
2	$CO + H_2O \Leftrightarrow CO_2 + H_2$	r_2
3	$CH_4 + 2H_2O \Leftrightarrow CO_2 + 4H_2$	r_3

components to simplify the notation, which is given in and index i is used, to represent this number in equations.

i	1	2	3	4	5	6	7
component	N_2	O_2	H_2	CH_4	H_2O	CO	CO_2

Similarly, each reforming reaction is assigned with a number and index j is used to represent this number in equations, as shown in the Table B.6.

In (B.25), a_{ij} represents the stoichiometric matrix for the reactions:

$$[a_{ij}] = \begin{bmatrix} 0 & 0 & 0 \\ 0 & 0 & 0 \\ 3 & 1 & 4 \\ -1 & 0 & -1 \\ -1 & -1 & -2 \\ 1 & -1 & 0 \\ 0 & 1 & 1 \end{bmatrix}$$

In (B.25), r_j, $j = 1, 2, 3$ represent reaction rates and are calculated by [8]

$$\begin{aligned} r_1 &= \frac{k_1}{p_{H_2}^{2.5}} \left(p_{CH_4} p_{H_2O} - \frac{p_{H_2}^3 p_{CO}}{K_1} \right) / (DEN)^2 \\ r_2 &= \frac{k_2}{p_{H_2}} \left(p_{CO} p_{H_2O} - \frac{p_{H_2} p_{CO_2}}{K_2} \right) / (DEN)^2 \\ r_3 &= \frac{k3}{p_{H_2}^{3.5}} \left(p_{CH_4} p_{H_2O}^2 - \frac{p_{H_2}^4 p_{CO_2}}{K_3} \right) / (DEN)^2 \end{aligned} \tag{B.26}$$

In (B.26), DEN is given by

$$DEN = 1 + K_{CO}^{ads} p_{CO} + K_{H_2}^{ads} p_{H_2} + K_{CH_4}^{ads} p_{CH_4} + K_{H_2O}^{ads} p_{H_2O} / p_{H_2} \tag{B.27}$$

In (B.26), k_1, k_2 and k_3 are rate coefficients for the reforming reactions.

$$k_j = A_{kj} \exp(\frac{-E_j}{RT}), \qquad j = 1, 2, 3 \tag{B.28}$$

In (B.26), K_1, K_2 and K_3 are the equilibrium constants for the reforming reactions, which are calculated as follows.

$$\begin{aligned} K_1 &= \exp(-26830/T + 30.114) \quad [bar^2] \\ K_2 &= \exp(4400/T - 4.036) \quad [\ - \ ] \\ K_3 &= \exp(-22430/T + 26.078) \quad [bar^2] \end{aligned} \tag{B.29}$$

In (B.27), $K_{CO}^{ads}, K_{H_2}^{ads}, K_{CH_4}^{ads}$ and $K_{H_2O}^{ads}$ are the adsorption constants, which are calculated by

$$K_i^{ads} = A_{K_i^{ads}} \exp(\frac{-\Delta \overline{h}_i^{ads}}{RT}), \qquad i = H_2, CH_4, H_2O, CO \tag{B.30}$$

It is assumed that the exhaust flows at outlet can be described by the choked exhaust flow equation [5], which is given by

$$\dot{m}_{out} = \sqrt{k(p - p_{out})} \tag{B.31}$$

The reformer volume, pressure, and temperature are assumed to be related by the ideal gas equation,

$$pV = \sum_{i=1}^{N} (N_i) RT, \quad N = 7 \tag{B.32}$$

Also, the partial pressure of each component within the reformer, is calculated by using the ideal gas equation,

$$p_i V = N_i RT, \quad i = 1...7 \tag{B.33}$$

As there is no pressure loss within the reformer, the pressure of the inflow streams is equal to the pressure within the reformer:

$$p_{in,fuel} = p_{in,steam} = p \tag{B.34}$$

Since it is assumed that there is perfect mixing within the reformer volume, the mass fraction of each component within reactor is equal to the mass fraction in the outlet flow.

Energy balance

One energy balance is developed for the whole reformer volume [7, Chap.13] and the following energy balance equation (B.35) is used [4].

$$mC_p^s \frac{dT}{dt} = \sum_{i=1}^{N} \dot{N}_i^{in,fuel}(\Delta\overline{h}_i^{in,fuel} - \Delta\overline{h}_i) + \sum_{i=1}^{N} \dot{N}_i^{in,steam}(\Delta\overline{h}_i^{in,steam} - \Delta\overline{h}_i) - \sum_{j=1}^{M} \Delta\overline{h}_j^{rx} r_j + P_{heat}, \qquad N = 7, M = 3 \tag{B.35}$$

In (B.35), P_{heat} represents the amount of heat power supplied to the reactor. Also, it is to be noted that the molar specific enthalpy of a component depends on the temperature and pressure of the component.

B.3 Combustion chamber

B.3.1 Introduction

The combustion chamber has n_{in} inlet streams and one outlet stream. It burns the fuel coming from all the inlet flows in the presence of oxygen. The requirement is that enough oxygen should be supplied to the combustor. In this model, the fuel can be methane, hydrogen or carbonmonoxide or a mixture of these fuels. The following reactions are being considered during the combustion.

$$\begin{aligned} 2H_2 + O_2 &\rightarrow 2H_2O \\ CH_4 + 2O_2 &\rightarrow 2H_2O + CO_2 \\ 2CO + O_2 &\rightarrow 2CO_2 \end{aligned} \tag{B.36}$$

B.3.2 Model assumptions

The following are the assumptions made in the combustor model.

1. The pressure of all the inlet flows is the same.

Table B.7: Combustor model parameters

Symbol	Definition	Units	Value
R	Universal gas constant	J/(mol·K)	8.3145
mC_p^s	Solid heat capacity	J/K	
a_{ij}	Stoichiometric matrix for the reactions	entry	
n_{rx}	Number of reactions		3
n_{in}	Number of inlets		
α	Pressure loss factor		

2. As the combustion process is very rapid, it is modeled as an instantaneous process.

3. The model is a bulk model; all the physical variables are assumed to be uniform over the combustion chamber.

4. The output pressure depends linearly on the input pressure.

B.3.3 Parameters and variables

Parameters

The parameters used in the model are listed in the following Table B.7. In the table, i represents component and j represents reaction.

Variables

Variables used in the model are listed in the following Table B.8. In the table, i represents component and j represents reaction.

B.3.4 Interfaces

The model interfaces are shown in the figure B.6. The model can have any number of inlets and it has one outlet. All the interfaces are material stream interfaces and there is no energy stream interface to the combustor.

Table B.8: Table Caption

Symbol	**Definition**	**Units**
N_i	Number of moles of the component i in combustor	mol
r_j	Reaction rate of reaction j	mol/s
$\dot{N}_i^{in}$	Total molar flow rate of component i from all the inlets	mol/s
$\dot{N}_i^{out}$	Molar flow rate of component i at outlet	mol/s
p_{in}	Pressure of the inlet streams	Pa
p	Pressure inside the combustion chamber	Pa
p_{out}	Pressure of the outlet stream	Pa
T	Temperature in combustor	K
$\Delta\overline{h}_j^{rx}$	Molar specific enthalpy change of reaction j	J/mol
$\Delta\overline{h}_i^{f}$	Molar specific enthalpy formation of component i in combustor	J/mol
$\Delta\overline{h}_i$	Molar specific enthalpy of component i in combustor	J/mol
$\overline{h}_i^{abs}$	Molar specific enthalpy of component i in combustor	J/mol
$\Delta\overline{h}_{i,in}$	Total Molar specific enthalpy of component i from all the inlets	J/mol
λ	Oxygen ratio	

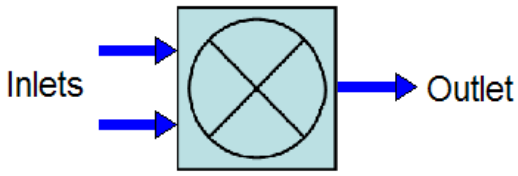

Figure B.6: Combustor interfaces

Table B.9: Combustor reactions

j	**Reaction**	**Reaction rate (r_j)**
1	$2H_2 + O_2 \rightarrow 2H_2O$	r_1
2	$CH_4 + 2O_2 \rightarrow 2H_2O + CO_2$	r_2
3	$2CO + O_2 \rightarrow 2CO_2$	r_3

B.3.5 Equations

In each inlet stream, there can be the following components; Nitrogen (N_2), Oxygen (O_2), Hydrogen (H_2), Methane (CH_4), Steam (H_2O), Carbonmonoxide (CO), and Carbondioxide (CO_2). A number is assigned to each of these components to simplify the notation, and index i is used, to represent this number in equations.

i	1	2	3	4	5	6	7
component	N_2	O_2	H_2	CH_4	H_2O	CO	CO_2

Similarly, each reforming reaction is assigned with a number, which is given in the following table and index j is used to represent this number in equations. And the corresponding reaction rate is also represented in the Table B.9.

In (B.37), a_{ij} represents the stoichiometric matrix for the reactions:

$$[a_{ij}] = \begin{bmatrix} 0 & 0 & 0 \\ -1 & -2 & -1 \\ -2 & 0 & 0 \\ 0 & -1 & 0 \\ 2 & 2 & 0 \\ 0 & 0 & -2 \\ 0 & 1 & 2 \end{bmatrix}$$

Mass balance

For mass balance, the control volume is the whole combustion chamber. The mass balance is expressed in terms of molar flows, as given in (B.37) [7, Chap.13].

$$\dot{N}_i^{in} + \sum_{j=1}^{n_{rx}} a_{ij} r_j = \dot{N}_i^{out}, \qquad i = 1...7,\ n_{rx} = 3 \tag{B.37}$$

Energy balance

For energy balance, the control volume is the whole combustion chamber. Since the combustion reactions are fast, the static energy balance is used [4], which is given by

$$\sum_{i=1}^{N} \dot{N}_i^{in}(\Delta\overline{h}_{i,in} - \Delta\overline{h}_i) - \sum_{j=1}^{M} \Delta\overline{h}_j^{rx} r_j = 0, \qquad N = 7, M = 3 \tag{B.38}$$

Oxygen ratio

The oxygen ratio (λ) is defined as the ratio between the amount of oxygen available to the amount of oxygen required for the complete combustion of the fuel,

$$\lambda = \frac{\text{amount of oxygen available for combustion}}{\text{amount of oxygen required for the complete combustion of fuel}} \tag{B.39}$$

If this value is greater than one, then the model guarantees the complete combustion of the fuel [1]. For example, if this combustion model is used for the SOFC application, then there is no need to care about the oxygen ratio. In that case, usually there is sufficient amount of oxygen available for the complete combustion.

Pressure relation

It is assumed that the pressure of all the incoming flows is the same. Also the pressure of the combustion chamber equals to the pressure of the inlet flows,

$$p_{in} = p \tag{B.40}$$

There is a 2% loss of pressure from the combustion chamber to the outlet flow,

$$p_{out} = \alpha p, \quad \alpha \in \langle 0, 1 \rangle \tag{B.41}$$

Table B.10: Heat exchanger model parameters

Symbol	Definition	Units	Value
U	Heat transfer coefficient of the wall	W/(m^2·K)	
A	Area of contact	m^2	
τ	Time constant		

B.4 Heat exchanger

B.4.1 Introduction

A very simple model of a counter-flow heat exchanger is presented. In the counter-flow heat exchanger, there is a counter-flow of cold and hot streams. During this counter-flow, there is an exchange of heat from the hot stream to the cold stream. The amount of the heat power exchanged depends on the heat transfer coefficient of the exchanger wall and also the average temperature difference between the hot and cold streams. The temperature change of the streams is not instantaneous.

B.4.2 Model assumptions

The following are the assumptions made in the model,

1. The model is a lumped one. All the physical parameters are assumed to be uniform over the heat exchanger. This may be a crude assumption.

2. There is no pressure loss within the heat exchanger.

B.4.3 Parameters and variables

Parameters

The parameters used in the model are listed in the following Table B.10.

Variables

Variables used in the model are listed in the following Table B.11.

Table B.11: Heat exchanger model variables

Symbol	Definition	Units
$\dot{m}_{cold}$	Mass flow rate of the cold stream	kg/s
$\dot{m}_{hot}$	Mass flow rate at the hot stream	kg/s
p_{cold}	Pressure of the cold stream	Pa
p_{out}	Pressure of the outlet stream	Pa
T_{in}^{cold}	Temperature of the cold inflow	K
T_{out}^{cold}	Temperature of the cold outflow	K
T_{in}^{hot}	Temperature of the hot inflow	K
T_{out}^{hot}	Temperature of the hot outflow	K
ΔT	Differential temperature	K
C_p^{cold}	Average mass specific heat capacity of the cold stream	J/kg
C_p^{hot}	Average mass specific heat capacity of the heat stream	J/kg

B.4.4 Interfaces

The interfaces of the model are shown in figure B.7. It is a counter flow heat exchanger having two inlets; one for cold flow inlet stream and the other for hot flow inlet stream, and two outlets; one for cold flow outlet stream and the other for hot flow outlet stream as shown in figure B.7. Here all the interfaces are associated with the material streams and there is no energy stream interface associated with the model.

B.4.5 Equations

Mass balance

As there is no mixing of the cold and hot streams, there is a continuous flow in the respective streams. This can be represented in the form of a equation (B.42).

$$\begin{aligned} \dot{m}_{in}^{cold} &= \dot{m}_{out}^{cold} \\ \dot{m}_{in}^{hot} &= \dot{m}_{out}^{hot} \end{aligned} \tag{B.42}$$

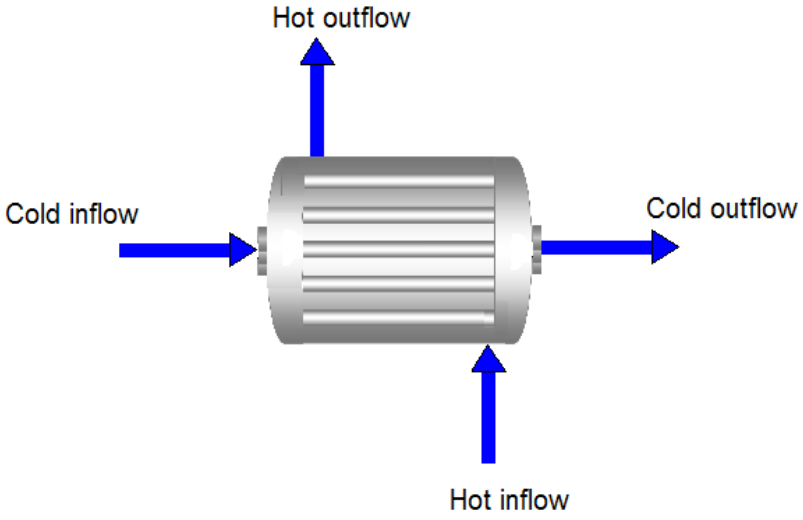

Figure B.7: Heat exchanger interfaces

Energy balance

The amount of heat power (q) that is being exchanged between the cold and hot streams is given by (B.43). In (B.43), ΔT is calculated from (B.44).

$$q = UA\Delta T \tag{B.43}$$

$$\Delta T = f((T_{in}^{hot} - T_{out}^{cold}), (T_{out}^{hot} - T_{in}^{cold})) \tag{B.44}$$

Heat exchanger cannot react instantaneously to the changes in the inflow conditions. Hence a first order time delay is included to the temperature calculated by (B.43), which for hot stream is given in (B.45), and for cold stream is given in (B.46).

$$\frac{dT_{out}^{hot}}{dt} = \frac{1}{\tau}\left(T_{in}^{hot} - T_{out}^{hot} + \frac{-q}{\dot{m}_{hot}C_p^{hot}}\right) \tag{B.45}$$

$$\frac{dT_{out}^{cold}}{dt} = \frac{1}{\tau}\left(T_{in}^{cold} - T_{out}^{cold} + \frac{q}{\dot{m}_{cold}C_p^{cold}}\right) \tag{B.46}$$

In the heat exchanger it is assumed that there is no pressure loss both in the cold and in the hot streams.

B.5 Compressor

B.5.1 Introduction

A compressor is a device which compresses any fluid by increasing its pressure and reducing its volume. There are many types of compressors that can be used depending on the application [6]. Especially for fuel cell application the following are the different types: roots compressor,Lysholm or screw compressor, centrifugal or radial type and axial flow compressor [3]. Here the compressor model represents a generic compressor whose characteristics depends on the compressor chart. The model gives the outlet temperature, outlet pressure and the power required for compression given the constant isentropic efficiency.

B.5.2 Model assumptions

1. It is assumed that the compressor has constant isentropic efficiency.

2. The working gas (fluid) is assumed to obey the ideal gas equation.

3. Adiabatic reversible state change with constant heat capacity is assumed during the compression.

B.5.3 Parameters and variables

Parameters

The compressor model parameters are listed in Table B.12.

Variables

The compressor model variables are listed in Table B.13.

B.5.4 Interfaces

The compressor interfaces are shown in figure B.8.

Table B.12: Compressor model parameters

Symbol	**Definition**	**Unit**	**Value**
R	Universal gas constant	J/(mol·K)	8.3145
A_{ref}	Reference area	m^2	
l	Length	m	
V	Volume	m^3	
γ	Isentropic exponent for the working fluid		
η_a	Adiabatic (isentropic) efficiency		
C_p	Specific heat at constant pressure	J/(mol·K)	
C_v	Specific heat at constant volume	J/(mol·K)	

Table B.13: Compressor model variables

Symbol	**Definition**	**Unit**
T_{in}	Inlet temperature	K
T_{out}	Outlet temperature	K
T_s	Isentropic temperature	K
P_{in}	Inlet pressure	Pa
P_{out}	Outlet pressure	Pa
$\dot{m}$	Mass flow rate through the compressor	kg/s
P	Compressor power	W
N	Shaft speed	rpm
ω	Shaft speed	rad/s
Δh_{in}	Mass specific enthalpy of the inlet stream	J/kg
Δh_{out}	Mass specific enthalpy of the outlet stream	J/kg
Δh	Mass specific enthalpy change from inlet to the outlet	J/kg
Δh_s	Isentropic mass specific enthalpy change from inlet to outlet	J/kg

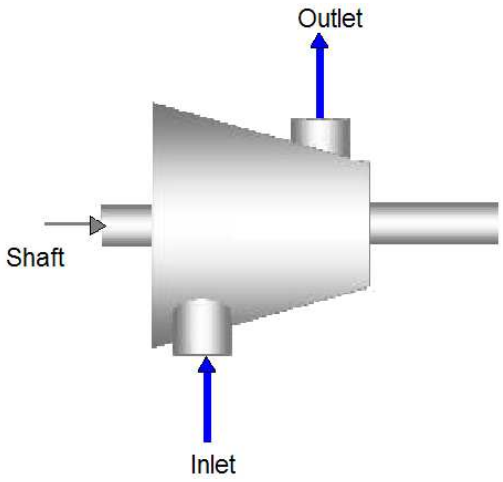

Figure B.8: Compressor interfaces

B.5.5 Equations

The inlet temperature and the isentropic outlet temperature are related to the pressure ratio which is given by, [3]

$$\frac{T_s}{T_{in}} = \left(\frac{p_{out}}{p_{in}}\right)^{\frac{\gamma-1}{\gamma}} \tag{B.47}$$

This relation is derived by assuming the adiabatic reversible state change for an ideal gas with constant heat capacity, equivalently

$$pV^{\gamma} = const \tag{B.48}$$

and using the ideal gas equation,

$$pV = nRT \tag{B.49}$$

In (B.47), γ is given by

$$\gamma = \frac{C_p}{C_v} \tag{B.50}$$

The isentropic enthalpy difference is the product of the real (actual) enthalpy difference and the adiabatic efficiency,

$$\begin{aligned} \Delta h_s &= \eta_a \Delta h \\ \Delta h &= \Delta h_{in} - \Delta h_{out} \end{aligned} \tag{B.51}$$

The power required by the compressor is given by,

$$P = \dot{m}\Delta h \tag{B.52}$$

B.5.6 Compressor map

The static relation among speed, mass flow and pressure ratio of a compressor is known as the compressor map. The model can be used with any provided compressor map. Here the compressor map is obtained by curve fitting the typical compressor map taken from [3]. The compressor map is shown in figure B.9, which gives the relation among the mass flow rate, the pressure ratio and speed while the inlet temperature and the pressure are maintained at $25°C$ and atmospheric pressure respectively. Basically, the compressor map shows the following relation,

$$\frac{p_{out}}{p_{in}} = \Phi(N_{factor},\ \dot{m}_{factor}) \tag{B.53}$$

In (B.53), N_{factor} and $\dot{m}_{factor}$are given by the following relations [3]:

$$\begin{aligned} \dot{m}_{factor} &= \frac{\dot{m}\sqrt{T_{in}}}{p_{in}} \\ N_{factor} &= \frac{N}{\sqrt{T_{in}}} \\ N &= \frac{60\omega}{\pi} \end{aligned} \tag{B.54}$$

B.6 Turbine

B.6.1 Introduction

Turbine is used to expand the compressed fluid to generate mechanical power [6]. The turbine is frequently used to rotate a compressor to compress the incoming air or fuel gas. In some cases there may be excess power that can be used to generate electrical power from generator fitted to the same shaft [3]. There are many types of turbine cycles but the following two are the important ones; centripetal or radial flow turbine and axial flow turbine. The turbine model calculates outlet pressure, temperature and power output given the isentropic efficiency of the turbine. The mass flow is calculated by a choked nozzle equation.

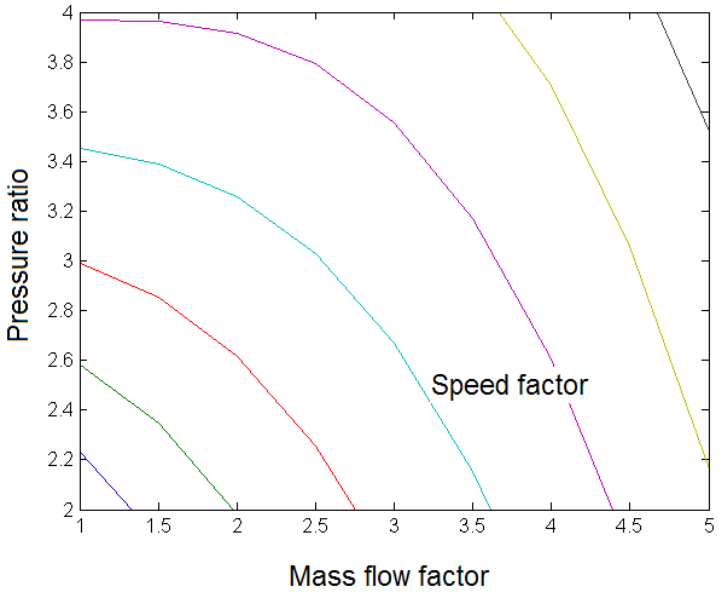

Figure B.9: Compressor map

B.6.2 Model assumptions

1. The model assumes constant isentropic efficiency.
2. The working fluid is assumed to satisfy the ideal gas equation.
3. Adiabatic reversible state change with constant heat capacity is assumed during the compression.

B.6.3 Parameters and variables

Parameters

The turbine model parameters are given in Table B.14.

Variables

The model variables are listed in Table B.15.

Table B.14: Turbine model parameters

Symbol	**Definition**	**Unit**	**Value**
R	Universal gas constant	J/(mol·K)	8.3145
C_p	Specific heat at constant pressure	J/(mol·K)	
C_v	Specific heat constant volume	J/(mol·K)	
$\dot{m}_d$	Design mass flow rate	kg/s	
T_{in}^d	Design inlet temperature	K	
p_{in}^d	Design inlet pressure	Pa	
γ	Isentropic exponent for the working fluid		
η_a	Adiabatic isentropic efficiency		

Table B.15: Turbine model variables

Symbol	**Definition**	**Unit**
$\dot{m}$	Mass flow rate	kg/s
T_{in}	Inlet temperature	K
T_{out}	Outlet temperature	K
p_{in}	Inlet pressure	Pa
p_{out}	Outlet pressure	Pa
P	Power	W
Δh_{in}	Mass specific enthalpy at the inlet	J/kg
Δh_{out}	Mass specific enthalpy at the outlet	J/kg
Δh	Mass specific enthalpy change from inlet to outlet	J/kg

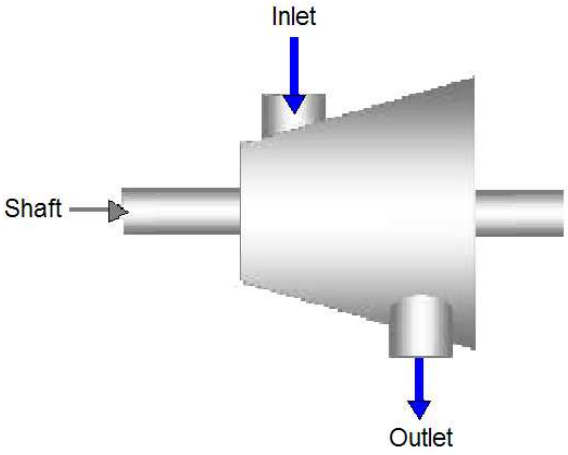

Figure B.10: Turbine interfaces

B.6.4 Interfaces

The turbine model interfaces are shown in figure B.10.

B.6.5 Equations

The inlet temperature and the isentropic outlet temperature are related to the pressure ratio, which is given by [3],

$$\frac{T_s}{T_{in}} = \left(\frac{p_{out}}{p_{in}}\right)^{\frac{\gamma-1}{\gamma}} \tag{B.55}$$

This relation is derived by assuming the adiabatic reversible state change for an ideal gas with constant heat capacity, equivalently

$$pV^{\gamma} = const \tag{B.56}$$

and using the ideal gas equation,

$$pV = nRT \tag{B.57}$$

In (B.55), γ is given by

$$\gamma = \frac{C_p}{C_v} \tag{B.58}$$

Table B.16: Shaft model parameters

Symbol	Definition	Unit	Value
M	Rotating mass	kg	
r	Radius of the shaft	m	

The isentropic enthalpy difference is the product of the real (actual) enthalpy difference and the adiabatic efficiency,

$$\begin{aligned} \Delta h_s &= \eta_a \Delta h \\ \Delta h &= \Delta h_{in} - \Delta h_{out} \end{aligned} \tag{B.59}$$

The power generated by turbine is given by ,

$$P = \dot{m} \Delta h \tag{B.60}$$

The mass flow rate is calculated by using the choked nozzle equation (B.61). In this the operating mass flow rate is related to the design point.

$$\left(\frac{p_{in}}{p_{in}^d}\right)^2 = \left(\frac{\dot{m}}{\dot{m}_d}\right)^2 \left(\frac{T_{in}}{T_{in}^d}\right) \tag{B.61}$$

B.7 Shaft

B.7.1 Introduction

Shaft is modeled as a rotating mass driven by the mechanical power (that can be developed by a turbine).

B.7.2 Parameters and variables

Parameters

The model parameters are listed in Table B.16.

Variables

The model variables are listed in Table B.17.

Table B.17: Shaft model variables

Symbol	Definition	Unit
N	Rotation speed	rpm
ω	Angular velocity	rad/s
P	Power	W
I	Inertia	kg-m^2

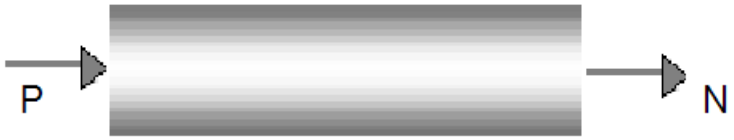

Figure B.11: Shaft interfaces

B.7.3 Interfaces

The shaft interfaces are shown in figure B.11.

B.7.4 Equations

The inertia of the rotating mass is calculated from,

$$I = \frac{1}{2}Mr^2 \tag{B.62}$$

The rotating speed (N) and the angular velocity (ω) are related by,

$$\omega = \pi N/30 \tag{B.63}$$

The shaft speed is calculated from the dynamic relation [1],

$$\dot{\omega} = P/(I\omega) \tag{B.64}$$

References

[1] L. Imsland, D. Snarheim, R. Ulfsnes, O. Bolland, and B. A. Foss. Modeling and control of a o2/co2 gas turbine cycle for co2 capture. *In proceedings of DYCOPS, Boston*, 2004.

[2] F. P. Incropera and D. P. De Witt. *Fundamentals of Heat and Mass Transfer*. Wiley, USA, 2002.

[3] J. Larminie and A. Dicks. *Fuel Cell Systems Explained*. Wiley, England, 2003.

[4] M. D. Lukas, K. Y. Lee, and H. Ghezel-Ayagh. An Explicit Dynamic Model for Direct Reforming Carbonate Fuel Cell Stack. *IEEE Transactions on Energy Conversion*, 16(3), September 2001.

[5] J. Padulles, G. W. Ault, and J. R. McDonald. An integrated SOFC dynamic model power systems simulation. *Journal of Power Sources*, 86(1):495–500, 2000.

[6] H. I. H. Saravanamuttoo, G. F. C. Rogers, and H. Cohen. *Gas Turbine Theory*. Prentice Hall, England, 2001.

[7] P. Thomas. *Simulation of Industrial Processes For Control Engineers*. Butterworth-Heinemann, Wobourn, MA, USA, 1999.

[8] J. Xu and G. F. Froment. Methane Steam Reforming, Methanation and Water-Gas Shift: I. Intrinsic Kinetics. *AIChE Journal*, 35(1):88–96, 1989.